POLYDIMETHYLSILOXANE-BASED SELF-HEALING COMPOSITE AND COATING MATERIALS

BY

SOO HYOUN CHO

B.S., Pohang University of Science and Technology, 1993
M.S., Pohang University of Science and Technology, 1995

DISSERTATION

Submitted in partial fulfillment of the requirements
for the degree of Doctor of Philosophy in Materials Science and Engineering
in the Graduate College of the
University of Illinois at Urbana-Champaign, 2006

Urbana, Illinois

ABSTRACT

This thesis describes the science and technology of a new class of autonomic polymeric materials which mimic some of the functionalities of biological materials. Specifically, we demonstrate an autonomic self-healing polymer system which can heal damage in both coatings and bulk materials. The new self-healing system we developed greatly extends the capability of self-healing polymers by introducing tin catalyzed polycondensation of hydroxyl end-functionalized polydimethylsiloxane and polydiethoxysiloxane based chemistries. The components in this system are widely available and comparatively low in cost, and the healing chemistry also remains stable in humid or wet environments. These achievements significantly increase the probability that self-healing could be extended not only to polymer composites but also to coatings and thin films in harsh environments.

We demonstrate the bulk self-healing property of a polymer composite composed of a phase-separated PDMS healing agent and a microencapsulated organotin catalyst by chemical and mechanical testing. Another significant research focus is on self-healing polymer coatings which prevent corrosion of a metal substrate after deep scratch damage. The anti-corrosion properties of the self-healing polymer on metal substrates are investigated by corrosion resistance and electrochemical tests. Even after scratch damage into the substrate, the coating is able to heal, while control samples which do not include all the necessary healing components reveal rapid corrosion propagation. This self-healing coating solution can be easily applied to most substrate materials, and is compatible with most common polymer matrices. Self-healing has the potential to extend the lifetime and increase the reliability of thermosetting polymers used in a wide variety of applications ranging from microelectronics to aerospace.

ACKNOWLEDGEMENTS

It was a big challenge and opportunity for me to decide to study at the University of Illinois at Urbana-Champaign. I think it was my fortune to have as my advisor, Prof. Paul V. Braun, throughout my graduate study. I greatly appreciate his valuable advice and thoughtful counseling whenever I encountered obstacles to progress in my research. I would like to thank my co-advisor, Prof. Scott R. White, for his enthusiasm and insight into self-healing research. As a research group leader, he gave me continued support and encouragement.

Many thanks are extended to my thesis committee, Profs. Nancy R. Sottos, Jennifer A. Lewis, and James Economy, for their useful suggestions and helpful discussion. I also acknowledge Profs. Philippe H. Geubelle and Jeffrey S. Moore for useful advice in research group meetings. In addition, I would like to express my thanks to Prof. Pierre Wiltzius for his thoughtful concerns and support.

It was a valuable experience to work in the interdisciplinary self-healing research group. I would like to thank my colleagues, Dr. Joe Rule, Gerald Wilson, Michael Keller, Jason Kamphaus, Dr. Magnus Andersson, Ben Blaiszik, Katie Toohey, Amit Patel, Onur Amagan, Gina Miller, and Dr. Byron McCaughey, in the Autonomic Healing Research Group for their extremely useful help and discussion. It was a great pleasure to work with them throughout my research period.

I also want to acknowledge Dr. Huilin Tu, Dr. Zenbin Ge, Dr. Steph Rinne, Dr. Weon Sik Chae, Dr. Dong-Guk Yu, Dr. Ryan Kershner, Xindi Yu, Margaret Shyr, Robert Shimmin, Dan Krogstat, Christy Chen, James Rinne and the rest of the Braun and Wiltzius group members,

for their helpful discussion and technical support on my research achievement. I really enjoyed my school life under pleasant circumstances with my group members.

I would like to thank the staff in the Imaging Technology Group in Beckman Institute and Center for Microanalysis of Materials at the University of Illinois at Urbana-Champaign for their profound technical support. I also gratefully thank Amy Lynch for her kind support throughout my graduate studies.

I gratefully acknowledge Prof. Chan Eon Park for giving me a scientific insight during my master's degree. I'm also grateful to the people in Pohang Iron and Steel Company (POSCO) for providing me an opportunity to study abroad in the U.S.

I would like to express my special thanks to my family. My parents, brother, and sisters gave me all their heart to sustain me. My wife, Jung Min, always supported me with continuous love and trust. My study was only possible by means of her tremendous help and sacrifice. My daughter, Jihee, gave me lots of pleasure and motivation for living. I cannot find more proper words to express my thanks for their help.

This thesis is supported by AFOSR Aerospace and Materials Science Directorate grant number F49620-03-1-0179, and Northrop Grumman Ship Systems grant number NG SRA 04-307 PO number 51-19655-011. Many parts of the microscopic observation in this thesis were performed in the Center for Microanalysis of Materials, at the Frederick Seitz Materials Research Laboratory, University of Illinois at Urbana-Champaign, which is partially supported by the U.S. Department of Energy under grant DEFG02-91-ER45439. The majority of synthesis and characterization in this thesis was performed in the Autonomous Materials System Laboratory and in the Imaging Technology Group at Beckman Institute, University of Illinois at Urbana-Champaign.

TABLE OF CONTENTS

LIST OF ABBREVIATIONS x

LIST OF TABLES xi

LIST OF FIGURES xii

CHAPTER 1. INTRODUCTION 1
1.1 Self-healing Function 1
1.2 Previous Self-healing Work 2
1.3 Polydimethylsiloxane (PDMS) Chemistry 6
1.3.1 Silicone Chemistry 6
1.3.2 Platinum Catalyzed Hydrosilylation 8
1.3.3 Tin Catalyzed Polycondensation 9
1.4 References 10

CHAPTER 2. SELF-HEALING POLYMER COMPOSITE 12
2.1 Motivation 12
2.2 PDMS Based Self-healing Materials 13
2.3 Phase Separation 17
2.3.1 Preliminary Study for Phase Separation Behavior 17
2.3.2 Phase Separation Behavior of PDMS in Matrix 22
2.3.3 PDMS Solubility in Epoxy Vinyl Ester Matrix 23
2.4 Catalyst Microencapsulation 24
2.4.1 Interfacial Polymerization 24
2.4.2 Characterization of Microcapsules 26
2.5 Surface Morphology of Fractured Self-healing Polymer Composite 30
2.6 Fracture Test of Self-healing Composite 31
2.6.1 Tapered Double-Cantilever-Beam (TDCB) Test 31
2.6.2 Self-healing under Water Environments 37
2.7 Conclusions 38
2.8 Experimental 39
2.8.1 Microcapsule Synthesis 39
2.8.2 Vinyl Ester Matrix Polymerization and Sample Formation 40
2.8.3 Fracture Testing and Healing Efficiency 41
2.8.4 Fracture Testing of the Samples Healed under Water Environments 41
2.9 References 42

CHAPTER 3. LOW TEMPERATURE SELF-HEALING 45
3.1 Viscosity of PDMS Healing Agent 45
3.2 Catalytic Activity 49

3.3 Conclusions....52
3.4 Experimental....52
3.4.1 Small Scale Bullet Sample Test....53
3.5 References....53

CHAPTER 4. SELF-HEALING COATINGS....54
4.1 Motivation....54
4.2 Self-healing Coating System....54
4.3 Self-healing Coating Fabrication....56
4.3.1 Self-healing Coatings with Bar Coater....57
4.3.2 Self-healing Coatings with Doctor Blade type Coater....58
4.4 Anti-corrosion Property of the Self-healing Coatings....59
4.5 Electrochemical Test....61
4.5.1 Electrochemical Test Facility....61
4.5.2 Electrochemical Current....62
4.6 Surface Morphology of the Self-healing....64
4.7 Cross Sectional Observation....65
4.7.1 Optical Microscopy....65
4.7.2 Scanning Electron Microscopy....66
4.7.3 Electroless Nickel Coating....68
4.7.4 Direct SEM Observation....71
4.7.5 Heat Treatment....73
4.8 Surface Profile....75
4.9 Conclusions....77
4.10 Experimental....77
4.10.1 Coating Fabrication....77
4.10.2 Corrosion Test....78
4.10.3 Electrochemical Test....79
4.10.4 SEM Sample Preparation for Cross-sectional Observation....79
4.10.5 Surface Profilometry....79
4.11 References....80

CHAPTER 5. TWO MICROCAPSULE SELF-HEALING SYSTEM....81
5.1 Investigation for Self-healing Coating Media....81
5.2 Two Microcapsule Self-healing System for Epoxy Matrix....82
5.3 Temperature Dependence of the Healing Property....86
5.4 TKAS Catalyst synthesis....88
5.5 Microencapsulation of the TKAS Catalyst....90
5.6 Healing Property with the TKAS Catalyst....91
5.7 Self-healing Coatings with Two Microcapsule System....93
5.8 Healing in water environments....94
5.8.1 Healing in Pure and Salt Water Environment....94
5.8.2 Healing in water with different pH conditions....95
5.9 Adhesion Strength of Self-healing Coatings....97

5.9.1 Chemical Treatment with Silane Coupling Agent 97
5.9.2 Mechanical Treatment with Sand Blasting 99
5.9.3 Primer Coating 100
5.10 Dual Layered Self-healing Coatings 102
5.11 Conclusions and Outlook 103
5.12 Experimental 104
5.12.1 Microcapsule Synthesis 104
5.12.2 Sample Preparation for Fracture Test with TDCB Geometry 105
5.12.3 Synthesis of TKAS Catalyst 105
5.12.4 Microencapsulation of the TKAS catalyst 105
5.12.5 Corrosion Test of the Samples Healed in Water Environments 106
5.13 References 106

CHAPTER 6. CONCLUSIONS AND FUTURE WORK 107

AUTHOR'S BIOGRAPHY 110

LIST OF ABBREVIATIONS

PMMA	poly(methyl metacrylate)
MEKP	methyl ethyl ketone peroxide
ROMP	ring opening metathesis polymerization
DCPD	dicyclopentadiene
PDMS	polydimethylsiloxane
HOPDMS	hydroxyl end functionalized polydimethylsiloxane
PDES	polydiethoxysiloxane
DBTL-Sn	di-n-butyltin dilaurate
EVE	epoxy vinyl ester
DETA	diethylenetriamine
BPO	benzoylperoxide
DMA	dimethylaniline
PBD	polybutadiene
THF	tetra hydro furan
SEM	scanning electron microscope
TDI	toluene 2,4-diisocyanate
EG	ethylene glycol
TGA	thermogravimetric analysis
TDCB	tapered double cantilever beam
RH	relative humidity
DMDN-Sn	dimethyldineodacanoate tin
DBBE-Sn	di-n-butyl bis(2-ethylenehexanoate) tin
HEA	hydroxyethyl acrylate
MMA	methyl methacrylate
TMPTA	trimethylolpropane triacrylate
GPC	gel permeation chromatograph
PDI	poly-dispersity index

LIST OF TABLES

Table 2.1: The size values of phase separated PBD droplets. 20

Table 2.2: The size values of phase separated PDMS droplets 22

Table 2.3: Elemental analysis of separated prepolymer phase and control samples. 24

Table 2.4: The size values of phase separated PDMS droplets according to the mechanical stirring speeds. 28

Table 2.5: Average maximum load of self-healed vinyl ester. One standard deviation in square brackets. 37

Table 3.1: Average maximum load for control and *in situ* samples according to temperature. 46

Table 3.2: The size values of phase separated PDMS droplets 47

Table 3.3: Maximum load of self-healed samples with various viscosity PDMS by TDCB test. 48

Table 3.4: Fracture load of self-healed samples with new catalysts by TDCB test. 52

Table 4.1: The electrochemical current values of the test specimens by electrochemical tests. 64

Table 4.2: Procedures of electroless nickel coating with 20-8192 EDGEMET®KIT. 70

Table 5.1: Result of thermal curing reaction of melamine curing agent for epoxy and PDMS after 24 hours according to temperatures. 82

LIST OF FIGURES

Figure 1.1: A thermally re-mendable crosslinked polymeric material healed by reversible Diels-Alder reaction; (a) Image of a broken specimen before thermal treatment and (b) Image of the specimen after thermal treatment. Figure adapted from ref. [8].. 3

Figure 1.2: Self-healing system using a microencapsulated healing agent; (a) Autonomic healing concept with microencapsulated DCPD and Grubbs's catalyst (adapted from [14]) and (b) self-healing material with wax-protected Grubbs' catalyst microspheres (adapted from [16]). 5

Figure 1.3: Reaction schemes for synthesis of PDMS; (a) silicone synthesis from silica, (b) methylchlorosilanes synthesis from the reaction of elemental silicone with methylchloride, (c) synthesis of polysiloxane from hydrolysis and condensation of methylchlorosilane, and (d) synthesis of PDMS by acid or base catalyzed ring opening polymerization of octamethylcyclotetrasiloxane (adapted from [22]). 7

Figure 1.4: Reaction scheme for Pt catalyzed hydrosilylation of PDMS (adapted from [22]). 8

Figure 1.5: Reaction scheme for tin catalyzed polycondensation of PDMS [24].. 9

Figure 2.1: Reaction Scheme for the polycondensation of HOPDMS and PDES in the presence of the DBTL-Sn catalyst. 14

Figure 2.2: Chemical structure of epoxy vinyl ester. 15

Figure 2.3: Schematic of self-healing process: a) self-healing composite consisting of microencapsulated catalyst (yellow) and phase-separated healing-agent droplets (white) dispersed in a matrix (green); b) composite containing a pre-crack; c) crack propagating into the matrix releasing catalyst and healing agent into the crack plane; d) a crack healed by polymerized PDMS (crack width exaggerated). 16

Figure 2.4: Confocal micrographs of phase separated PBD droplets with molecular weight (a) $\overline{M}_n$ =1,000 and (b) $\overline{M}_n$ =1,800 from epoxy before and after matrix polymerization. The images are obtained in scanning modes for surface observation (XYZ direction) and cross sectional observation (XZY direction). 18

Figure 2.5: Fluorescence confocal micrographs of phase separated PBD ($\overline{M}_n$ =1,000 & 1,800) droplets from epoxy including fluorescent dye (Rodamine 6G) before and after matrix polymerization. The images are obtained in scanning modes for surface observation (XYZ direction) and cross sectional observation (XZY direction). 19

Figure 2.6: Scanning electron micrographs of fracture plane in (a) epoxy matrix and epoxy with 10 wt% of PBD (b) before and (c) after extraction by THF. 20

Figure 2.7: Scanning electron micrographs of fracture plane in epoxy with (a) 10 wt%, (b) 20 wt%, and (c) 30 wt% of PBD ($\overline{M}_n$ =1,000); (d) 10 wt%, (e) 20 wt%, (f) 30 wt% of PBD ($\overline{M}_n$ =1,800) after extraction by THF. 21

Figure 2.8: Scanning electron micrographs of fracture plane in epoxy with (a) 10 wt%, (b) 20 wt%, and (c) 30 wt% of DCPD after extraction by THF. 22

Figure 2.9: Optical microscopic images of epoxy with (a) 10 wt%, (b) 20 wt%, and (c) 30 wt% of PDMS (DOW, SYLGARD184). 23

Figure 2.10: Scanning electron micrographs of fracture plane in epoxy with (a) 10 wt%, (b) 20 wt%, and (c) 30 wt% of PDMS (DOW, SYLGARD184). 23

Figure 2.11: Reaction schemes for synthesis of urethane prepolymer. 25

Figure 2.12: Reaction schemes for encapsulation using interfacial polymerization. 25

Figure 2.13: Schematics of interfacial polymerization for catalyst microencapsulation. 26

Figure 2.14: Microscopic images of synthesized microcapsules: (a) Optical microscope image of catalyst containing microcapsules and (b) SEM image of a representative microcapsule showing its smooth, uniform surface. 27

Figure 2.15: Fractured surface of self-healing polymer composite with phase separated healing materials and broken microcapsule. 27

Figure 2.16: Diameter of catalyst containing microcapsules (shown with standard deviation) as a function of stirring speed. The insert shows an optical microscope image of microcapsules formed at 1000 rpm. 29

Figure 2.17: Thermal behavior of synthesized microcapsules by TGA. 30

Figure 2.18: Fracture surface of self-healing polymer composite. (a) Empty microcapsule and voids left by the phase separated healing agent before healing reaction; (b) Broken microcapsule and voids left by the phase separated healing agent before healing reaction; (c) Broken microcapsule; (d) Cured PDMS layer after healing reaction. 31

Figure 2.19: Tapered-double-cantilever-beam geometry based on modification to the geometry. All dimensions in mm. Figure adapted from ref. [42, 43]. 32

Figure 2.20: Load–displacement curves of virgin TDCB samples with (1, black) and without (2, red) post curing at 50 ˚C. Test sample contains 4 wt% adhesion promoter, 12 wt% PDMS, and 3.6 wt% microcapsules. 33

Figure 2.21: Optical microscopic images of virgin sample with TDCB geometry according to the crack propagation. Arrow represents the position of propagated crack [44]. 34

Figure 2.22: Load–displacement curves of TDCB samples: a) virgin sample (1, black), and injection-healed sample with (2, red) and without (3, blue) adhesion promoter; b) first fracture of sample containing 4 wt% adhesion promoter, 12 wt% PDMS, and 3.6 wt% microcapsules (4, black) and after self-healing (5, blue). The injection-healed sample (2, red) with adhesion promoter is shown again for comparison. 36

Figure 2.23: Load–displacement curves of TDCB samples containing 4 wt% adhesion promoter, 12 wt% PDMS, and 3.6 wt% microcapsules healed in air at low relative humidity (1, black), in air at high relative humidity (2, red), and immersed in water (3, blue). 38

Figure 3.1: Fractured surface of composite of phase separated PDMS healing materials, (a) S42 (viscosity 14,000 cP) and (b) S35 (viscosity 4,000 cP), with epoxy vinyl ester matrix. 46

Figure 3.2: Result from monotonic fracture tests with TDCB geometry for virgin samples and fractured samples healed at 30 ˚C with a) S42 (viscosity 14,000 cP) and b) S35 (viscosity 4,000 cP). 47

Figure 3.3: Chemical structures for original catalyst a) DBTL-Sn ($C_{32}H_{64}O_4Sn$, M.W. 631.55) and new versions of organotin catalysts b) DMDN-Sn ($C_{22}H_{44}O_4Sn$, M.W. 491.29), c) DBBE-Sn ($C_{24}H_{48}O_4Sn$, M.W. 519.34) and d) Tin-II ($C_{36}H_{66}O_4Sn$, M.W. 680.69).....49

Figure 3.4: Optical microscopic images of synthesized microcapsules containing new organotin catalysts. 50

Figure 3.5: Results from monotonic fracture tests with new catalysts containing microcapsules for virgin and fractured samples healed at a) room temperature and b) 30 ˚C. 51

Figure 4.1: Schematic of self-healing process. a, self-healing coating containing microencapsulated catalyst (yellow) and phase separated or encapsulated healing-agent droplets (blue) in a matrix (pink) on a metallic substrate (grey); b, damage to the coating layer releases catalyst (green) and healing agent; c, diffusive mixing of healing agent and catalyst in the damaged region; d. damage healed by crosslinked PDMS, protecting the substrate from the environment. 56

Figure 4.2: a) Bar coater applicator for fabricating coated steel samples. b) Set-up for corrosion tests in an aqueous solution of sodium chloride. c) Epoxy vinyl ester coated steel corrosion test sample after scribing and 120 h exposure to salt water. 57

Figure 4.3: Procedure for surface coating fabrication with doctor blade coater. a) Application of coating solution by pipette. b) Coating thickness adjustment by threaded dials. C) Coated steel test sample. 58

Figure 4.4: Corrosion test results for control and self-healing coatings. The polymers are composed of a, matrix (epoxy vinyl ester) and adhesion promoter (methylacryloxy propyl triethoxy silane, 3 wt%); b, matrix, adhesion promoter, and 3 wt% of tin catalyst (dimethyldineodecanoate tin containing microcapsules); c, matrix, adhesion promoter, and phase separated PDMS healing agent (12 wt% mixture of HOPDMS and PDES); d, the self-healing coating consisting of matrix, adhesion promoter, microencapsulated catalyst, and PDMS healing agent. The corrosion test samples are 75 x 150 mm^2 (width x length). Samples were healed at 50 °C. Images are taken after immersion in salt water for 120 hours. 59

Figure 4.5: Corrosion test result of specimens of control and in situ samples according to dipping times in 5 wt% NaCl aqueous solution. Polymer coating solution is composed of control a, matrix (epoxy vinyl ester) and adhesion promoter (methylacryloxy propyl triethoxy silane, 3 wt%); control b, matrix, adhesion promoter, and microencapsulated tin catalyst (dimethyldineodecanoate tin, 3 wt% of total microcapsules); control c, matrix, adhesion promoter, and phase separated PDMS healing agent (12 wt%, mixture of HOPDMS and PDES); *In situ*, matrix, adhesion promoter, microencapsulate catalyst, and PDMS healing agent (self-healing). The size of corrosion test samples is 75×150 mm^2 (width ×length). Samples were healed at 50 °C. 60

Figure 4.6: Electrochemical corrosion test set-up. The current is measured both over the scratched region and away from the scratch (red circle to right). 62

Figure 4.7: Electrochemical test result of polymer coated metal substrate in pure water. (a) Scratched part of control sample and (b) scratched part of self-healing sample. 63

Figure 4.8: Electrochemical test result of polymer coated metal substrate in 1 M sodium chloride aqueous solution. (a) Unscratched part of specimens and (b) Scratched part of control (black) and self-healed sample (red). 64

Figure 4.9: SEM acquired from metal substrate, control, and self-healing coatings. SEM of a scratch in (a) metal substrate, (b) control, and (c) self-healing coating after allowing for healing. 65

Figure 4.10: Cross sectional view of the self-healing coatings on a metal substrate by optical microscopy. (a) Undamaged part and (b) damaged part of the self-healing coated sample. 66

Figure 4.11: Cross sectional view of the self-healing coatings on a metal substrate by scanning electron microscopy. (a) Secondary electron image of sample 1 (image was taken from the scratched region) and (b) back scattered image of sample 2. 67

Figure 4.12: Cross sectional view of the self-healing coatings on a metal substrate (sample in figure 4.11b) by elemental mapping of scanning electron microscopy for (a) carbon, (b) oxygen, (c) silicone, and (d) iron. 68

Figure 4.13: Procedures of sample preparation for cross sectional view of the self-healing coatings on a metal substrate by scanning electron microscopy with electroless nickel coating. 69

Figure 4.14: Cross sectional view of the self-healing coatings on a metal substrate by scanning electron microscopy with electroless nickel coating at the interface between epoxy molding and self-healing coated sample. (a) Lower magnification and (b) higher magnification..... 70

Figure 4.15: Cross sectional view of the self-healing coatings on a metal substrate with electroless nickel coating at the interface between epoxy molding and self-healing coated sample by elemental mapping of scanning electron microscopy for (a) carbon, (b) silicone, (c) iron, and (d) nickel. 71

Figure 4.16: Procedures of sample preparation for cross sectional view of the self-healing coatings on a metal substrate by scanning electron microscopy without epoxy molding. 72

Figure 4.17: Cross sectional view of the self-healing coatings on a metal substrate by scanning electron microscopy without epoxy molding. (a) Lower magnification and (b) higher magnification. 73

Figure 4.18: Cross sectional view of the self-healing coatings on a metal substrate treated at 170 °C for 24 hours by scanning electron microscopy. (a) Sample 1 and (b) sample 2. 74

Figure 4.19: Cross sectional view of the self-healing coatings on a metal substrate treated at 170 °C for 24 hours by scanning electron microscopy. Samples are tilted for observing the bottom surface of damages after healing reaction. Tilted images of sample 1 by (a) 30° and (b) 60°. 74

Figure 4.20: Surface profile of undamaged parts of test sample by surface profilometry. (a) metal substrate and (b) polymer coating layer. 75

Figure 4.21: Surface profile of collected from control (no self-healing) and self-healing coatings after damage and sufficient time to allow healing reactions to take place. Red dots indicate the surface morphology beyond the thickness limitation by instrument. 76

Figure 5.1: Optical microscopic images of PDMS containing microcapsules. 83

Figure 5.2: Maximum load changes of healed TDCB specimens according to the amount of PDMS and catalyst containing microcapsules. The samples were healed at 50 °C. 84

Figure 5.3: Maximum load values of manually healed TDCB specimens by injecting PDMS healing agent according to adhesion promoter change. 85

Figure 5.4: Monotonic fracture test results of two microcapsule self-healing polymer (TDCB geometry) for virgin and fractured samples healed at 50 °C. The self-healing composite is composed of epoxy with amine curing agent, 3 wt% of adhesion promoter ((3-trimethoxysilylpropyl)dimethylene triamine), 14 wt% of PDMS (S32, viscosity 1,600 cP) containing microcapsules, and 3 wt% of tin catalyst (dimethyldineodacanoate tin) containing microcapsules....86

Figure 5.5: Monotonic fracture test results of two microcapsule self-healing polymer (TDCB geometry) for virgin and fractured samples healed at a) 30 °C and b) 50 °C. The self-healing composite is composed of epoxy with amine curing agent, 3 wt% of adhesion promoter [(3-trimethoxysilylpropyl) dimethylene triamine], 14 wt% of PDMS (S32, viscosity 1,600 cP) containing microcapsules, and 3 wt% of tin catalyst (dimethyldineodacanoate tin) containing microcapsules. 87

Figure 5.6: Reaction scheme for the polycondensation of hydroxyl end functionalized PDMS with an alkyl ester tin catalyst in the presence of moisture (adapted from [4]). 89

Figure 5.7: Experimental set-up for synthesis of the TKAS catalyst. 89

Figure 5.8: Optical microscopic image of newly synthesized catalyst containing microcapsules. 90

Figure 5.9: Results from monotonic fracture tests with TDCB geometry for virgin samples and fractured samples healed at a) room temperature and b) 30 °C using the TKAS catalyst. The self-healing composite is composed of epoxy with amine curing agent, 3 wt% of adhesion promoter [(3-trimethoxysilylpropyl) dimethylene triamine], 14 wt% of PDMS (S32, viscosity 1,600 cP) containing microcapsules, and 3 wt% of TKAS catalyst containing microcapsules..... 91

Figure 5.10 Results from monotonic fracture tests (TDCB geometry) for virgin samples and fractured samples healed at 50 °C for (a) two microcapsule containing system and (b) one microcapsule containing system. The amount of TKAS catalyst containing microcapsules added in the sample was 3 wt%. 92

Figure 5.11: Corrosion test result of specimens of control and in situ samples healed at 50 °C after 120 hours in 5 wt% NaCl aqueous solution. Coating solution is composed of (a) matrix with 3 wt% of adhesion promoter; (b) matrix, 3 wt% of adhesion promoter, and 3 wt% of catalyst containing microcapsules; (C) matrix, 3 wt% of adhesion promoter, and 14 wt% of PDMS containing microcapsules; (d) matrix, 3 wt% of adhesion promoter, 3 wt% of catalyst containing microcapsules, and 14 wt% of PDMS containing microcapsules (*in situ* sample)..... 93

Figure 5.12: Corrosion test result of specimens healed at 50 °C after 120 hours in 5 wt% NaCl aqueous solution. The first set of (a) control and (b) *in situ* samples was healed in pure water, and the second set of (c) control and (d) *in situ* samples was healed in salt water (5 wt% NaCl aqueous solution). 95

Figure 5.13: Corrosion test result of specimens healed at 50 °C after 72 hours in 5 wt% NaCl aqueous solution. (a) Control and (b) *in situ* sample healed in water bath having pH 2; (c) Control and (d) in situ sample healed in water bath having pH 4; (e) Control and (f) in situ sample healed in water bath having pH 10; (g) Control and (h) in situ sample healed in water bath having pH 12. 96

Figure 5.14: Corrosion test result of specimens of control and in situ samples healed at 30 °C after 120 hours in 5 wt% NaCl aqueous solution. Coating solution is composed of (a) matrix with 3 wt% of adhesion promoter; (b) matrix, 3 wt% of adhesion promoter, and 3 wt% of catalyst containing microcapsules; (C) matrix, 3 wt% of adhesion promoter, and 14 wt% of PDMS containing microcapsules; (d) matrix, 3 wt% of adhesion promoter, 3 wt% of catalyst containing microcapsules, and 14 wt% of PDMS containing microcapsules (*in situ* sample).....98

Figure 5.15: Reaction scheme for forming adhesion bonds by reaction of γ-glycidoxy propyl trimethoxysilane with epoxy on a metal surface [adapted from reference 4].....99

Figure 5.16: Corrosion test result of specimens of control and *in situ* samples healed at 30 °C after 120 hours in 5 wt% NaCl aqueous solution. Coating solution is composed of (a) matrix with 3 wt% of adhesion promoter; (b) matrix, 3 wt% of adhesion promoter, and 3 wt% of catalyst containing microcapsules; (C) matrix, 3 wt% of adhesion promoter, and 14 wt% of PDMS containing microcapsules; (d) matrix, 3 wt% of adhesion promoter, 3 wt% of catalyst containing microcapsules, and 14 wt% of PDMS containing microcapsules (*in situ* sample). Metal substrates were treated by sand blasting to induce mechanical adhesion. 100

Figure 5.17: Corrosion test result of specimens of (a) control and *in situ* samples healed at (b) room temperature, (c) 30 °C, and (d) 50 °C after 120 hours in 5 wt% NaCl aqueous solution. The self-healing coating solution is composed of epoxy with diethylenetriamine (DETA), 3 wt% of adhesion promoter, 14 wt% of PDMS containing microcapsules, and 3 wt% of tin catalyst (synthesized, $Si[OSn(n\text{-}C_4H_9)_2OOCCH_3]_4$) containing microcapsules. Metal substrates were coated by primer bottom layer to induce adhesion strength prior to the self-healing coating. 101

Figure 5.18: Corrosion test result of specimens of (a) control and *in situ* samples with (b) one layered self-healing coating and (c) dual layered self-healing coating healed at 50 °C after 120 hours in 5 wt% NaCl aqueous solution. The control sample is coated by Intergard 264. The self-healing coating solution is composed of Intergard 264, 14 wt% of PDMS containing microcapsules, and 3 wt% of tin catalyst (DMDN-Sn) containing microcapsules. 102

CHAPTER 1

INTRODUCTION

1.1 Self-healing Function

The modern world uses a large variety and amount of synthetic polymers in industry and daily life. The current society can be called "a polymer age" due to the use of many synthetic polymer materials. However, there is a significant difference between natural biomaterials and artificial polymers. Natural biomaterials such as our human body can automatically heal damage or injury, while conventional synthetic polymers do not have this self-healing property.

Various polymers with high functionality and advanced properties are being developed to replace traditional materials. These polymers sometimes are used in severe environments, such as the deep ocean or space, which are difficult to access. In addition, some polymers are used inside the human body, such as artificial organs and bone cement. The detection of damage and repair to these advanced materials is difficult even though their failure results in considerable expense and loss of effort and time. Thus, the importance of a healing effect in synthetic polymers is much more necessary for advanced applications.

Synthetic polymers with a self-healing effect can deliver a number of merits and resolve many unsolvable problems in common polymers. We can find one example of these problems in anti-corrosion coatings. In terms of the economical aspect, the annual cost of corrosion in the U.S. is approximately $276 billion per year, which corresponds to 3.1 percent of the U.S. gross domestic product (GDP) [1]. Thus, metal substrates need to be coated by a polymer layer, but this layer cannot protect the substrate once it sustains scratch or chip damage. Once there is sufficient damage, the coating layer must be reapplied. This thesis is motivated by these current needs to develop advanced synthetic polymers with a self-healing function.

1.2 Previous Self-healing Work

Since there has been so much demand for autonomic healing in artificial materials, there have been a number of previous attempts to add self-healing functionality to polymers glasses and concrete [2-4]. It has been known for some time that when a thermoplastic polymer such as poly(methyl methacrylate) (PMMA) is damaged, it can be repaired by heat or solvent treatments that causes diffusion of the thermoplastic polymer across the crack plane. Basically, the solvent or heat brings the sample above its glass transition temperature and the polymer chains can diffuse and entangle [5-7]. However, these kinds of treatments that require external intervention such as heat, pressure, ultra violet radiation, or solvent are not descriptive of a self-healing system. Moreover, it is necessary to know there is damage in the sample in the first place prior to external treatment of the damaged region.

A more advanced system, using a thermally re-mendable cross-linked polymeric material, for a thermoset polymer was recently reported by Chen and Wudl [8, 9]. This material can undergo repeated healing by reversible Diels-Alder reaction with multi-dienes and multi-dineophiles. The report proved that about 30% of the covalent bonds can be reversibly disconnected and reconnected by temperature change, so that it can heal the fracture of samples multiple times without a catalyst, additional monomer, or special surface treatment (figure 1.1). However, this system requires a specially synthesized monomer, and in addition, a high temperature treatment of above 120 °C. Since external intervention is required, this is not truly autonomic healing.

(a) 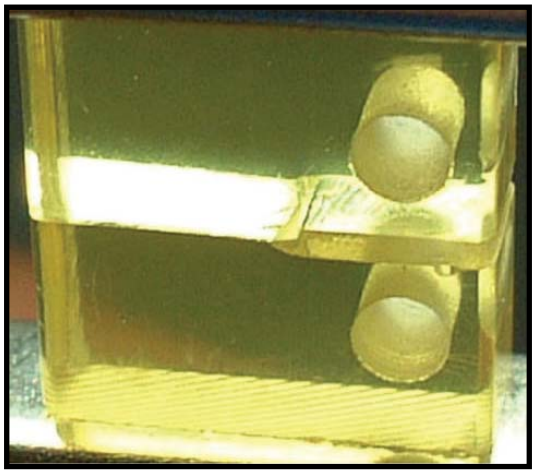 (b) 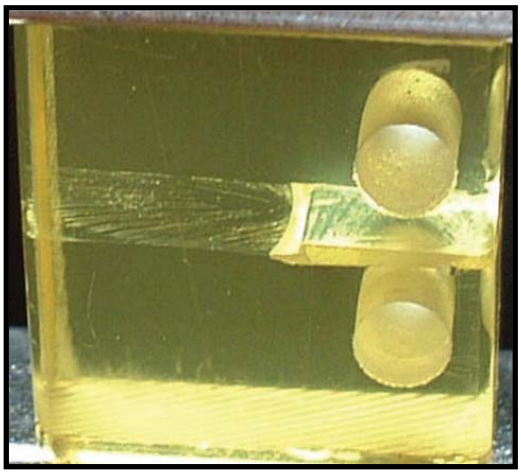

Figure 1.1 A thermally re-mendable crosslinked polymeric material healed by reversible Diels-Alder reaction; (a) Image of a broken specimen before thermal treatment and (b) Image of the specimen after thermal treatment. Figure adapted from ref. [8].

One example of true self-healing materials is a system composed of an encapsulated healing agent in a matrix polymer. In this system, the healing reaction is only triggered when the encapsulated healing agent is released by a mechanical damage event. The first study of this kind used macroscale glass tubes which contained cyanoacrylate or two-part epoxy resin in an epoxy matrix [10]. It was proved that encapsulated healing agents have the possibility for self-healing in the cracked damage by polymerization of the released healing agent from the glass capillary. However, making glass tubes containing monomers and distributing them inside a matrix is a difficult and time-consuming process, which make this material too difficult to be practical. Self-healing with an encapsulated healing agent starts to gain importance when a microencapsulated monomer, which can be dispersed through the matrix, is used. Using microcapsules enables self-healing polymer mass production, even distribution, and effective healing in the case of relatively small cracks inside a matrix. Early self-healing research using a

microencapsulated monomer involved epoxy pre-polymer and free-radical polymerization of a styrene-based monomer initiated by Co(II) naphthenate and methyl ethyl ketone peroxide (MEKP) in a polyester matrix [11-12], but those were not very successful. The problem was insufficient microcapsule rupture by crack invasion and incomplete polymerization of the monomer by the initiator [13].

A breakthrough in self-healing research was developed by White et al., which induced living ring opening metathesis polymerization (ROMP) of dicyclopentadiene (DCPD) in the presence of ruthenium (Ru) based Grubbs' catalyst [14]. The healing agent, DCPD, is microencapsulated by in situ polymerization of urea-formaldehyde, which forms a shell outside of the DCPD liquid droplet. The size of microcapsules is determined by mechanical stirring speeds, typically 10-1000 μm in the range of 200-2000 rpm [15]. These microcapsules effectively deliver the healing agent to the cracked plane, induce polymerization by contact with the catalyst, and finally seal the damage. The healing efficiency of this system, calculated by the relative ratio of healed toughness to virgin toughness, was reported as 75% [14]. However, this self-healing polymer needs relatively large (2.5 wt%) amount of embedded Grubbs' catalyst, which is quite expensive ($45/g). A small amount of unprotected Grubbs' catalyst could not accomplish a successful healing reaction because of poor dispersion of the catalyst in the matrix, which causes exposure of only a few large particles on the crack plane [16]. Moreover, Grubbs' catalyst is susceptible to deactivation by contact with the amine curing agent used for epoxy matrix polymerization [16].

Rule et al. used Grubbs' catalyst encapsulated microspheres with paraffin wax to protect the catalyst from the amine curing agent [16-17]. Catalyst containing microspheres are synthesized by mixing molten wax and Grubbs's catalyst in hot water with ethylene-maleic

anhydride copolymer as a surfactant under mechanical stirring, followed by quenching in ice water [17-18]. When a crack propagates into a matrix, the healing agent released from the microcapsules dissolves the wax and induces the healing reaction [17-18]. Wax-protected catalyst microspheres can also improve the dispersion property of the catalyst in the matrix, and consequently induce the uniform exposure of the catalyst to the cracked plane [16, 18]. The healing efficiency calculated by the ratio of internal work between the healed sample and the virgin sample is reported as a maximum 93% [16]. Although less catalyst is required by wax protected catalyst microspheres, this system still uses Grubbs' catalyst, which has some limitations.

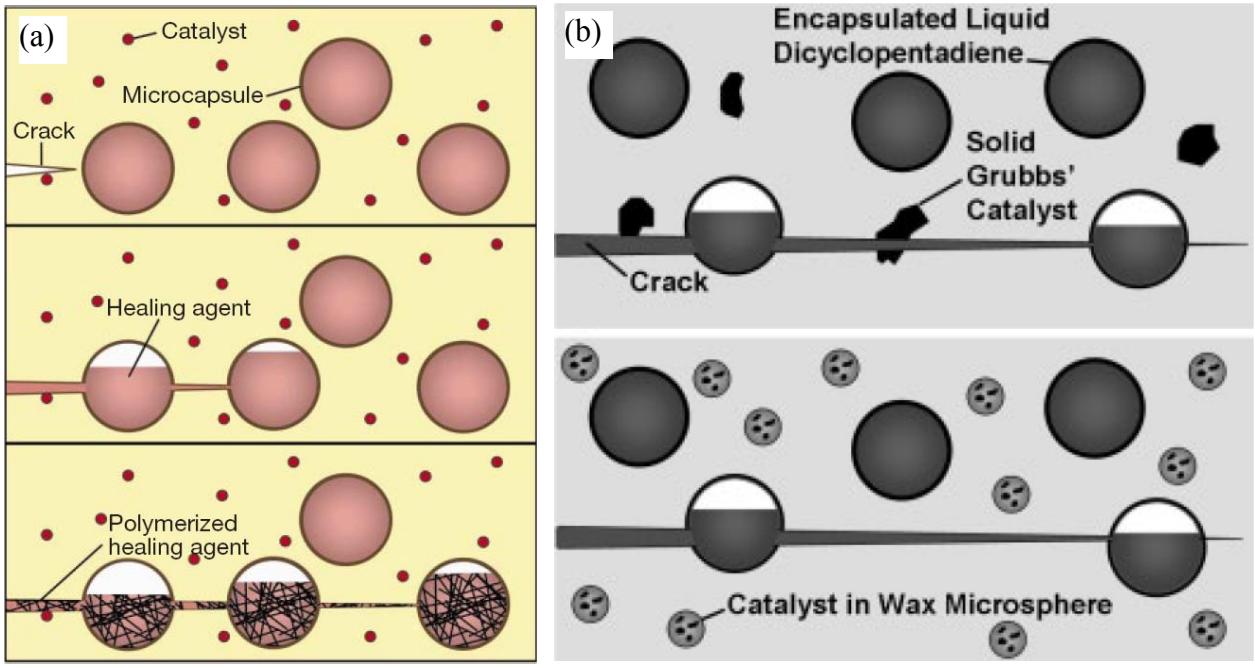

Figure 1.2 Self-healing system using a microencapsulated healing agent; (a) Autonomic healing concept with microencapsulated DCPD and Grubbs's catalyst (adapted from [14]) and (b) self-healing material with wax-protected Grubbs' catalyst microspheres (adapted from [16]).

1.3 Polydimethylsiloxane (PDMS) Chemistry

Sriram and Rule described the required properties of a healing agent for self-healing material [13, 18]. Basically, unique characteristics for self-healing materials are: a long period of activity and stability, good deliverability, high reactivity, minimal shrinkage, and no negative effect on physical properties of materials either before or after healing [13, 18]. Moreover, Rule also pointed out limitations of self-healing chemistry using DCPD and Grubbs' catalyst. Those drawbacks are: a slow rate of healing, a narrow operating temperature range, the high cost of Grubbs' catalyst, the severely limited availability of Grubbs' catalyst, and a large extent of pre-healing damage [18]. Some of these limitations are improved by microencapsulated Grubbs' catalyst with paraffin wax [16]. However, to devise a more practical material, it is necessary to access a chemistry which is more environmentally stable and economically viable. For this purpose, PDMS is chosen as a healing agent in our study and we made much progress in previously mentioned limitations. Although PDMS is not a hard polymer with strong mechanical properties, it has a number of useful unique properties, especially for self-healing coatings.

1.3.1 Silicone Chemistry

A chemical grade of elemental silicon for methylchlorosilanes synthesis can be achieved by carbo-electro reduction process at high voltage and temperature (>1200 °C) from silica (figure 1.3-a) [21, 22]. Silicone became commercially important with Roscow's discovery of the synthesis of methylchlorosilanes from the reaction of elemental silicone with methylchloride, according to figure 1.3-b [19-20, 22]. The products are separated by distillation and isolation after reaction. Polysiloxane is obtained from hydrolysis and condensation of methylchlorosilane,

which produces linear and cyclic polysiloxanes (figure 1.3-c). PDMS is finally synthesized by either acid or base catalyzed ring opening polymerization of octamethylcyclotetrasiloxane with hexamethyldisiloxane (figure 1.3-d) [22]. In addition the physical properties of PDMS can be greatly improved by addition of reinforcing fillers such as silica, effectively fumed silica with high surface area [22].

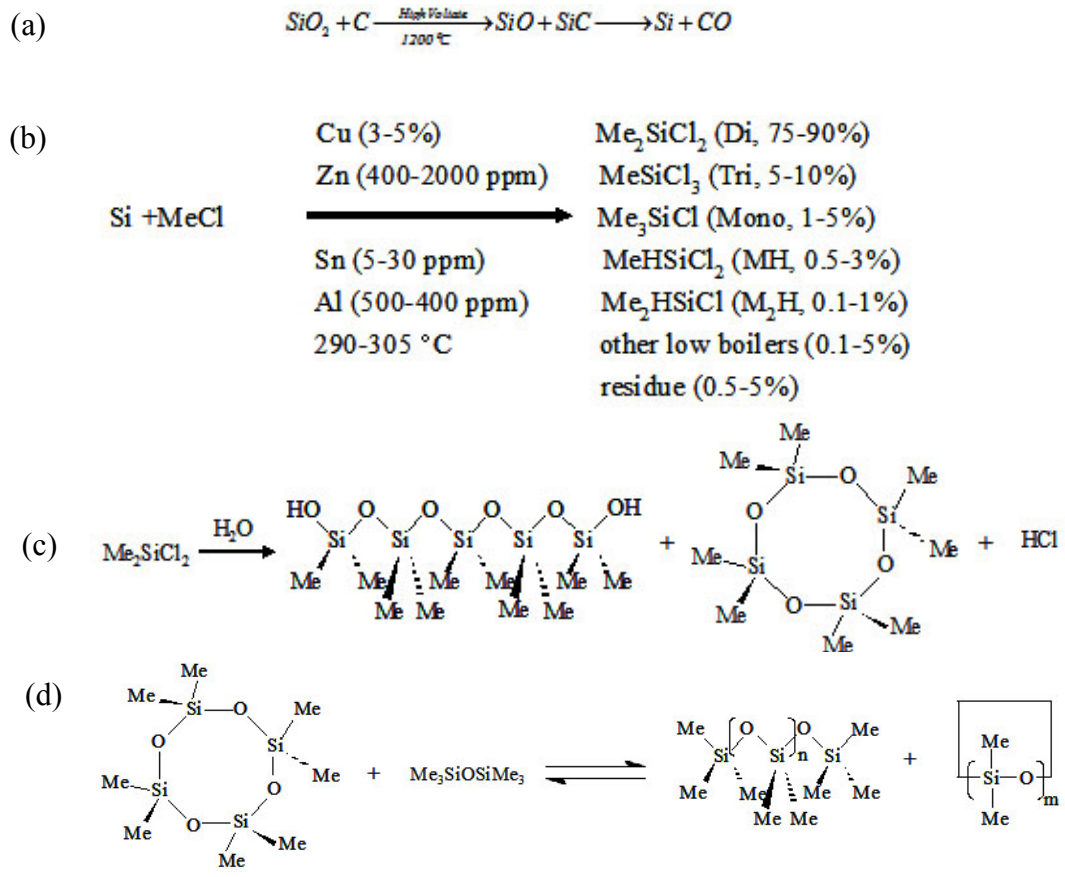

Figure 1.3 Reaction schemes for synthesis of PDMS; (a) silicone synthesis from silica, (b) methylchlorosilanes synthesis from the reaction of elemental silicone with methylchloride, (c) synthesis of polysiloxane from hydrolysis and condensation of methylchlorosilane, and (d) synthesis of PDMS by acid or base catalyzed ring opening polymerization of octamethylcyclotetrasiloxane (adapted from [22]).

1.3.2 Platinum Catalyzed Hydrosilylation

Many commercially available silicone products are based on hydrosilylation reaction chemistry. The hydrosilylation forms silicon carbon bonds by the reaction of vinyl functionalized PDMS with multi-Si-H-containing PDMS in the presence of a platinum catalyst, typically Karstedt's catalyst, and an inhibitor to control the reaction rate. The final product is a highly crosslinked polymer network (figure 1.4) [22]. The reaction is mainly affected by: the molecular weight of the vinyl functionalized polymer, the amount of Si-H functional groups, the ratio of vinyl to Si-H functional groups, and the amount of platinum catalyst and inhibitor [22]. The reaction can be hindered by contact with certain chemicals, curing agents, and plasticizers. Those are organotin compounds, silicone rubber containing organotin catalysts, sulphur, polysulphides, polysulphones, other sulphur containing materials, amines, urethanes, amides and azides [23]. In my thesis, platinum catalyzed hydrosilylation was first considered as a healing chemistry because of its possible polymerization reaction at room temperature. Furthermore, it was a commonly available commercial product and had useful properties of polymerized PDMS. However, it is inappropriate due to the previously mentioned restrictions.

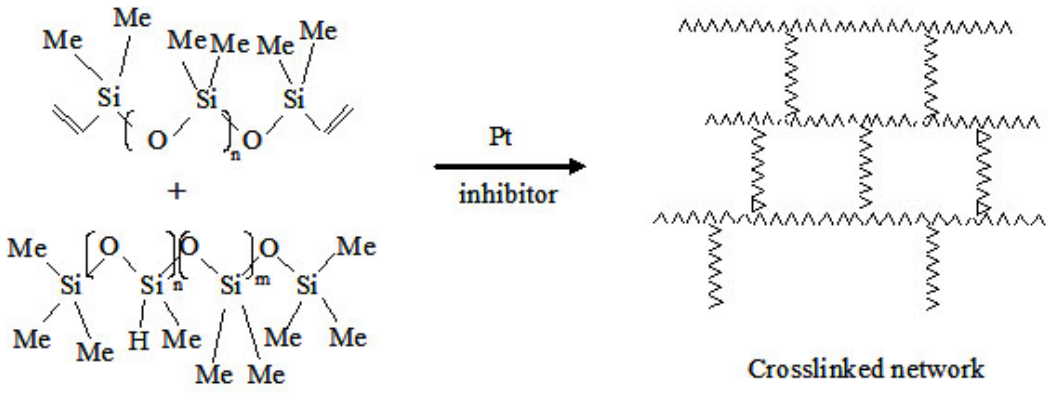

Figure 1.4 Reaction scheme for Pt catalyzed hydrosilylation of PDMS (adapted from [22]).

1.3.3 Tin Catalyzed Polycondensation

The primary reaction for self-healing curing chemistry in my thesis is the tin catalyzed polycondensation of hydroxyl end functionalized PDMS (HOPDMS) with alkoxysilane. This PDMS polycondensation can occur to produce a crosslinked PDMS polymer network at room temperature with certain catalysts (figure 1.5). Those catalysts are amine and carboxylic acid salt of Pb, Zn, Zr, Sb, Fe, Cd, Sn, Ba, Ca, and Mn [24-25]. Among these catalysts, organotin compounds were finally chosen in my study because this catalyst causes a minimal number of side reactions [25]. Although organotin has been used as a catalyst for polycondensation of PDMS for many years, the reaction mechanism and its function is not precisely defined. The main reasons the function is hard to define are that there are a relatively small number of hydroxyl groups on HOPDMS and the final product is a crosslinked gel, both of which make monitoring of the reaction by chemical or spectroscopic methods difficult [25].

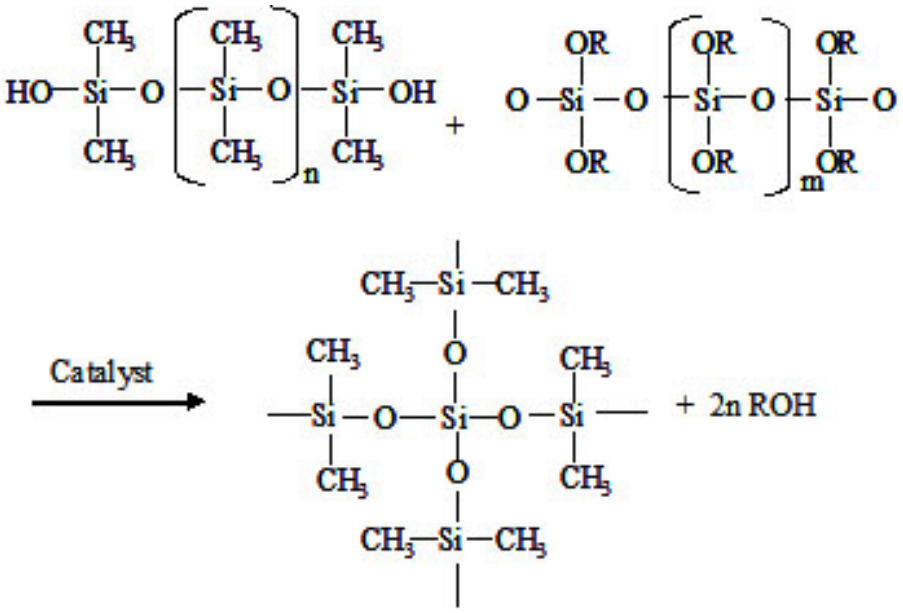

Figure 1.5 Reaction scheme for tin catalyzed polycondensation of PDMS [24].

Most of commercially available products for polycondensation reactions use an organotin catalyst, generally dialkyltin dicarboxylates or tin dicarboxylates [26]. Although the reaction mechanism is not clearly understood yet, some reports suggest that the reaction rate mostly depends on steric and electronic effects [25-26]. Shah reported that the length of the carboxylic groups bonded to the tin atom is an important factor for the catalytic activity of organotin catalysts [25]. That also means a longer length of ester and alkyl groups bonded to tin atoms causes a decrease of catalytic activity, but the catalytic activity decrease has saturation above 32 total carbon atoms [25]. The polycondensation of HOPDMS with PDES in the presence of an organotin catalyst occurs at room temperature, and is not hindered by contact with oxygen, moisture, and peroxide initiator. It was this stability that leads us to we adopt this reaction as the basis of our self-healing chemistry.

1.4 References

1. G. H. Koch, M. P. Brongers, N. G. Thompson, Y. P. Virmani, J. H. Payer, FHWA funds Cost of Corrosion Study. Report FHWA-RD-01-156, September 2001.

2. S. S. Sukhotskaya, V. P. Mazhorava, N. T. Yu, *Hydrotechnical Construction* **1983**, *17*, 295-296.

3. C. Edvardsen, *ACI Materials Journal* **1999**, *96*, 448-454.

4. B. Stavrinidis, D. G. Holloway, *Physics and Chemistry of Glasses* **1983**, *24*, 19-25.

5. K. Jud, H. H. Kausch, *Polymer Bulletin* **1979**, *1*, 697-707.

6. C. B. Lin, S. Lee, K. S. Liu, *Polym. Eng. Sci.* **1990**, *30*, 1399-1406.

7. H. C. Hsieh, T. J. Yang, S. Lee, *Polymer* **2001**, *42*, 1227-1241.

8. X. X. Chen, M. A. Dam, K. Ono, A. Mal, H. B. Shen, S. R. Nutt, K. Sheran, F. Wudl, *Science* **2002**, *295*, 1698-1702.

9. X. X. Chen, F. Wudl, A. K. Mal, H. B. Shen, S. R. Nutt, *Macromolecules* **2003**, *36*, 1802-1807

10. C. Dry, *Composite Structures* **1996**, *35*, 263-269.

11. D. Jung, *Performance and Properties of Embedded Microspheres in Self Repairing Applications*; University of Illinois at Urbana-Champaign: Urbana, Illinois, 1997.

12. A. Hegeman, *Self-Repairing Polymers: Repair Mechanisms and Micromechanical Modeling*; University of Illinois at Urbana-Champaign: Urbana, Illinois, 1997.

13. S. R. Sriram, *Development of Self-Healing Polymer Composites and Photoinduced Ring Opening Metathesis Polymerization*; Univeristy of Illinois at Urbana-Champaign, 2001.

14. S. R. White, N. R. Sottos, P. H. Geubelle, J. S. Moore, M. R. Kessler, S. R. Sriram, E. N. Brown, S. Viswanathan, *Nature* **2001**, *409*, 794-797.

15. E. N. Brown, M. R. Kessler, N. R. Sottos, S. R. White, *Journal of Microencapsulation* **2003**, *20*, 719-730.

16. J. D. Rule, E. N. Brown, N. R. Sottos, S. R. White, J. S. Moore, *Adv. Mater.* **2005**, *17*, 205-208.

17. D. F. Taber, K. J. Frankowski, *J. Org. Chem.* **2003**, *68*, 6047.

18. J. D. Rule, *Polymer Chemistry for Improved Self-healing Composite Materials*, University of Illinois at Urban-Champaign, 2005.

19. B. Kanner, K. M. Lewis, *Catalyzed Direct Reactions of Silicones*; K. M. Lewis, D. G. Rethwisch, Eds.; Elsevier Science Publishers B. V.: Amsterdam, **1993**, 1-49.

20. L. N. Lewis, *The Chemistry of Organosilicon Compounds*, Part 3; Z. Rappoport, Ed., John Wiley: Sussex, England, 1998.

21. J. H. Downing, R. H. Kaiser, J. E. Wells, *Catalyzed Direct Reactions of Silicones*; K. M. Lewis, D. G. Rethwisch, Eds.; Elsevier Science Publishers B. V.: Amsterdam, **1993**, 67.

22. L. N. Lewis, *From Sand to Silicones, an Overview of the Chemistry of Silicones*, GE Technical Report (98CRD092), 1998.

23. Dow Corning, Product information: Silicone Elastomer, Ref. no. 10-1024A-01, 1998.

24. G. B. Shah, R. W. Winter, *J. Appl. Poly. Sci.* **1996**, *61*, 1649-1654.

25. G. B. Shah, *J. Appl. Poly. Sci.* **1998**, *70*, 2235-2239.

26. F. W. Van der Weij, *Macromol. Chem.* **1980**, *181*, 2541-2548.

CHAPTER 2

SELF-HEALING POLYMER COMPOSITE

Significant components of this chapter were published as S. H. Cho, H. M. Andersson, S. R. White, N. R. Sottos, P. V. Braun, "Polydimethyl-siloxane Based Self-healing Materials" *Advanced Materials* **2006**, *18*, 997-1000.

2.1 Motivation

Self-healing represents a new paradigm for active and responsive materials inspired by natural biomaterials. Self-healing is expected to extend the lifetime and increase the reliability of materials for many applications. Specifically we are studying self-healing thermosetting polymers, which are used in a wide variety of applications ranging from microelectronics to aerospace. Living organisms are well known to heal their structural damages in contrast to current artificial polymers. To introduce the natural healing concept into synthetic materials, a number of crack-healing approaches have been studied for many years [1-23]. However, most of these systems can not be considered as truly self-healing materials because they require an external initiation event to heal. As first demonstrated by White et al. [24], and subsequently in additional publications [25-30], polymer composites can be engineered to truly chemically self-heal. The previous studies confirmed the healing effect in damaged parts of polymer composites when an internal crack is propagated into matrix material. However, the chemistry of previous system possesses some inherent shortcomings. Most significantly, they are unstable to environmental exposure such as air, amine and peroxide initiator, and economically expensive.

With this in mind, we developed a new environmentally stable self-healing system for extending the capability of self-healing polymers.

2.2 PDMS Based Self-healing Materials

This research aims to develop a new self-healing system by introducing environmentally stable healing chemistry and demonstrate the concept of phase separated healing agents in polymer matrices. Phase separation of the healing agent is an approach that may be applicable to a broad class of new healing chemistries for structural polymers. Although inspired by the previous self-healing methodology [24], in which the monomeric healing agent was encapsulated and the catalyst was dispersed as particulate throughout an epoxy matrix, this new system contains a number of distinct differences. The siloxane-based healing agent mixture is not encapsulated, rather it is phase-separated in the matrix while the catalyst is encapsulated. In this thesis, we created a new, chemically stable self-healing materials system based on the tin-catalyzed polycondensation of phase-separated droplets containing hydroxyl end-functionalized polydimethylsiloxane (HOPDMS) and polydiethoxysiloxane (PDES). The catalyst, di-*n*-butyltin dilaurate (DBTL), is contained within polyurethane microcapsules embedded in a vinyl ester matrix and is released when the capsules are broken by mechanical damage.

To introduce the PDMS curing chemistry into the self-healing system, we investigated the room temperature reactions of PDMS in the presence of catalysts. A well known hydrosilylation reaction [31], platinum catalyzed addition cure, is not appropriate for the self-healing system because many chemicals, curing agents and plasticizers found in common thermosets can inhibit this catalyst curing reaction. Thus, we investigated as our healing chemistry the polycondensation-based curing of PDMS. The polycondensation of HOPDMS

with PDES occurs rapidly at room temperature in the presence of amine and carboxylic acid salt of various metal elements [32]. Because side reactions are limited, organotin catalysts are highly desirable for curing PDMS based systems, even in open air [32-33]. This environmental stability to water and air is of critical importance for practical realization of self-healing, and was a prime motivation for this catalyst system. A schematic chemical reaction is shown in figure 2.1.

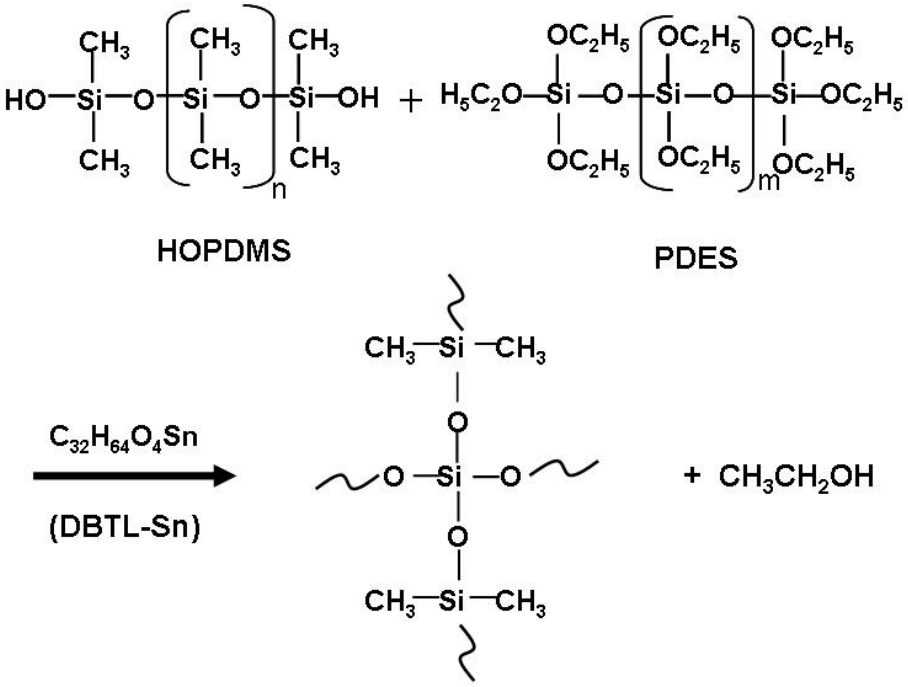

Figure 2.1 Reaction Scheme for the polycondensation of HOPDMS and PDES in the presence of the DBTL-Sn catalyst.

Generally, an amine curing agent such as diethylenetriamine (DETA, Ancanmine®) is used for epoxy polymerization, which is also used in the previous self-healing methodology. In the case of epoxy with an amine curing system, this amine curing agent can also polymerize PDMS liquid droplets during epoxy matrix polymerization. Thus, other matrices such as epoxy vinyl ester (EVE), hydroxyethyl acrylate (HEA), methyl methacrylate (MMA), and

trimethylolpropane trimethacrylate (TMPTA), which are polymerized by a radical initiator, were investigated for the PDMS-based self-healing system. Among these, epoxy vinyl ester (figure 2.2) is considered first as a matrix material in this thesis due to its useful mechanical properties. Furthermore, the epoxy vinyl ester is rapidly cured at room temperature using 1wt% of benzoylperoxide (BPO) and 0.1wt% of dimethylaniline (DMA) as the initiator and activator, respectively.

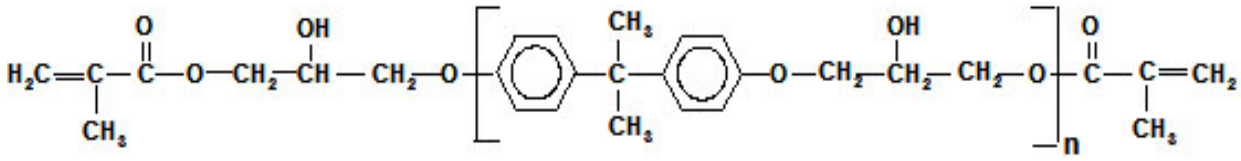

Figure 2.2 Chemical structure of epoxy vinyl ester.

Successful self-healing requires that both the healing agent and the catalyst be closely located within the matrix. However, they must not react until desired, that is, until a crack propagates in the material. Thus, both the healing agent and catalyst can not be freely dispersed in the matrix. The low solubility of siloxane-based polymers enables the HOPDMS–PDES mixture and catalyst containing microcapsules to be directly blended with the vinyl ester prepolymer, forming a distribution of stable phase-separated droplets and protected catalyst. The microcapsules consist of a polyurethane shell surrounding a DBTL-Sn chlorobenzene mixture. No reactions take place between the HOPDMS and PDES prior to exposure to the catalyst. When the matrix cracks, a mixture of catalyst released from microcapsules and the healing agent wets the entire crack plane. Addition of an adhesion promoter to the matrix optimizes wetting and bonding of the crack faces. After the healing agent mixture cures, the crack is self-healed (Figure 2.3 a–d).

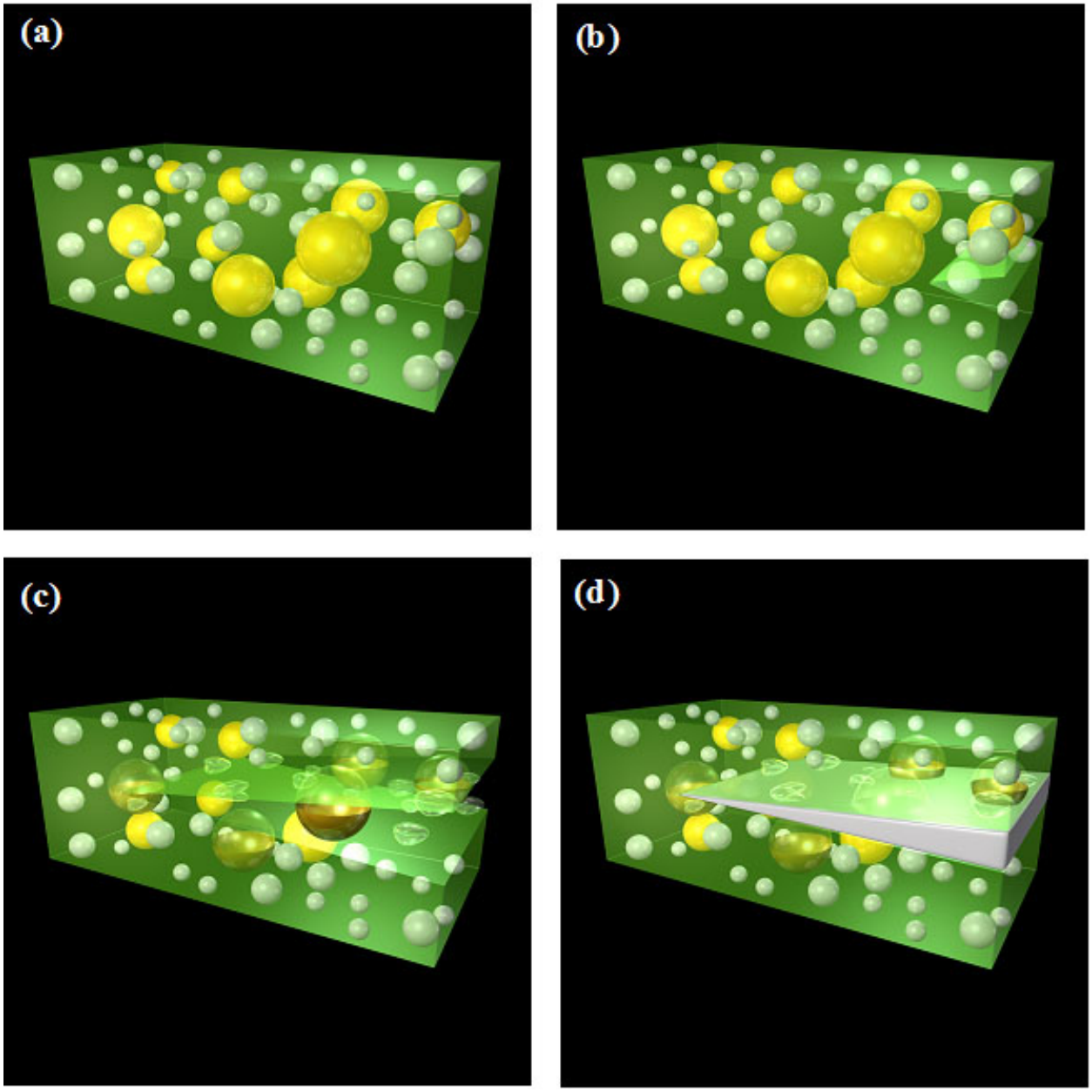

Figure 2.3 Schematic of self-healing process: a) self-healing composite consisting of microencapsulated catalyst (yellow) and phase-separated healing-agent droplets (white) dispersed in a matrix (green); b) composite containing a pre-crack; c) crack propagating into the matrix releasing catalyst and healing agent into the crack plane; d) a crack healed by polymerized PDMS (crack width exaggerated).

2.3 Phase Separation

The approach of this thesis research was inspired by the previous self-healing methodology [24], where the healing agent was encapsulated. However, in my self-healing system the healing agents are simply phase separated in the matrix, which induces smaller and more uniform distribution of the healing agent in the polymer matrix as well as an easy manufacturing process upon simple mixing with the matrix.

2.3.1 Preliminary Study for Phase Separation Behavior

Before the actual phase separation study with PDMS as a healing agent, it was first tried to investigate the phase separation behavior of polybutadiene (PBD) in an epoxy (EPON®828) matrix regarding thermodynamic incompatibility such as molecular weight difference. Commercially available PBDs (Sigma-Aldrich) whose molecular weights ($\overline{M}_n$) are 1,000 and 1,800 were used. Basically, PBD is chemically immiscible with epoxy due to the large difference of hydrophobicity, and the very small entropy of mixing of polymers, so it exists as liquid droplets inside the matrix upon mixing with epoxy.

The morphology of phase separated PBD droplets is first observed by a conventional laser scanning confocal microscope (Leica, DMIRBE microscope and SP-2 scan-head). Confocal micrographs showed that PBD is successfully phase separated from the matrix in the spherical domain even with small amount of addition (10 wt%) to the matrix (figure 2.4), even before crosslinking of the matrix. After matrix polymerization at room temperature, the phase separated PBD domains were very obvious because of the increase in thermodynamic incompatibility. Phase separation behavior of PBD is not significantly affected by molecular weight as long as it has sufficient molecular weight for thermodynamic incompatibility.

Confocal micrographs were obtained both in xyz mode for surface observation and in xzy mode for cross section.

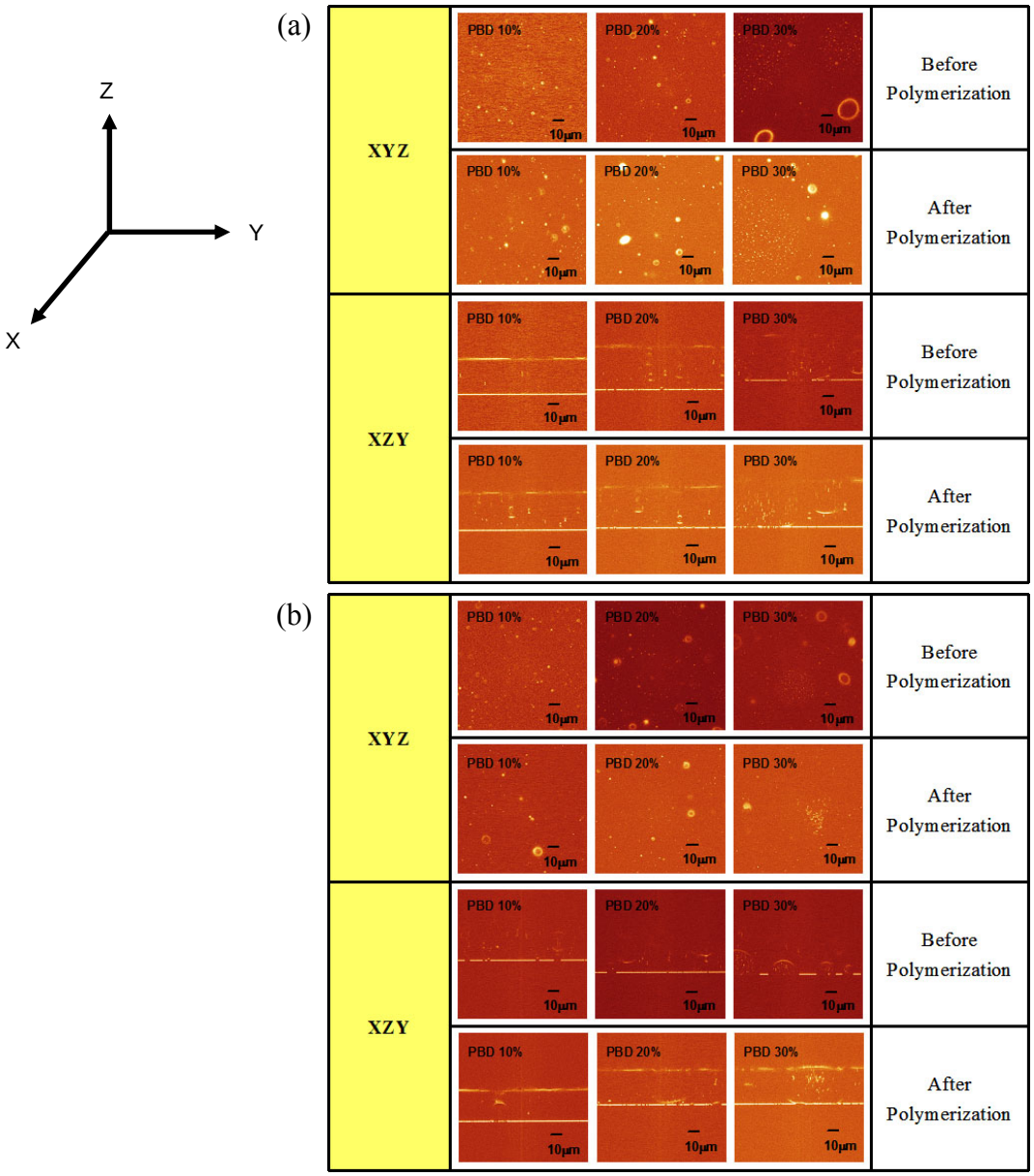

Figure 2.4 Confocal micrographs of phase separated PBD droplets with molecular weight (a) $\overline{M}_n$ =1,000 and (b) $\overline{M}_n$ =1,800 from epoxy before and after matrix polymerization. The images are obtained in scanning modes for surface observation (XYZ direction) and cross sectional observation (XZY direction).

To obtain clearer images for the phase separation behavior, a fluorescent dye, Rodamine 6G, was added into the epoxy matrix, which has very little solubility in PBD. The phase separated morphology of PBD droplets was evident as black dots in fluorescence confocal micrographs (figure 2.5). The number of phase-separated PBD droplets was increased as the amount of added PBD increased. The size of phase separated droplets is not related with the molecular weight of PBD but that was increase as the amount of added PBD increased (table 2.1).

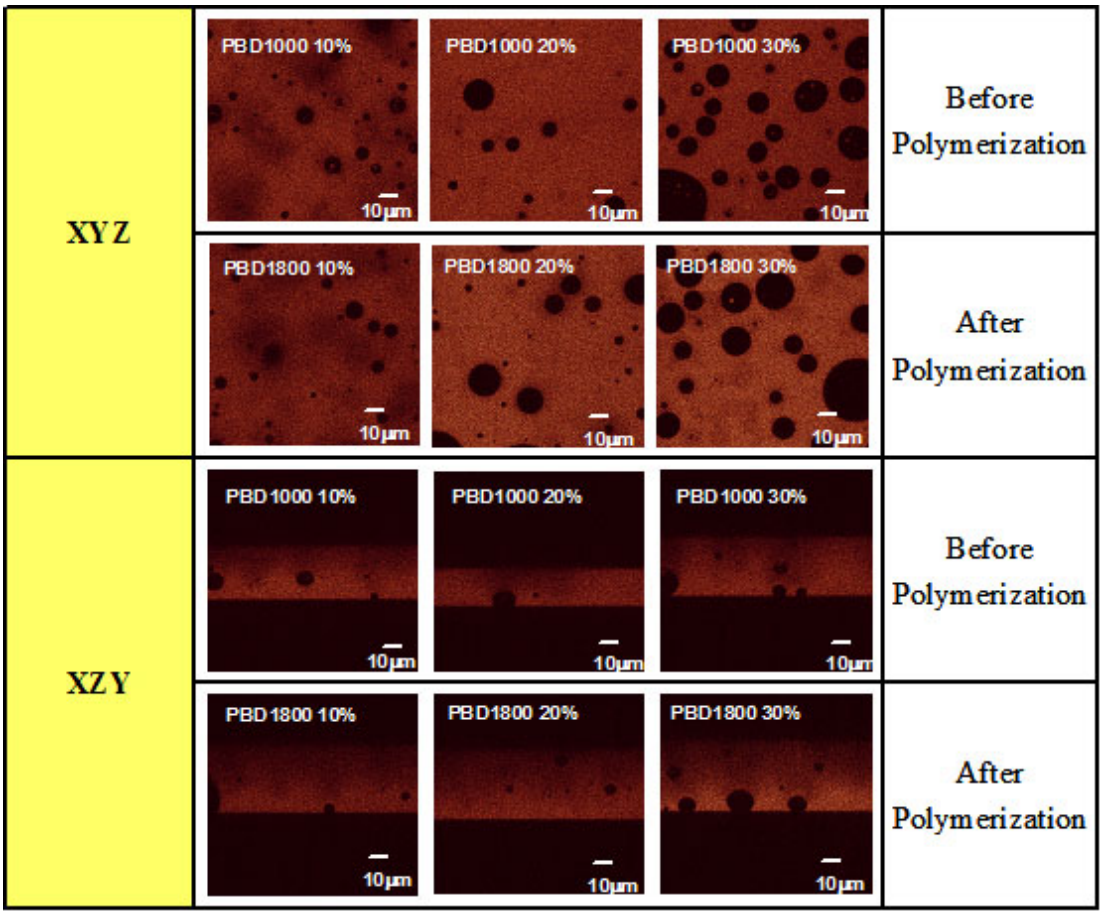

Figure 2.5 Fluorescence confocal micrographs of phase separated PBD ($\overline{M}_n$ =1,000 & 1,800) droplets from epoxy including fluorescent dye (Rodamine 6G) before and after matrix polymerization. The images are obtained in scanning modes for surface observation (XYZ direction) and cross sectional observation (XZY direction).

Table 2.1. The size values of phase separated PBD droplets.

Amount of PBD (wt%)	Size of droplets (μm) Average [±1 standard deviation]	
	PBD ($\overline{M}_n$ =1,000)	PBD ($\overline{M}_n$ =1,800)
10	5.5 [±3.1]	5.6 [±3.1]
20	7.9 [±3.9]	7.9 [±5.5]
30	10.7 [±3.7]	13.8 [±6.3]

The phase separated morphology was also investigated with scanning electron microscopy (SEM). Polymerized epoxy containing PBD droplets was fractured to observe the bulk morphology, followed by dipping in tetrahydrofuran (THF) to extract PBD liquid droplets, so that an obvious distinction between the phase separated domain and the matrix could be made (figure 2.6).

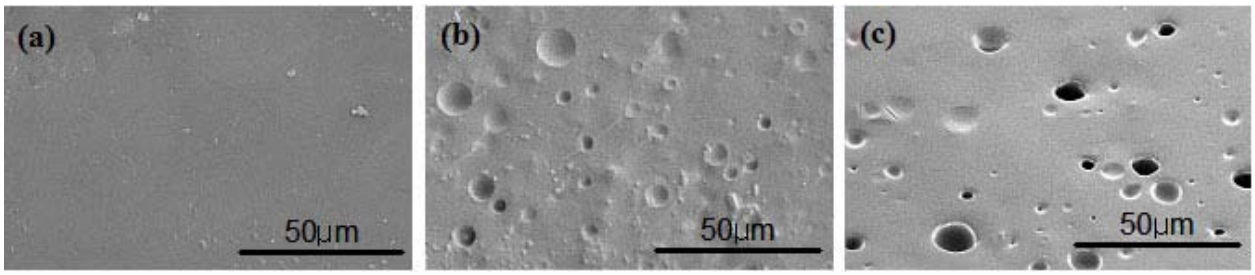

Figure 2.6 Scanning electron micrographs of fracture plane in (a) epoxy matrix and epoxy with 10 wt% of PBD (b) before and (c) after extraction by THF.

Phase-separated PBD domains were shown as spherical holes on the matrix surface, which represents liquid droplets existing after matrix polymerization (figure 2.7). SEM images proved successful phase separation with 10 wt% of PBD added to the epoxy, and consequently in consecutively observed phase separated domains according to the amount of PBD addition.

The previous self-healing system adopted dicyclopentadiene (DCPD) as a healing agent, which is encapsulated by a urea-formaldehyde shell [24]. Thus, the possibility for inducing

DCPD in the matrix by phase separation without any capsule formation is also investigated in this study. The fracture plane of polymerized epoxy with DCPD was observed by SEM according to the amount of DCPD after THF etching. Phase-separated droplets were only observed at 30 wt% of DCPD content, while there was not obvious phase separated morphology with 10 and 20 wt% additions (figure 2.8). In the result, more than a 30 wt% addition is required to induce DCPD in the form of phase separated liquid droplets in an epoxy matrix, which is a large amount. To increase incompatibility, I also investigated the phase separated morphology of DCPD oligomer which has 3 repeating units of the monomer, but it showed almost the same behavior as the monomer case according to the amount of DCPD. From this observation, DCPD seems not to be as promising a material for inducing the healing agent as phase separated liquid droplets without encapsulation.

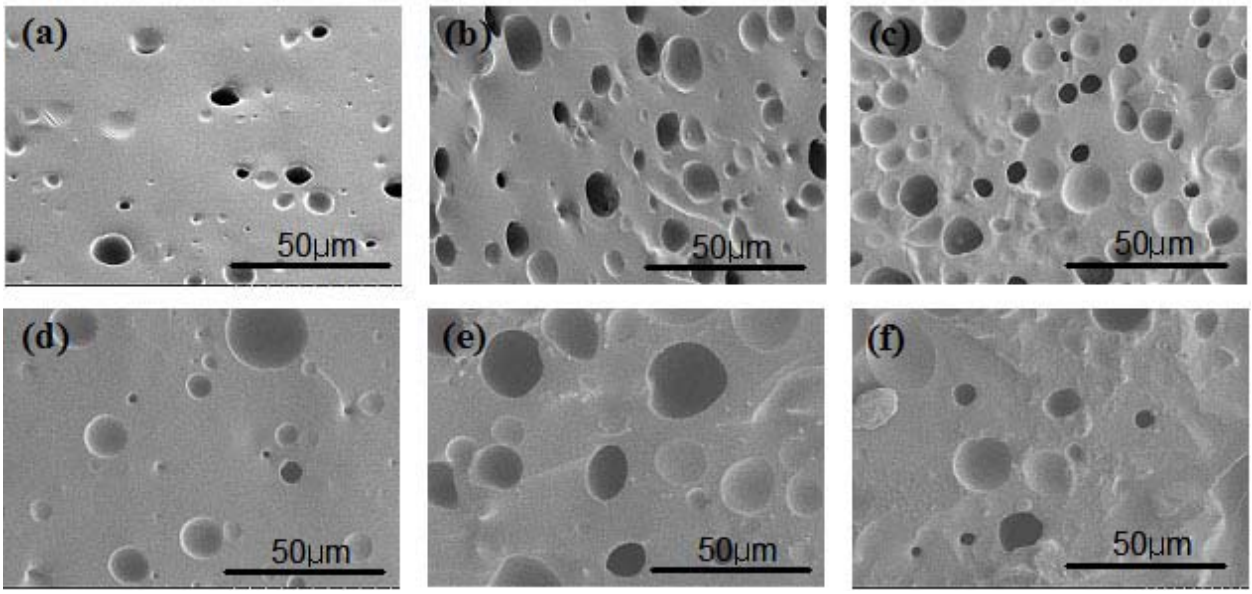

Figure 2.7 Scanning electron micrographs of fracture plane in epoxy with (a) 10 wt%, (b) 20 wt%, and (c) 30 wt% of PBD ($\overline{M}_n$ =1,000); (d) 10 wt%, (e) 20 wt%, (f) 30 wt% of PBD ($\overline{M}_n$ =1,800) after extraction by THF.

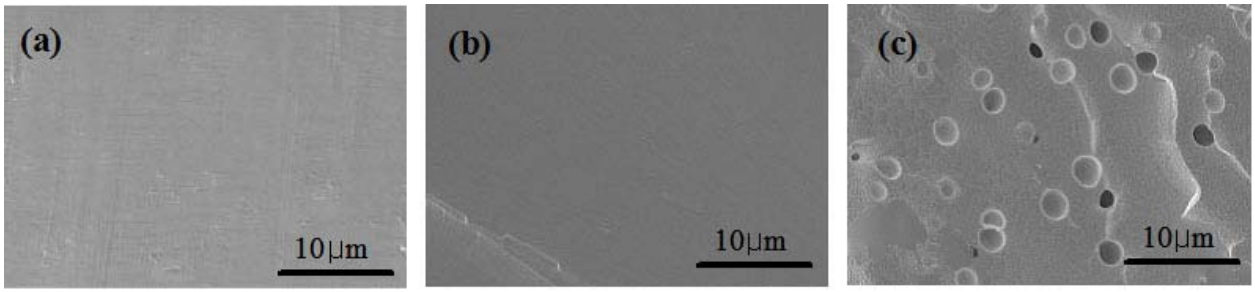

Figure 2.8 Scanning electron micrographs of fracture plane in epoxy with (a) 10 wt%, (b) 20 wt%, and (c) 30 wt% of DCPD after extraction by THF.

2.3.2 Phase Separation Behavior of PDMS in Matrix

A curing chemistry based on PDMS was considered for the new self-healing system because of the very low solubility of PDMS oligomers in most materials. Such a system will rapidly phase separate, yielding the desired droplets of healing agents dispersed in a polymer matrix. The healing agent, PDMS, is immiscible with the epoxy or epoxy vinyl ester matrix (DOW, DERAKANE 510A-40) we used. Through vigorous mixing, these healing agents disperse within the matrix. The phase separated PDMS droplets are successfully observed by optical microscopy and SEM started with 10 wt% of addition (figure 2.9 and 2.10). Phase separated PDMS domains exists in the form of liquid droplets in epoxy after matrix polymerization, so it can be used as healing agent in the case of damage. The size of the phase separated droplets is summarized in table 2.2.

Table 2.2. The size values of phase separated PDMS droplets.

Amount of PDMS (wt%)	Size of droplets (μm) Average [±1 standard deviation]
10	11.0 [±6.2]
20	12.8 [±9.4]
30	13.1 [±6.1]

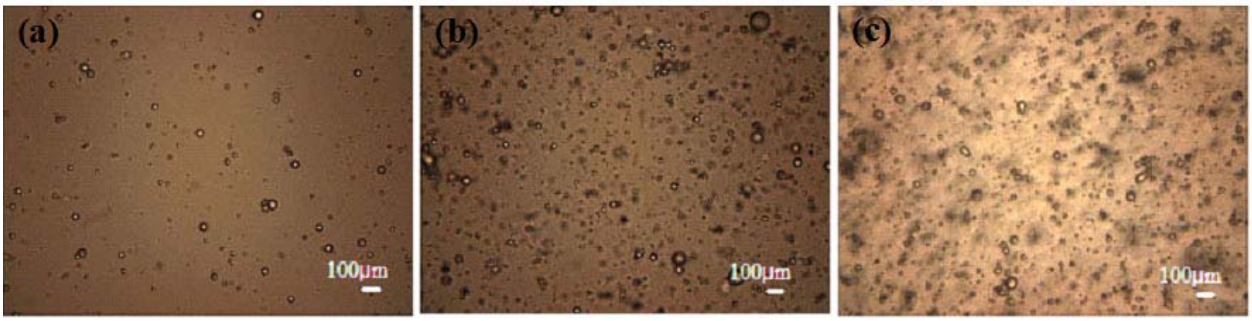

Figure 2.9 Optical microscopic images of epoxy with (a) 10 wt%, (b) 20 wt%, and (c) 30 wt% of PDMS (DOW, SYLGARD184).

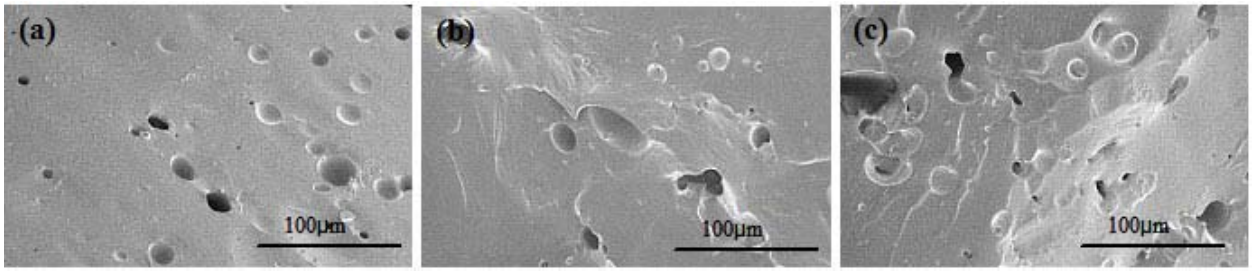

Figure 2.10 Scanning electron micrographs of fracture plane in epoxy with (a) 10 wt%, (b) 20 wt%, and (c) 30 wt% of PDMS (DOW, SYLGARD184).

2.3.3 PDMS Solubility in Epoxy Vinyl Ester Matrix

Prior to testing of the self-healing composite system, several processing variables were investigated. First, elemental analysis was used to confirm the immiscibility of the healing agent in the prepolymer. The vinyl ester prepolymer was vigorously mixed with HOPDMS, PDES, and adhesion promoter, and subsequently placed in a centrifuge to separate the prepolymer and dissolved adhesion promoter from the healing agents. The silicon content of the resulting prepolymer phase was almost the same as for a control sample consisting of a mixture of prepolymer and adhesion promoter (table 2.3). The elemental analysis proves the solubility of healing agent is very low in epoxy vinyl ester matrix, so it induces successful phase separation.

Table 2.3. Elemental analysis of separated prepolymer phase and control samples.

Element	A [epoxy vinyl ester + adhesion promoter]		B [HOPDMS +PDES]		C [epoxy vinyl ester + adhesion promoter) + (HOPDMS+PDES)]	
	Trial 1 (Si^{28})	Trial 2 (Si^{29})	Trial 1 (Si^{28})	Trial 2 (Si^{29})	Trial 1 (Si^{28})	Trial 2 (Si^{29})
C	62.44	62.83	32.38	32.21	60.21	59.28
H	5.52	5.60	8.10	8.19	5.51	5.33
N	0.44	0.27	0.19	0.42	0.30	0.19
Si	-	0.138	23.92	24.85	-	0.166

2.4 Catalyst Microencapsulation

2.4.1 Interfacial Polymerization

The DBTL-Sn catalyst is contained within microcapsules formed through interfacial polymerization, sequestering the catalyst from the PDMS healing agent. The interfacial polymerization of the polyurethane shell effectively avoids the aggregation of microcapsules [34-37]. In addition, it enables shell thickness control by changing the volume ratio of core and pre-polymer components and high yield. The microcapsules consist of a polyurethane shell surrounding a DBTL-Sn chlorobenzene mixture. The manufacturing process details are described in the experimental section.

Polyurethane microencapsulation is composed of two-step polymerization. Urethane prepolymer is first synthesized by toluene 2,4-diisocyanate (TDI) and 1,4-butanediol in cyclohexanone (figure 2. 11). The molecular weight of synthesized urethane prepolymer was 1,270 for number average ($\overline{M}_n$) and 1,690 for weigh average ($\overline{M}_w$) by gel permeation chromatograph (GPC), so poly-dispersity index (PDI) of prepolymer was 1.33.

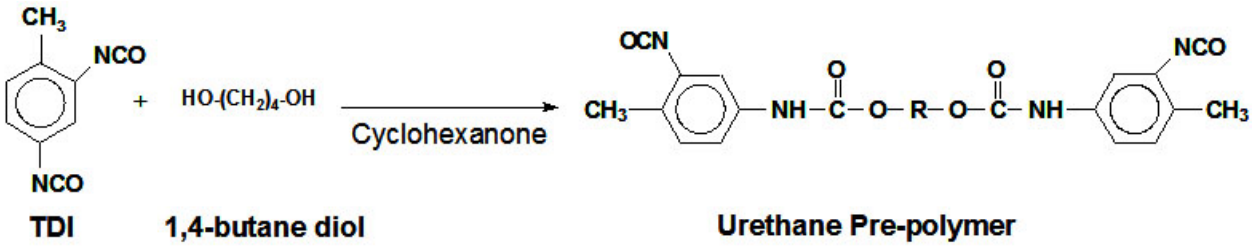

Figure 2.11 Reaction schemes for synthesis of urethane prepolymer.

The second step is the catalyst encapsulation using interfacial polymerization with synthesized urethane pre-polymer and ethylene glycol (EG) as a chain extender (figure 2.12). Liquid droplets of dissolved catalyst in chlorobenzene are stabilized by a suspending agent under mechanical stirring. Here the size of liquid droplets and final microcapsules is determined by mechanical stirring speeds. To increase the molecular weigh of urethane prepolymer, a chain extender is added into the solution during the polymerization reaction. Polyurethane shell is finally formed at the interface between aqueous phase and organic phase, so that the microcapsule contains a liquid mixture of tin catalyst and solvent (figure 2.13).

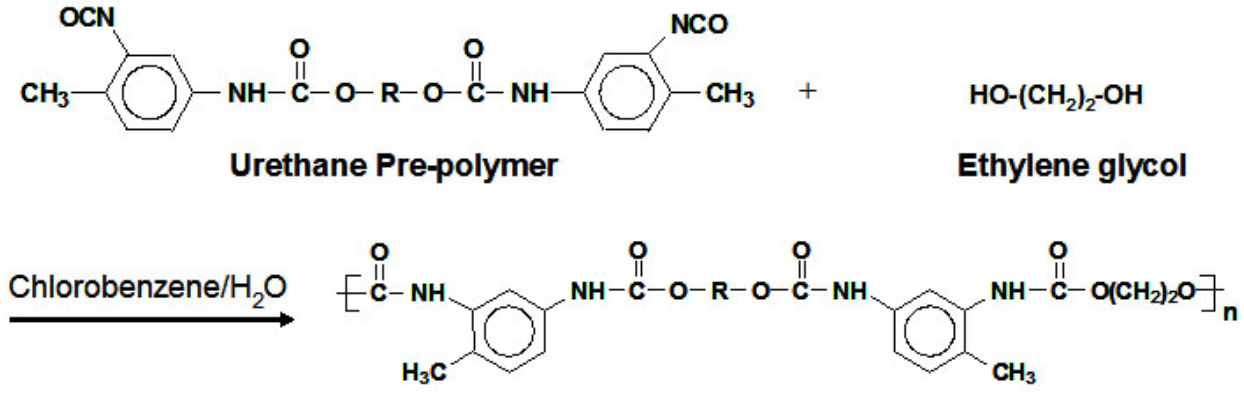

Figure 2.12 Reaction schemes for encapsulation using interfacial polymerization.

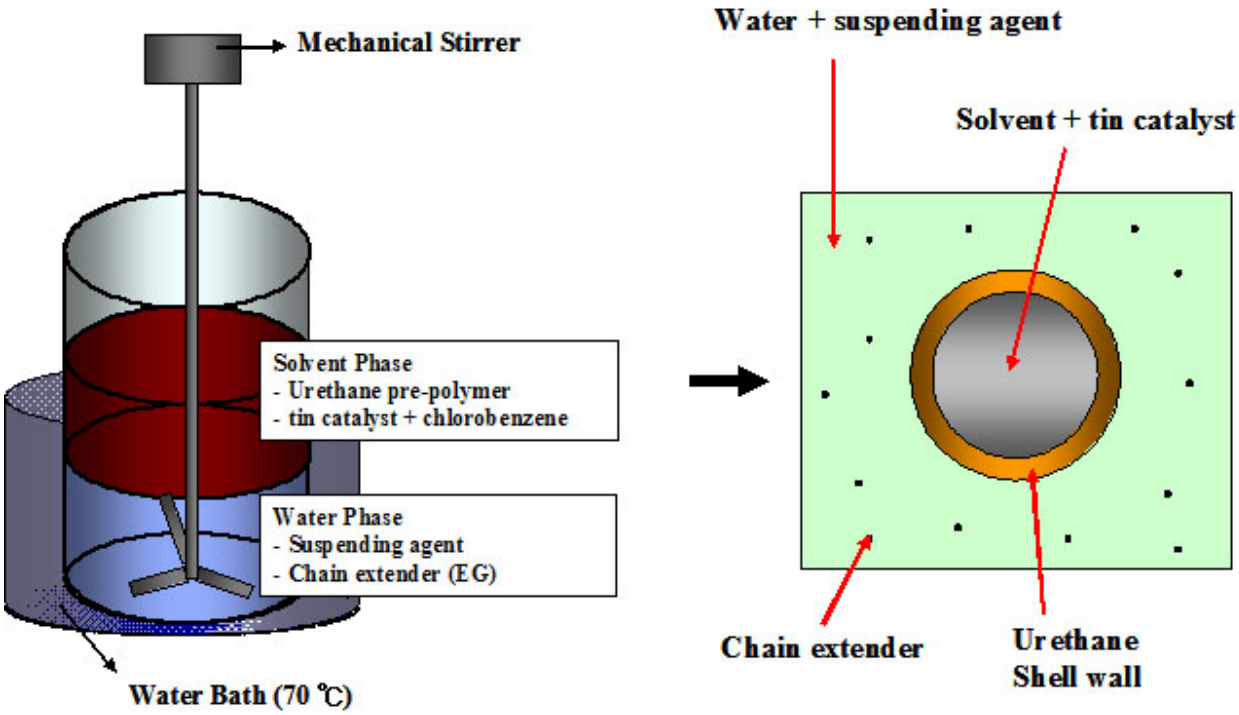

Figure 2.13 Schematics of interfacial polymerization for catalyst microencapsulation.

2.4.2 Characterization of Microcapsules

Synthesized microcapsules were investigated by both scanning electron microscopy (SEM) and optical microscopy (figure 2.14). From the result, it was pronounced that microcapsules successfully contained catalyst containing liquid droplets with a clean outer surface.

Size distributions of the phase separated droplets and catalyst containing microcapsules were determined through SEM and optical microscopy. Phase separated droplets of healing agent are created by vigorous mixing of vinyl ester prepolymer with adhesion promoter, HOPDMS, and PDES. The diameter of the phase separated droplets after mechanical stirring at 600 rpm ranged from 1-20 μm (figure 2.15). The droplet size was not a strong function of

stirring rate, and did not change significantly when samples were stirred between 100 and 2000 rpm (table 2.4).

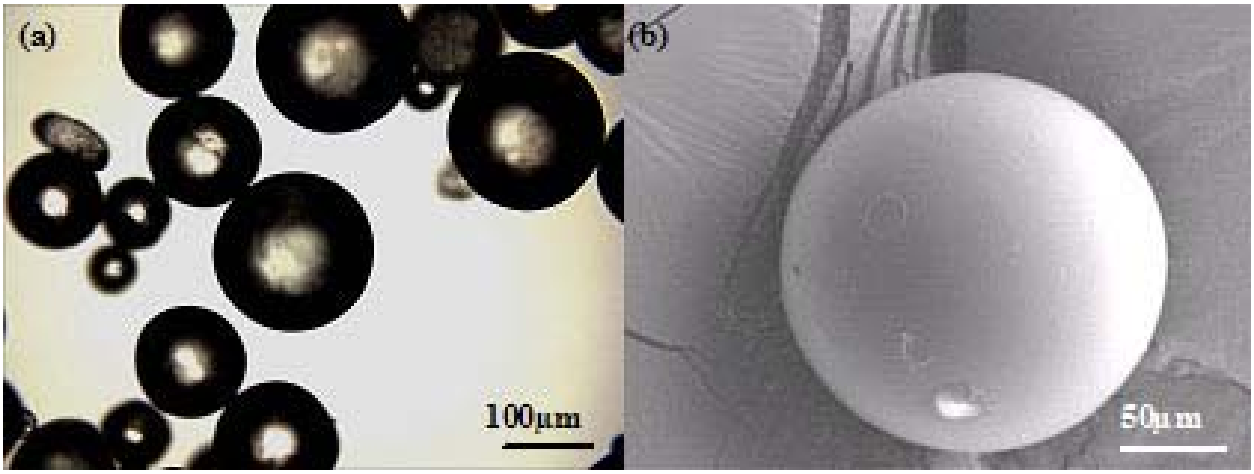

Figure 2.14 Microscopic images of synthesized microcapsules: (a) Optical microscope image of catalyst containing microcapsules and (b) SEM image of a representative microcapsule showing its smooth, uniform surface.

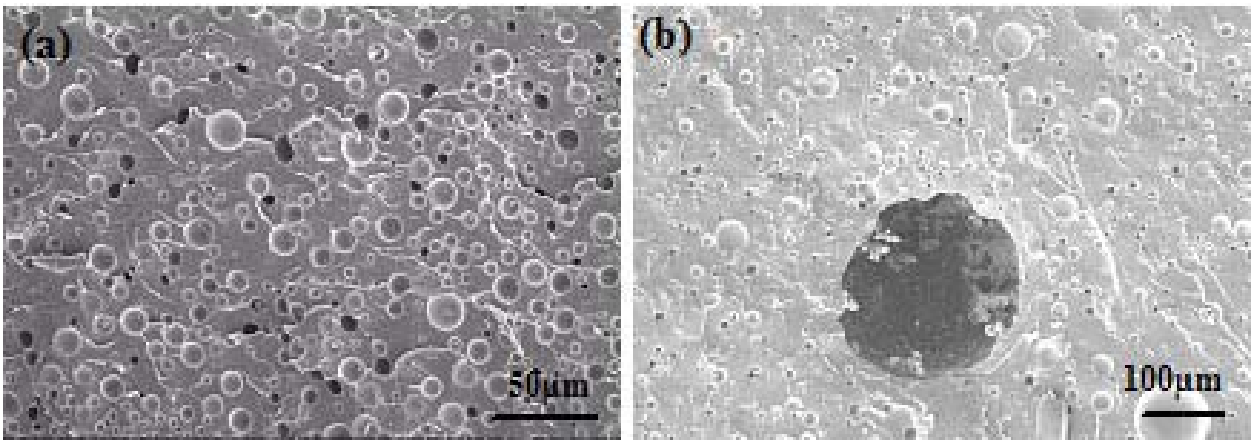

Figure 2.15 Fractured surface of self-healing polymer composite with phase separated healing materials and broken microcapsule.

Table 2.4. The size values of phase separated PDMS droplets according to the mechanical stirring speeds.

Stirring speeds (r.p.m.)	Size of droplets (μm) Average [±1 standard deviation]
100	11.9 [±4.7]
500	16.9 [±7.8]
1000	13.1 [±5.8]
2000	17.1 [±8.2]

Previously, it was reported that the size of microcapsules was successfully changed by the mechanical stirring speeds during urea-formaldehyde microencapsulation with DCPD [28]. In this thesis, the size of catalyst containing microcapsules can be also effectively changed by the mechanical stirring speeds during the interfacial polymerization. The average diameter of the DBTL-Sn catalyst containing microcapsules was a strong function of stirring rate and ranged from 50 to 450 μm according to the stirring speeds (figure 2.16). Each size of microcapsules can be separated by mechanical sieve after vacuum filtration and air dry. The size of microcapsules can be controlled by mechanical stirring speed but average microcapsule diameter in the experiments was selected to be from 150 to 200 μm. The ability to control the size of the various components enables us to tailor the self-healing system to both thin and thick layer systems.

Control test in which PDMS was mixed with the content of ruptured microcapsules revealed that significant catalytic activity was retained after encapsulation. In *ex situ* tests, mechanically fractured microcapsules effectively cured the PDMS healing agent, while intact microcapsules were not catalytically active in the case of mixing with the PDMS healing agent, indicating little or no catalyst was present on the exterior of the microcapsules.

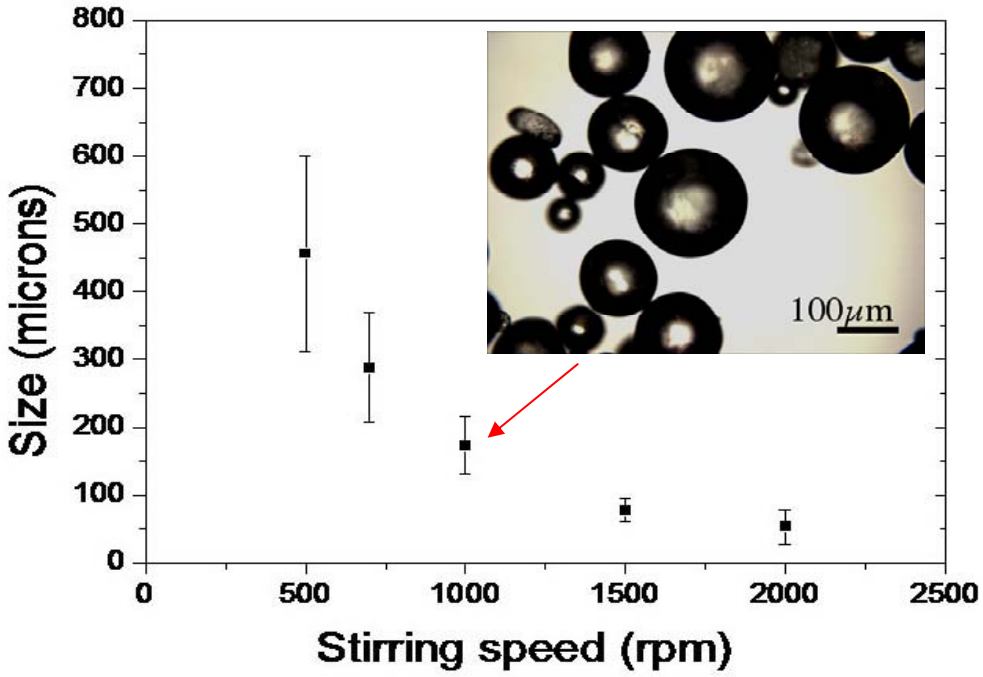

Figure 2.16 Diameter of catalyst containing microcapsules (shown with standard deviation) as a function of stirring speed. The insert shows an optical microscope image of microcapsules formed at 1000 rpm.

We investigated the thermal properties of micro-capsules by thermogravimetric analysis (TGA). As shown in figure 2.17, no weight change occurred up to the boiling point of chlorobenzene (131~132 ˚C) (contained within the microcapsules). The higher temperature flat region in the curve corresponds to the pyrolysis of urethane shell material. Thus, we estimate the synthesized microcapsules do not rapidly leak below the boiling point of the solvent and should have good thermal stability under common working environments. In addition, the fill content of the liquid mixture of tin catalyst and chlorobenzene in the microcapsules is about 85% in TGA analysis.

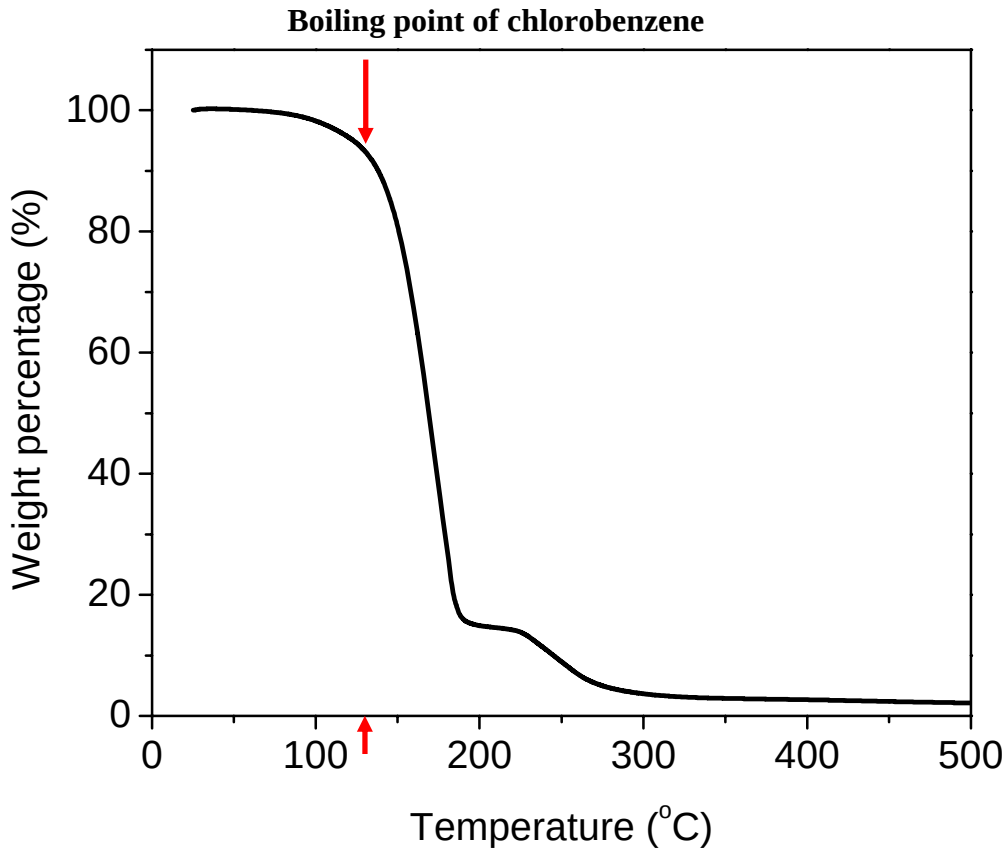

Figure 2.17 Thermal behavior of synthesized microcapsules by TGA.

2.5 Surface Morphology of Fractured Self-healing Polymer Composite

Phase separated PDMS liquid droplets and microencapsulated tin catalyst are successfully embedded in epoxy vinyl ester matrix, which consists of the self-healing polymer composites. The fracture surface of the composite before healing reaction obtained by SEM showed that broken empty microcapsules and voids, which represents presence of liquid phase of catalyst and PDMS healing agent (figure 2.18-a). The thickness of urethane shell wall was about 8~10 μm by SEM observation (figure 2.18c-d). Polymerized PDMS was observed on the fracture surface after healing reaction, which represents the successful healing reaction of the self-healing composite (figure 2.18-d).

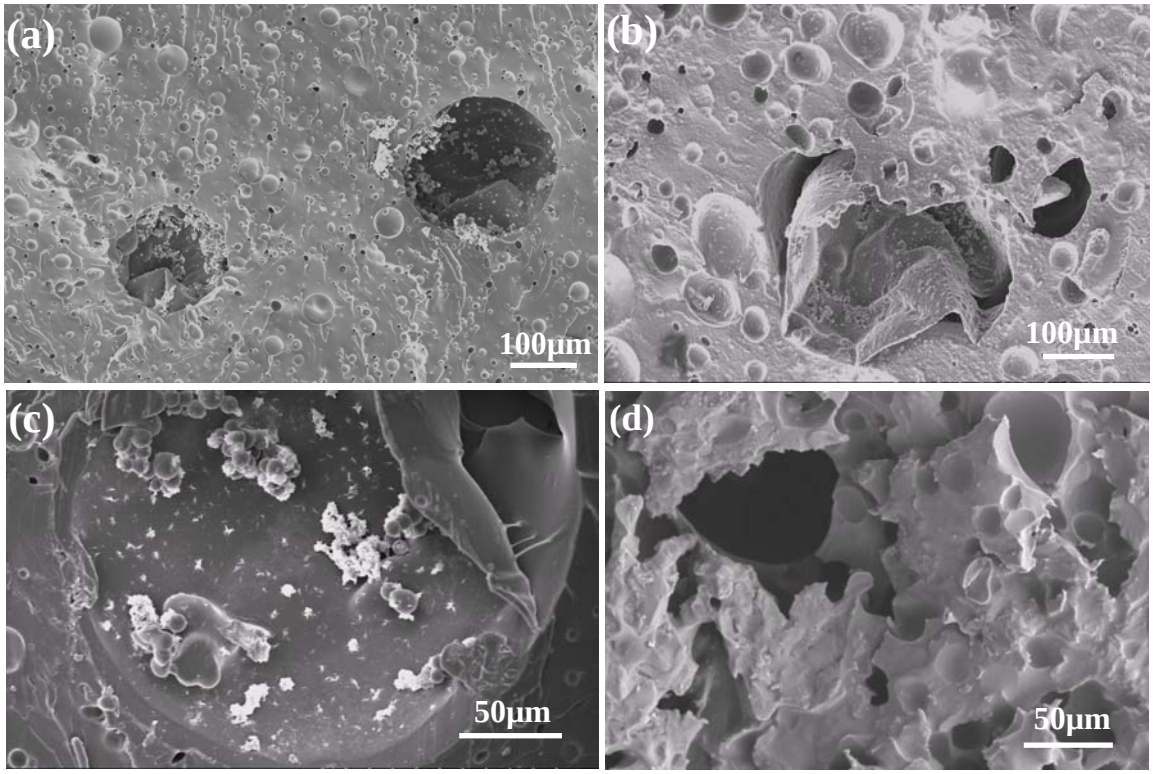

Figure 2.18 Fracture surface of self-healing polymer composite. (a) Empty microcapsule and voids left by the phase separated healing agent before healing reaction; (b) Broken microcapsule and voids left by the phase separated healing agent before healing reaction; (c) Broken microcapsule; (d) Cured PDMS layer after healing reaction.

2.6 Fracture Test of Self-healing Composite

2.6.1 Tapered Double-Cantilever-Beam (TDCB) Test

The performance of the self-healing composite was assessed via a fracture test protocol established previously by White et al. [24, 38]. This test utilizes a tapered double cantilever beam (TDCB) sample (figure 2.19), which ensures controlled crack growth along the centerline of the brittle specimen and provides a crack length independent measure of fracture toughness

for both virgin and healed materials [39-41]. The healing efficiency (η) is calculated using the protocol established by White et al.[24,25] as

$$\eta = \frac{K_{IC_{healed}}}{K_{IC_{virgin}}} = \frac{P_{c_{healed}}}{P_{c_{virgin}}}$$

where $K_{IC_{healed}}$ is the experimentally determined mode-I critical stress intensity of the healed specimen and $K_{IC_{virgin}}$ is the critical stress intensity of the virgin specimen. $P_{c_{healed}}$ is the critical fracture load of the healed specimen and $P_{c_{virgin}}$ is the critical fracture load of the virgin specimen.

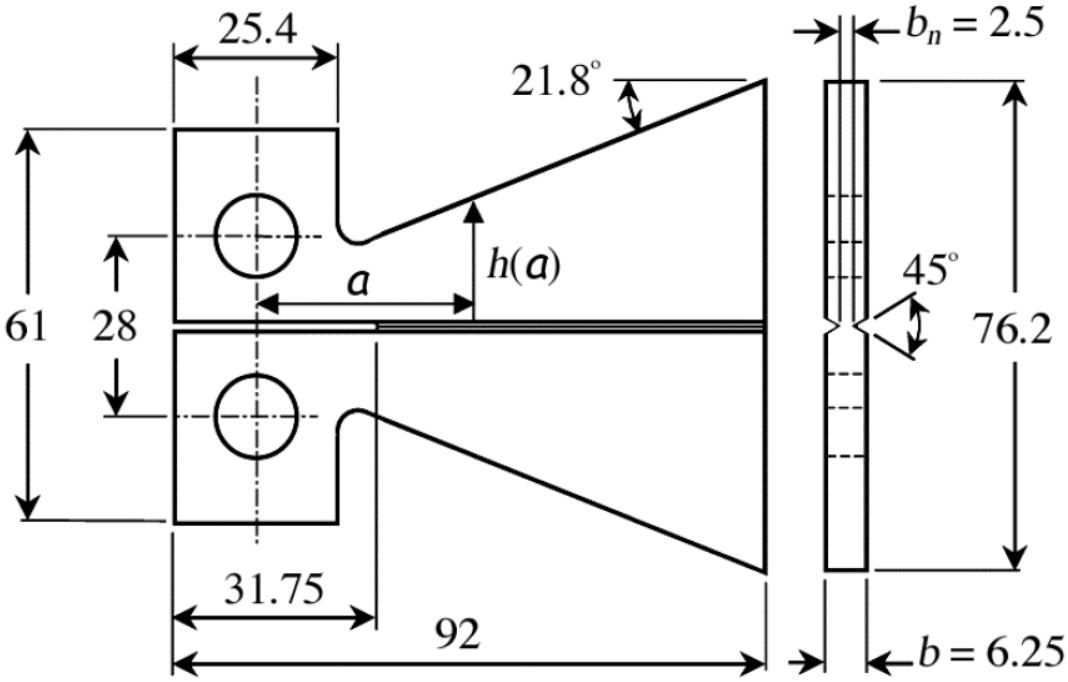

Figure 2.19 Tapered-double-cantilever-beam geometry based on modification to the geometry. All dimensions in mm. Figure adapted from ref. [42, 43].

In the preliminary testing the healing ability of the PDMS self-healing system was confirmed by small scale screening tests. Subsequently, we have confirmed the healing efficiency of PDMS system by TDCB fracture toughness testing. Fully *in situ* samples were

prepared of the self-healing composite as well as control samples in which the PDMS solution was manually coated on the broken surface of epoxy vinyl ester containing the adhesion promoter. The control tests removed the variables associated with delivery of phase separated healing agent and microencapsulated catalyst, while *in situ* samples contained both the phase-separated PDMS healing agent and the microencapsulated organotin catalyst, enabling the samples to self-heal after fracture. Load-displacement curve for *in situ* samples which are cured at room temperature reveals that the fracture behavior of polymer composite is nonlinear elastic. However, it shows linear load-displacement curve and higher maximum load value after post curing at 50 ˚C (figure 2.20).

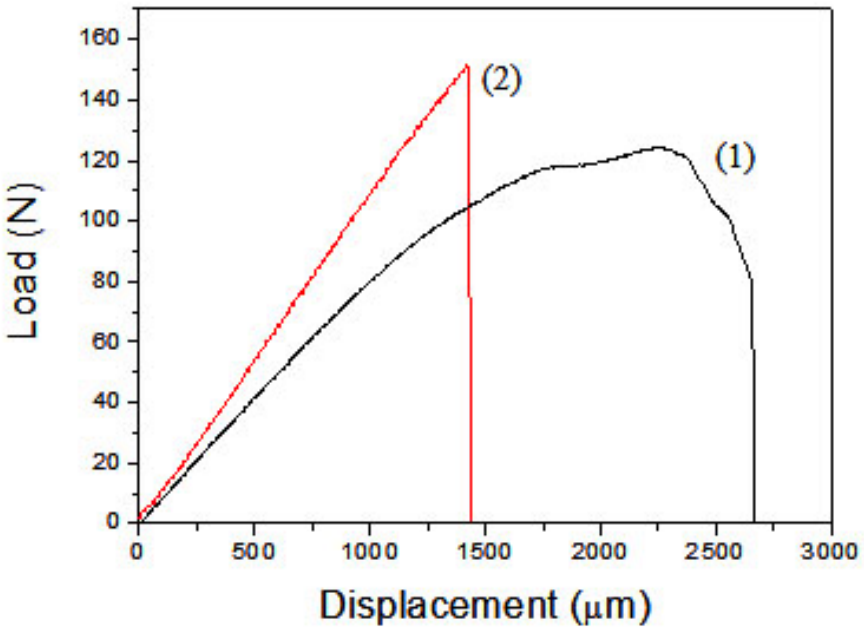

Figure 2.20 Load–displacement curves of virgin TDCB samples with (1, black) and without (2, red) post curing at 50 ˚C. Test sample contains 4 wt% adhesion promoter, 12 wt% PDMS, and 3.6 wt% microcapsules.

To reduce the amount of healing components, we used localized TDCB sample which is made of central core containing the healing components surrounded by a blank matrix part [44]. During the test process, we could observe that liquid was released on the fractured surface of TDCB sample (figure 2.21).

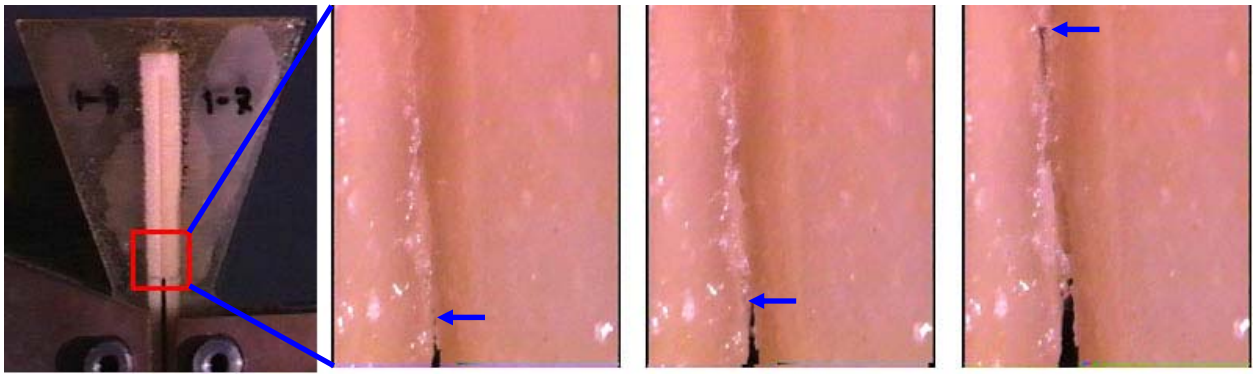

Figure 2.21 Optical microscopic images of virgin sample with TDCB geometry according to the crack propagation. Arrow represents the position of propagated crack [44].

In situ samples consisting of phase-separated PDMS healing agent and microencapsulated DBTL catalyst dispersed in the cured vinyl ester matrix initially showed low, but non-zero healing after mechanical damage. Post-fracture analysis of these specimens revealed that low η was a result of poor inherent adhesion of PDMS to the matrix. The adhesion promoter methylacryloxy propyl triethoxy silane ($C_{13}H_{26}O_5Si$) was added to the matrix to improve bond strength. A control experiment was introduced to study the effect of the adhesion promoter on fracture behavior (adhesive vs. cohesive failure) without the variables associated with delivery of phase separated healing agent and microencapsulated catalyst. Control samples were healed by injecting a solution of pre-mixed healing agent and catalyst into the crack plane of fully fractured samples. As shown in Figure 2.22-a, the addition of adhesion promoter more than doubled the η of the control samples. Experiments were then performed on the *in situ*

system with adhesion promoter added. Fracture test results show that the self-healing system and control samples attain similar levels of η (figure 2.22-b), indicating that self-healing was equally effective as manually mixing and injecting the PDMS and bonding the crack closed. A range of healing agent, microcapsule and adhesion promoter concentrations was investigated (table 2.5), with the maximum η for the *in situ* healed samples achieved for samples containing 12wt% PDMS, 4wt% adhesion promoter, and 3.6wt% microcapsules.

Also apparent from figure 2.22, the critical load to fracture of the virgin, *in situ* self-healing system (4) is significantly greater than for the neat vinyl ester matrix used for the control experiments (1). Thus, the inclusion of phase separated healing agent and microcapsules of catalyst increases the toughness of the vinyl ester matrix. For the concentrations corresponding to the results in figure 2.22-b, the increase in mode-I fracture toughness is approximately 88% based on the critical load at fracture. In addition, while both the virgin *in situ* and control tests exhibit characteristically linear (brittle) fracture behavior, the fracture of healed samples is a non-linear deformation and failure process, fortuitously absorbing additional energy in the fracture process. The increased fracture toughness of the matrix does, however, lead to lower effective η. Relative to the original vinyl ester matrix, η as high as 46% are achieved.

Although the η reported in table 2.5 are lower than obtained by White et al. for a self-healing epoxy based on Grubbs catalyst and encapsulated DCPD healing agent [20], this new PDMS based materials system still holds great promise. Low η are to be expected given the PDMS has significantly lower stiffness and fracture toughness than the matrix material. In many applications, however, simply filling or sealing the crack from harsh environments is as important as recovering full fracture strength in the test protocol. For example, the PDMS based

healing system has potential for healing surface cracks or scratches in protective coatings used in corrosive environments.

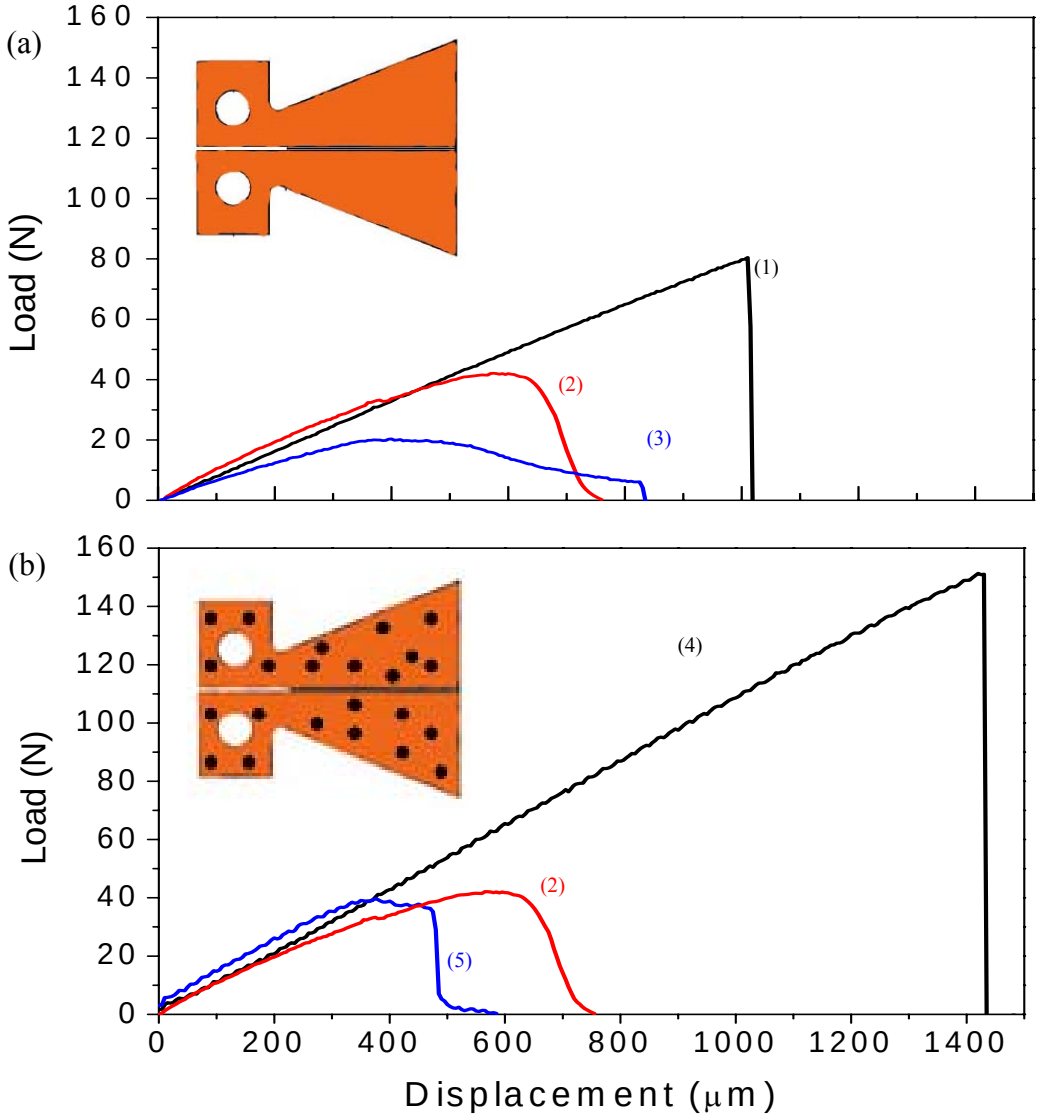

Figure 2.22 Load–displacement curves of TDCB samples: a) virgin sample (1, black), and injection-healed sample with (2, red) and without (3, blue) adhesion promoter; b) first fracture of sample containing 4 wt% adhesion promoter, 12 wt% PDMS, and 3.6 wt% microcapsules (4, black) and after self-healing (5, blue). The injection-healed sample (2, red) with adhesion promoter is shown again for comparison.

Table 2.5. Average maximum load of self-healed vinyl ester. One standard deviation in square brackets.

Composition[a]			Fracture load (N)	Healing efficiency (%)
PDMS (wt%)	Adhesion promoter (wt%)	Micro-capsule (wt%)		
8	4	2.4	14 [3]	9 [2]
		5.0	9 [5]	6 [3]
12	2	3.6	14 [2]	9 [1]
	4	3.6	37 [7]	24 [4]
	8	3.6	28 [5]	19 [4]
15	4	2.4	21 [1]	14 [1]
		4.5	37 [3]	24 [3]

[a] remainder is vinyl ester.

2.6.2 Self-healing under Water Environments

Healing under real-world conditions, for example in the presence of water is considerably more complex than in the laboratory frame. The effect of water on self-healing was examined by a simple experiment in which a TDCB sample was fractured, immersed in water prior to bringing the two sides together, and then healed under water. This sample was compared to samples healed in air under high (>90%) and low (10%) relative humidity (RH). The fracture load of the sample healed under water decreased only ~25% with respect to the other samples (figure 2.23), even though the system has not yet been optimized for healing under water.

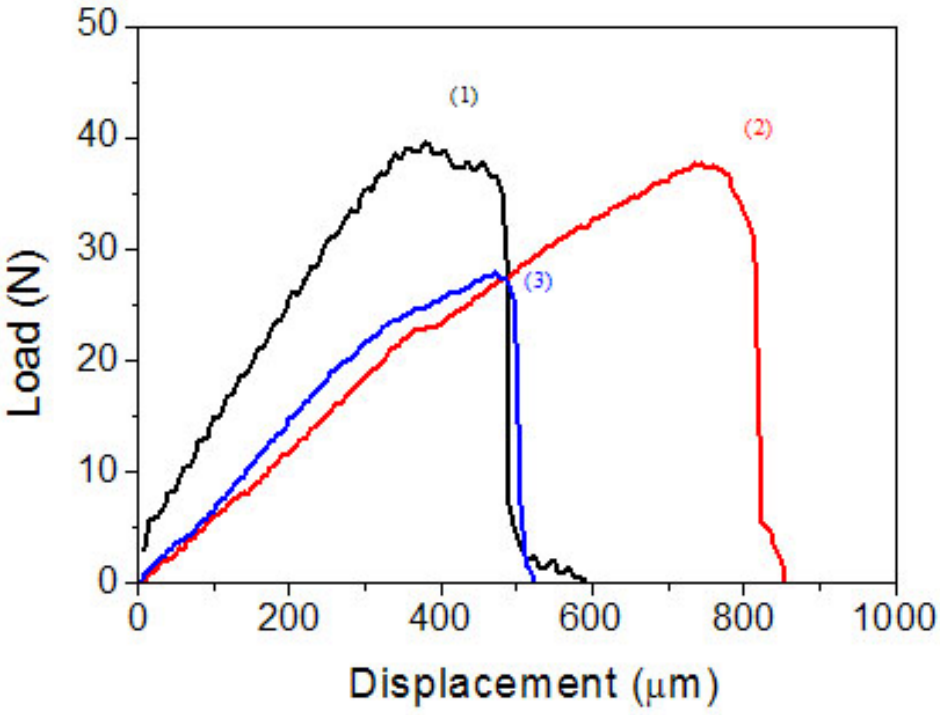

Figure 2.23 Load–displacement curves of TDCB samples containing 4 wt% adhesion promoter, 12 wt% PDMS, and 3.6 wt% microcapsules healed in air at low relative humidity (1, black), in air at high relative humidity (2, red), and immersed in water (3, blue).

2.7 Conclusions

In this chapter, the manufacturing method for catalyst containing microcapsules and phase separated PDMS healing agent in epoxy vinyl ester matrix was described. These components consist of a new self-healing materials system. Moreover, we proved that the interfacial polymerization of polyurethane shell is very effective to synthesize the catalyst containing microcapsules with spherical shape and good heat stability. The fracture test with TDCB sample geometry showed that the self-healing polymer composite has good healing property even under water environments. Consequently, we created a chemically stable self-

healing composite based on the tin-catalyzed polycondensation of phase-separated droplets containing HOPDMS and PDES. This system possesses a number of important advantages over the previous self-healing methodology, including a) the healing chemistry remains viable in humid or wet environments; b) the chemistry is stable to an elevated temperature (> 100 °C), enabling healing in higher-temperature thermoset systems. The thermal stability of the self-healing composite was tested with the post cured TDCB specimens at 100 °C for 24 hours in a convection oven. The polycondensation of HOPDMS and PDES without catalyst occurs from 150 °C in bulk mixing experiments; c) the components are widely available and comparatively low in cost. The price of the previous system is $53.5/g for Grubbs catalyst and $0.14/g for DCPD (Aldrich) and this system is $0.46/g for DBTL and $0.16/g for PDMS (Gelest); d) the concept of phase separation of the healing agent greatly simplifies processing, as the healing agent can now be simply mixed into the polymer matrix.

The materials system presented in this thesis greatly extends the capability of self-healing polymers by introducing a new, environmentally stable healing chemistry and demonstrating the concept of phase-separated healing agents in a structural polymer matrix. Phase separation of the healing agent is an approach that may be applicable to a broad class of new healing chemistries for structural polymers, and stability to water and air significantly increases the probability that self-healing could be extended to coatings and thin films in harsh environments.

2.8 Experimental

2.8.1 Microcapsule Synthesis

The urethane prepolymer was synthesized through the reaction of toluene 2,4-diisocyanate (TDI, Aldrich, 22.0 g, melting point, mp= 19.5–21.5 °C) and 1,4-butanediol (5.0 g)

in cyclohexanone (142 g, boiling point, bp760 = 155.6 °C) at 80 °C for 24 h. The solution of TDI and cyclohexanone was first mixed and allowed to react under mechanical stirring in a round-bottomed flask. 1,4-butanediol was then added at 5 $mLmin^{-1}$ using a syringe pump while stirring. To avoid formation of a gel during microencapsulation, the molar ratio of TDI to 1,4-butandediol was kept below 2.3. The cyclohexanone was evaporated under vacuum at 100 °C. The synthesized urethane prepolymer had excess isocyanate functional groups, which could be reacted to form a higher-molecular-weight polymer through the use of a chain extender. The amount of chain extender added was determined by titration of the isocyanate functional group in urethane prepolymer following ASTM D2572-97. To form the tin catalyst-containing urethane microcapsules, the urethane prepolymer (3.0 g) and DBTL (Gelest, 1 g) were dissolved in 32 g chlorobenzene and added to 28.8 g of a water solution containing 15 wt% gum Arabic (Aldrich, suspending agent). After the mixture was stirred for 30 min at 70 °C, 30 wt% (relative to the urethane prepolymer) of ethylene glycol (chain extender) was added into the solution at 5 $mLmin^{-1}$. Spherical microcapsules containing dissolved DBTL in chlorobenzene with smooth surfaces were obtained after 2 h at 70 °C with mechanical stirring at 1000 rpm.

2.8.2 Vinyl Ester Matrix Polymerization and Sample Formation

The specific self-healing polymer composite described in this thesis consisted of phase-separated liquid droplets of the PDMS-based healing agent and DBTL-catalyst-containing microcapsules dispersed in a mixture of vinyl ester (DOW DERAKANE 510A-40) and adhesion promoter. The vinyl ester was cured using benzoylperoxide (BPO) and dimethylaniline (DMA) as the initiator and activator, respectively. 1 wt% BPO was dissolved in the prepolymer. After the BPO was completely dissolved, the mixture of HOPDMS and PDES was added into the prepolymer with

mechanical stirring, followed by degassing under vacuum. The microcapsules containing DBTL were then mixed with the degassed solution and 0.1 wt% DMA, followed by a final degassing. This mixture was poured into a closed silicone rubber mold and cured for 24 h at room temperature. The sample was then cured at 50 °C for another 24 h.

2.8.3 Fracture Testing and Healing Efficiency

After preparation of TDCB specimens, a sharp pre-crack was created by gently tapping a razor blade into the molded starter notch in the samples. All fracture specimens were tested under displacement control, using pin loading and 5 μm/s displacement rate. Samples were tested to failure, measuring compliance and peak load. Samples were unloaded, allowing the crack faces to come back into contact, and healed in this state for 24 hours at 50 °C. Using the protocol established by White et al.[24,25], healing efficiency (η) is calculated as

$$\eta = \frac{K_{IC_{healed}}}{K_{IC_{virgin}}} = \frac{P_{c_{healed}}}{P_{c_{virgin}}}$$

where $K_{IC_{healed}}$ is the experimentally determined mode-I critical stress intensity of the healed specimen and $K_{IC_{virgin}}$ is the critical stress intensity of the virgin specimen. $P_{c_{healed}}$ is the critical fracture load of the healed specimen and $P_{c_{virgin}}$ is the critical fracture load of the virgin specimen. The healing efficiency and standard deviation are calculated from a minimum of five fracture tests (Table 2.2).

2.8.4 Fracture Testing of the Samples Healed under Water Environments

The preparation and first fracture of TDCB samples tested under humid and wet states were performed by the same methods as the dry state. A set of fractured TDCB samples were

immersed into a water bath for ~30 sec and reassembled in air without drying the samples. The reassembled samples were submerged back into the water bath, which was then placed into an oven for 24 hours at 50 °C. Another set of fractured TDCB samples were reattached in air and separately healed in same the oven for 24 hours at 50 °C to determine the effect of healing under high humidity. The healed specimens were tested to failure following the standard procedure.

2.9 References

1. H. C. Hsieh, T. J. Yang, S. Lee, *Polymer* **2001**, *42*, 1227-1241.
2. X. Chen, M. A. Dam, K. Ono, A. Mal, H. Shen, S. R. Nut, K. Sheran, F. Wudl, *Science* **2002**, *295*, 1698-1702.
3. X. Chen, F. Wudl, A. Mal, H. Shen, S. Nutt, *Macromolecules* **2003**, *36*, 1802-1807.
4. E. Vaccaro, J. H. Waite, *Biomacromolecules* **2001**, *2*, 906-911.
5. R. P. Wool, Polymer Interfaces: Structure and Strength; Hanser Gardner: Cincinnati, 1995.
6. S. S. Sukhotskaya, V. P. Mazhorava, Yu. N. Terekhin, *Hydrotechnical Construction* **1983**, *17*, 295-296.
7. C. Edvardsen, *ACI Materials Journal* **1999**, *96*, 448-454.
8. J. O. Outwater, D. J. Gerry, *Journal of Adhesion* **1969**, *1*, 290-298.
9. M. Zako, N. Takano, *J. Intell. Mater. Syst. Struct.* **1999**, *10*, 836-841.
10. C. Dry, *Comp. Struct.* **1996**, *35*, 263-269.
11. S.M. Wiederhorn, P.R. Townsend, *J. Am. Ceram. Soc.* **1970**, *53*, 486-489.
12. B. Stavrinidis, D.G. Holloway, *Phys. Chem. Glasses* **1983**, *24*, 19-25.
13. M. Inagaki, K. Urashima, S. Toyomasu, Y. Goto, M. Sakai, *J. Am. Ceram. Soc.* **1985**, *68*, 704-706.
14. K. Jud, H. H. Kausch, *Polym. Bull.* **1979**, *1*, 697-707.
15. K. Jud, H. H. Kausch, J. G. Williams, *J. Mater. Sci.* **1981**, *16*, 204-210.
16. H. H. Kausch, K. Jud, *Proc. Appl.* **1982**, *2*, 265-268.

17. E. P. Wang, S. Lee, J. Harmon, *J. Polym. Sci. B* **1994**, *32*, 1217-1227.

18. C. B. Lin, S. Lee, K. S. Liu, *Polym. Eng. Sci.* **1990**, *30*, 1399-1406.

19. I. Raghavan, R. P. Wool, *J. Appl. Polym. Sci.* **1999**, *71*, 775-785.

20. V. C. Li, Y. M. Lim, Y. Chan, *Composites Part B-Engineering* **1998**, *29*, 819-827.

21. P. T. Curtis, S. W. Travis, G. *Plastics Rubber and Composites* **1999,** *28*, 201-209.

22. M. Motuku, U. K. Vaidya, G. M. Janowski, *Smart Materials and Structures* **1999**, *8*, 623-638.

23. S. M. Bleay, C. B. Loader, V. J. Hawyes, L. Humberstone, P. T. Curtis, *Composites Part A-Applied Science and Manufacturing* **2001**, *32*, 1767-1776.

24. S. R. White, N. R. Sottos, P. H. Geubelle, J. S. Moore, M. R. Kessler, S. R. Sriram, E. N. Brown, S. Viswanathan, *Nature* **2001**, *409*, 794-797.

25. E. N. Brown, S. R. White, N. R. Sottos, *Journal of Materials Science* **2004**, *39*, 1703-1710.

26. M. R. Kessler, S. R. White, *Journal of Polymer Science Part A-Polymer Chemistry* **2002**, *40*, 2373-2383.

27. M. R. Kessler, N. R. Sottos, S. R. White, *Composite Part A* **2003**, *34*, 743-753.

28. E. N. Brown, M. R. Kessler, N. R. Sottos, S. R. White, *Journal of Microencapsulations* **2003**, *20*, 719-730.

29. J. D. Rule, J. S. Moore, *Macromolecules*. **2002,** *35*, 7878-7882.

30. J. D. Rule, E. N. Brown, N. R. Sottos, S. R. White, Moore, J. S. *Adv. Mater.* **2005**, *17*, 205-208.

31. L. Lewis, R. Colborn, H. Grade, G. Bryant, C. Sumpter, R. Scott, *Organometallics* **1995**, *14*, 2202-2213.

32. G. B. Shah, *J. Appl. Poly. Sci.* **1998**, *70*, 2235-2239.

33. F. W. Van der Weij, *Macromol. Chem.* **1980**, *181*, 2541-2548.

34. I. Kim, J. Seo, Y. Kim, *Polymer (Korea)* **2002**, *26*, 400-409.

35. K. Hong, S. Park, *Reactive & Functional Polymers* **1999**, *42*, 193-200.

36. Y. Frere, L. Danicher, P. Gramain, *European Polymer Journal* **1998**, *34*, 193-199.

37. J. Cho, A. Kwon, *C.* Cho, *Colloid Polym. Sci.* **2002**, *280*, 260-266.

38. E. N. Brown, N. R. Sottos, S. R. White, *Experimental Mechanics* **2002**, *42*, 372-379.

39. R. P. Wool, K. M. O'Conner, *J. Appl. Phys.* **1981**, *52*, 5953-5963.

40. S. Mostovoys, P.B. Crosley, E. J. Ripling, *J. Mater.* **1967**, *2*, 661-681.

41. M. Meiller, A. A. Roche, H. Sautereau, *Journal of Adhesion Science* **1999**, *13*, 773-788.

42. E. N. Brown, *Fracture and Fatigue of a Self-healing Polymer Composite Material*, University of Illinois at Urban-Champaign, 2003.

43. W. Beres, A. K. Koul, R. Thambraj, *Journal of Testing and Evaluation* **1997**, *25*, 536-542.

44. J. D. Rule, N. R. Sottos, S. R. White, *Effect of Microcapsule Size on the Performance of the Self-healing Polymers, Polymer*, in review.

CHAPTER 3

LOW TEMPERATURE SELF-HEALING

In most previous experiments, samples were healed at 50 °C, which although sufficient to demonstrate the principle of self-healing system, may be prohibitive for many real-world situations. To improve the healing property of the self-healing system at room temperature, and potentially even below room temperature, we investigated a highly effective new organotin catalyst for the polycondensation of HOPDMS with PDES, as well as optimized the viscosity of PDMS healing agent for better transport to the crack plane in this chapter.

3.1 Viscosity of PDMS Healing Agent

The focus in this chapter is to modify the self-healing system so that higher healing efficiencies can be achieved at room temperature, without losing many of the advantageous properties of the current system. One approach to accomplish this is to reduce the viscosity of the healing agent. The bulk chemistry of PDMS poly-condensation works at room temperature, and if we reduce the viscosity of the PDMS precursor for better transport properties, it should translate to better healing efficiencies at low temperature. As a reference, average maximum loads from monotonic fracture testing of control and *in situ* TDCB samples (the systems are described in chapter 2), containing a PDMS healing agent (S45) with a viscosity value of 40,000 cP, are summarized in table 3.1. The control sample is epoxy vinyl ester matrix with 4 wt% adhesion promoter. The *in situ* sample is composed of matrix, 4 wt% adhesion promoter, 12 wt% PDMS, and 3.6 wt% catalyst containing microcapsules. As this data shows, the efficiency of the healing decreases significantly as the temperature is reduced.

Table 3.1. Average maximum load for control and *in situ* samples according to temperature.

Temp. (℃)	control sample	*In situ* sample
	Average Maximum Load (N) [± 1 standard deviation]	
RT (20)	21 [±1]	5 [±3]
30	30 [±5]	17 [±13]
50	41 [±4]	37 [±7]

In order to achieve better self-healing efficiency at low temperatures, we have turned our attention to lower viscosity healing agents for improved fluid diffusion and mixing with catalyst. Specifically, two commercially available PDMS healing agents have been investigated: S42 and S35 from Gelest with viscosities of 14,400 cP and 4,000 cP, respectively. Generally, the lower viscosity PDMS may have a possible problem of unsuccessful phase separation with matrix material, because it also has lower molecular weight. However, we confirmed successful phase separation of two lower viscosity PDMS candidates by SEM (figure 3.1). The size of the phase separated droplets is decreased as the molecular weight of PDMS healing agent decreases (table 3.2). In the result, the average size of phase separated droplets with S35 was also smaller than the size of droplets with original PDMS healing agent (S45 in table 2.2) and S42.

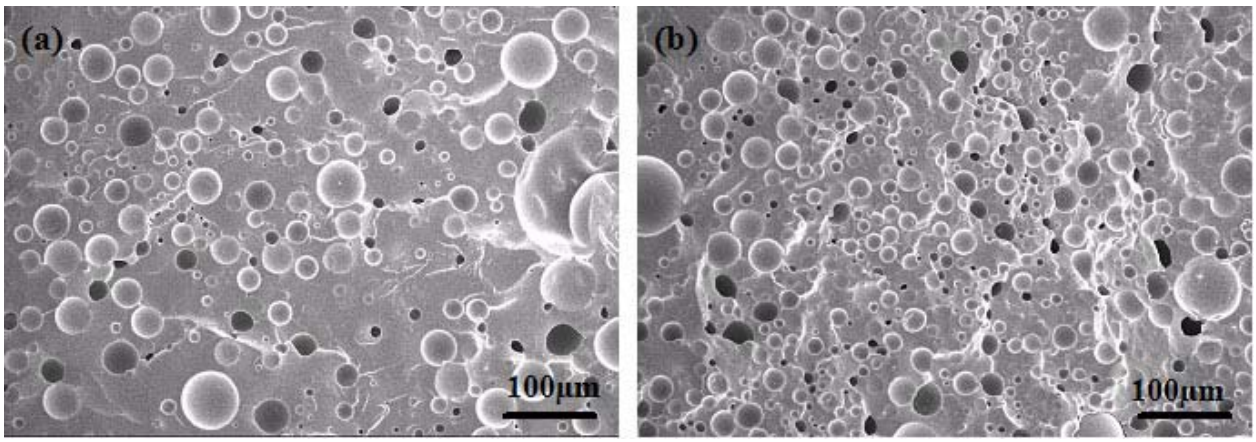

Figure 3.1 Fractured surface of composite of phase separated PDMS healing materials, (a) S42 (viscosity 14,000 cP) and (b) S35 (viscosity 4,000 cP), with epoxy vinyl ester matrix.

Table 3.2. The size values of phase separated PDMS droplets.

PDMS	Viscosity (cP)	Molecular Weight	Size of droplets (μm) Average [±1 standard deviation]
S42	14,000	77,000	15.9 [±10.2]
S35	4,000	49,000	9.8 [±4.8]

In the monotonic TDCB tests with healing at 30 ˚C , the lower molecular weight PDMS healing agent displays better healing efficiency than the original high viscosity agent at the same temperature (figure 3.2).

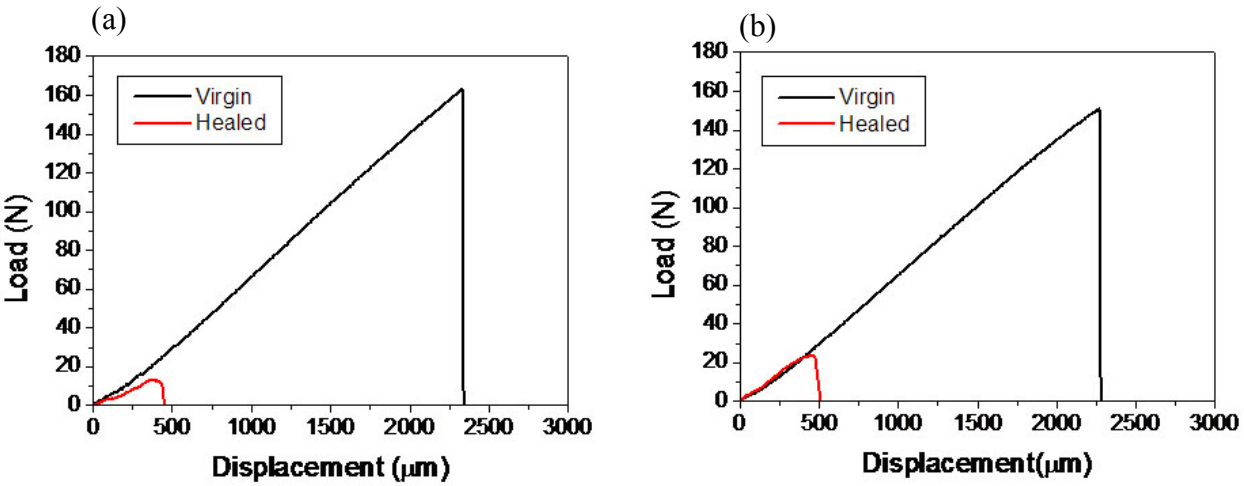

Figure 3.2 Result from monotonic fracture tests with TDCB geometry for virgin samples and fractured samples healed at 30 ˚C with a) S42 (viscosity 14,000 cP) and b) S35 (viscosity 4,000 cP).

In order to screen the optimum viscosity value, the preliminary test was performed by breaking and healing small scale bullet samples test with lower viscosity PDMS healing agents. The experimental details for the small scale bullet sample test are described in experimental section. Commercially available PDMS healing agents with various viscosity values were used in this test. The healing property of the bullet sample test was evaluated by manually testing the adhesion strength of healed samples. The bullet sample test healed at room temperature showed

very promising result. Also, the test result shows that the healing agent with intermediate viscosity seems to have better healing property than the lowest one. This result was verified by the TDCB fracture toughness test. The maximum load of self-healed samples was compared with TDCB geometry according to the viscosity values of the PDMS healing agent (Table 3.3). In the result, the healing property of the self-healing composite was improved by reducing the viscosity of the healing agent, and had the optimum viscosity range around 1,600~2,400 cP However, the PDMS healing agent with too low molecular weight, less than 4,000, did not successfully heal the damage because the healing agent was not properly included in matrix due to layered phase separation. The healing agents mixed with the matrix under mechanical stirring and they exist as the phase separated liquid droplets in the matrix after the matrix polymerization. However, the healing agent with the too low molecular weight was formed on top of the matrix layer in the form of liquid layer after matrix polymerization.

Table 3.3. Maximum load of self-healed samples with various viscosity PDMS by TDCB test.

PDMS	Viscosity (cP)	Molecular weight	% Hydroxyl group (OH)	Maximum load of healed specimen	
				RT	30°C
S12	13-26	400-700	4.5-7.5	No healing (layered phase separation)	
S15	36-68	2,000-3,500	0.9-1.2	No healing (layered phase separation)	
S27	560-640	18,000	0.2	16 N	21 N
S32	1,600	36,000	0.09	15 N	29 N
S35	4,000	49,000	0.07	17 N	29 N
S42	14,400	77,000	0.04	10 N	15 N
S45 (original)	40,000	110,000	0.03	5 N	17 N

3.2 Catalytic Activity

To further improve the PDMS self-healing system, we investigated other commercially available organotin catalysts with better catalytic activity than the current catalyst to determine if that would result in better healing due to the more effective reaction at low temperature. Thus, the combination of lower viscosity healing agent and a more effective catalyst should take us closer to the optimized low temperature PDMS self-healing system. The original organotin catalyst, DBTL-Sn, has long ligand chains (more that 30 total carbon atoms) attached to the tin atom. For better catalytic activity, we investigated other organotin catalysts which have shorter ligand chains than the current organotin catalyst or contain tin (II) rather than tin (IV) (figure 3.3). Basically, the number of carbon atoms in the alkyl and ester groups bonded to the tin atom is reciprocally proportional to the catalytic activity according to Shah's research [1, 2].

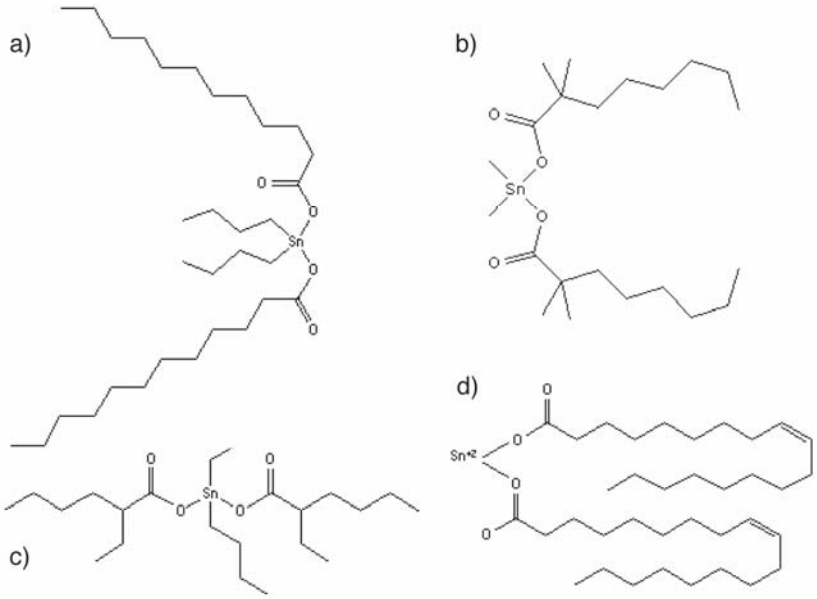

Figure 3.3 Chemical structures for original catalyst a) DBTL-Sn ($C_{32}H_{64}O_4Sn$, M.W. 631.55) and new versions of organotin catalysts b) DMDN-Sn ($C_{22}H_{44}O_4Sn$, M.W. 491.29), c) DBBE-Sn ($C_{24}H_{48}O_4Sn$, M.W. 519.34) and d) Tin-II ($C_{36}H_{66}O_4Sn$, M.W. 680.69).

In this study, we have successfully synthesized microcapsules containing three kinds of new organotin catalysts as shown in figure 3.4. For these catalysts, dimethyldineodacanoate tin has a shorter alkyl chain and di-n-butyl bis(2-ethylenehexanoate) tin has a shorter ester chain than the original catalyst. Furthermore, tin II oleate is Sn^{2+} type catalyst rather than Sn^{4+}. Thus, we expect that they may be more effective than the original catalyst. So, in the next phase of research we investigated the healing efficiency of epoxy vinyl ester systems with various types of lower viscosity PDMS precursors and more effective catalyst containing microcapsules for room temperature self-healing.

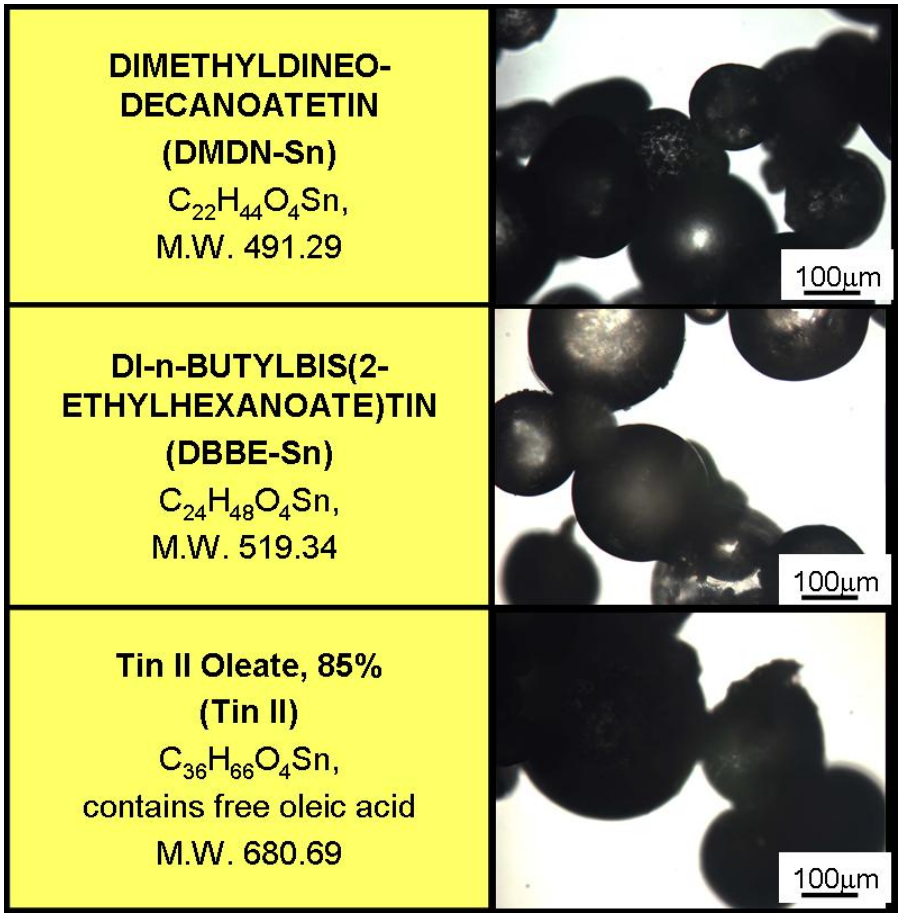

Figure 3.4 Optical microscopic images of synthesized microcapsules containing new organotin catalysts.

To confirm the healing property with these new catalyst-containing microcapsules, we did monotonic tests with TDCB samples. Figure 3.5 and table 3.4 shows the monotonic test result by using lower molecular weight PDMS (S35) and new catalyst containing microcapsules. In the test result, the healing efficiency is increased by using new catalysts at low temperature. The maximum fracture load using DMDN-Sn catalyst was around 20N at room temperature and it was around 30N at 30 ˚C which is almost the same value as the injected control sample test. For the catalytic activity, tin II catalyst almost instantaneously polymerized the PDMS precursor in the case of bulk mixing. However, in actual mechanical testing, the healing property of the tin II catalyst was the worst. If the healing reaction would be too rapid, the self-healing system could not have the sufficient time for diffusion from broken microcapsules to the crack plane. This means that the catalysts may have a reactivity window for a successful healing reaction. In the next step, we tried to optimize the self-healing system for room temperature by further investigation of the viscosity of PDMS healing agent and more effective organotin catalysts.

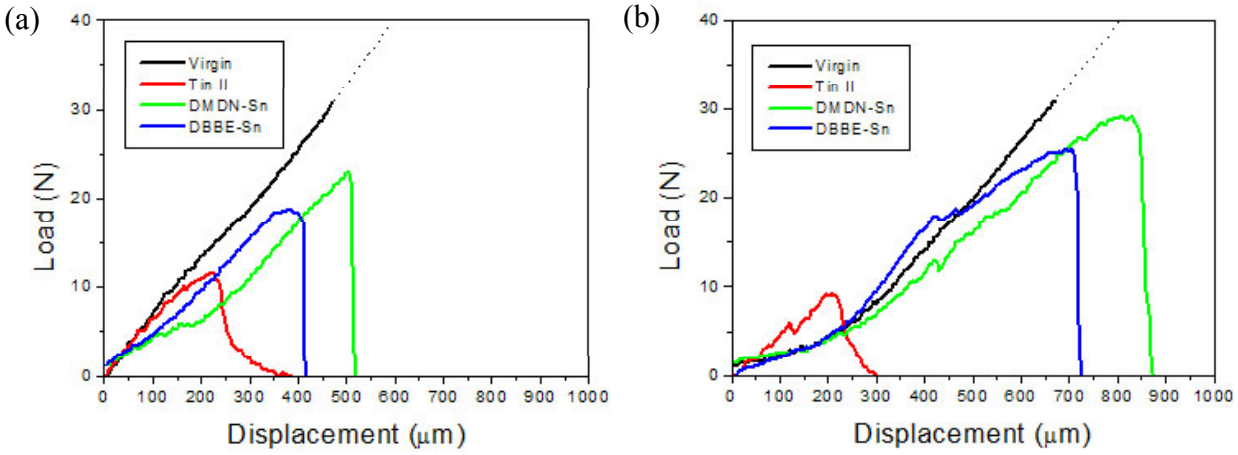

Figure 3.5 Results from monotonic fracture tests with new catalysts containing microcapsules for virgin and fractured samples healed at a) room temperature and b) 30 ˚C.

Table 3.4. Fracture load of self-healed samples with new catalysts by TDCB test.

Catalyst	Fracture load of healed specimen Average Maximum Load (N) [± 1 standard deviation]	
	RT	30°C
DMDN-Sn	14 [±7]	26 [±0.2]
DBBE-Sn	17 [±0.6]	26 [±4]
Tin II	9 [±3]	7 [±3]

3.3 Conclusions

Certain modifications of the original concept, based on phase-separated PDMS healing agent and microencapsulated organotin catalyst, have been necessary to optimize the properties of the self-healing system. The preliminary result suggested that the temperature dependence of the original PDMS self-healing could be partly attributed to the viscosity of the healing agent and that a lower viscosity healing agent would improve fluid transport at lower temperatures. We since then successfully demonstrated higher healing efficiency at 30°C with a lower molecular weight PDMS healing agent than with the original high viscosity agent. To further improve the PDMS self-healing system, other commercially available organotin catalysts with better catalytic activity than the original catalyst were investigated. The changes of those components in self-healing system drove better healing property at reduced temperatures.

3.4 Experimental

The method for urethane microencapsulation with organotin catalyst was described in chapter 2, and monotonic fracture test with TDCB geometry was also covered in chapter 2.

3.4.1 Small Scale Bullet Sample Test

The preliminary tests are performed to compare the healing property of the self-healing composites by small scale bullet sample test. The composed self-healing solution is poured to the bullet shaped mold, and cured at room temperature for 24 hours. The bullet samples are broken at the middle part and re-attached by holding with clamp and metal plate. Samples are healed at room temperature, 30 °C, and 50 °C in a convection oven. The healing property of the test specimens is evaluated by the feeling of adhesion strength ranged from 1 to 5.

3.5 References

1. G. B. Shah, R. W. Winter, *J. Appl. Poly. Sci.* **1996**, *61*, 1649-1654.
2. G. B. Shah, *J. Appl. Poly. Sci.* **1998**, *70*, 2235-2239.

CHAPTER 4

SELF-HEALING COATINGS

Significant components of this chapter are in preparation as S. H. Cho, S. R. White, P. V. Braun, "Self-healing Polymer Coatings" (2006).

4.1 Motivation

Our prior work for the self-healing materials has focused on bulk systems [1], however as we demonstrate here, a very promising new area for autonomic materials may be self-healing coatings. We and others have demonstrated self-healing for repair of bulk mechanical damage in polymers as well as the use of self-healing to dramatically increase the fatigue life of polymers. These systems rely on various approaches for introducing self-healing into material including encapsulation [2-6], phase separation [1], reversible polymerization [7], polyionomers [8], microvascular networks [9], and nanoparticle phase separation [10]. Here we demonstrate, for the first time, self-healing polymer coatings, a very important, yet largely unexplored area of research. Self-healing coatings have the potential to substantially reduce corrosion across a diverse array of applications, potentially dramatically reducing the immense economic cost of corrosion. Importantly, the approach we describe is general, and as we demonstrate, is highly effective for both model and industrially important coatings systems.

4.2 Self-healing Coating System

Inherently, a self-healing coating must be highly stable to environmental effects because it is almost impossible to prevent oxygen and water diffusion through thin polymer films.

Fortunately, we have already demonstrated a self-healing chemistry based on the tin-catalyzed polycondensation hydroxyl end-functionalized polydimethylsiloxane (HOPDMS) and polydiethoxysiloxane (PDES) [1], and thus it was not necessary to develop a new healing chemistry for self-healing coatings. This chemistry is attractive because it is air and water stable, and will operate even after exposure to elevated temperatures (up to 150 °C), an important property since many coatings undergo a thermal cure. The mechanical properties of PDMS are not exceptional; in our prior work, this was reflected in the generally low tensile strength of the damaged region of the sample after healing relative to the starting epoxy. In a coatings application, the mechanical strength of the healing agent is rather unimportant, rather, it is the ability of the healing agent to fill the damage to the coating and the chemical stability of the system that are of paramount importance. Figure 4.1 presents a schematic of a coating damage event, and the subsequent self-healing process in the self-healing coating system described in this thesis. Self-healing coatings are composed of microencapsulated catalysts and phase separated or encapsulated healing-agent droplets in a matrix on a metallic substrate. No reactions take place between the HOPDMS and PDES prior to exposure to the catalyst in a matrix. When the self-healing coating layer is damaged by cracking or scratches, the catalyst released from microcapsules and the healing agent wets the damaged plane. Diffusive mixing event of healing agent and catalyst follows in the damaged region. Finally, the damage of coating layer is healed by crosslinked PDMS, which protects the substrate from the environment.

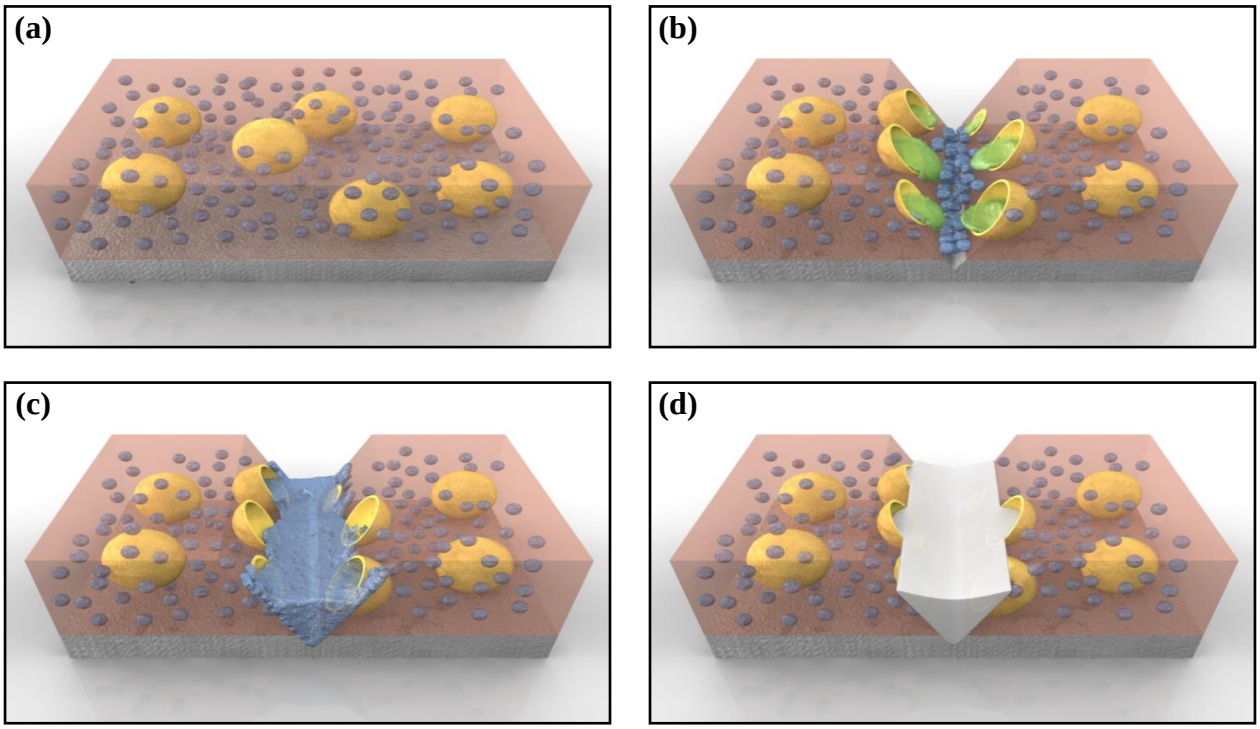

Figure 4.1 Schematic of self-healing process. a, self-healing coating containing microencapsulated catalyst (yellow) and phase separated or encapsulated healing-agent droplets (blue) in a matrix (pink) on a metallic substrate (grey); b, damage to the coating layer releases catalyst (green) and healing agent; c, diffusive mixing of healing agent and catalyst in the damaged region; d. damage healed by crosslinked PDMS, protecting the substrate from the environment.

4.3 Self-healing Coating Fabrication

To apply the self-healing coatings on a metal substrate, we first investigated the optimum fabrication method of the self-healing coatings. Self-healing polymer solution can be coated on the metal substrates by means of various coating tools such as bar coater, doctor blade type coater or spay coater.

4.3.1 Self-healing Coatings with Bar Coater

Self-healing polymer was first spread on the metal substrates by a bar coater (figure 4.2a). The bar coater has wound wire on the bar which is related with the coating thickness. It is very easy and convenient coating tool for thin coating but it revealed a problem, especially for highly viscous solutions. For thick coatings, the result was an uneven stripe shaped coating layer (figure 4.2c). The test samples for corrosion test were coated by the epoxy vinyl ester based solution on the cold rolled steel sheet. For the healing reaction, the coated samples were scribed (×-cut) by a razor blade and healed at 50 ˚C for 24 hours. The test specimens were dipped in salt water for the accelerated corrosion test (figure 4.2b). Figure 4.2c shows the corrosion test results of the *in situ* sample coated by bar coater after 120 hours of the corrosion test. The coating thickness was around 175 μm with No. 75 bar coater according. In the corrosion test result, the corrosion propagation was not uniform on the sample surface due to the uneven coating layer so that we could not distinguish actual corrosion propagation between control and *in situ* samples. Thus, other, more effective coating tools for applying the coating solution were necessary to investigate.

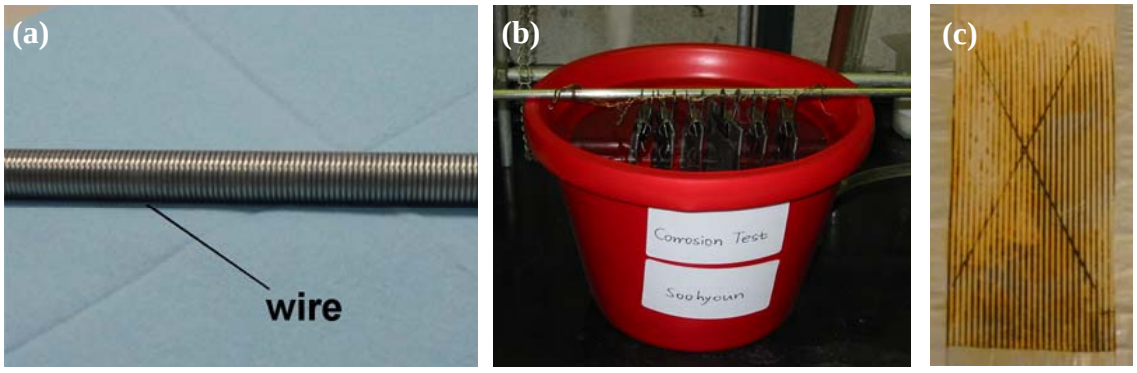

Figure 4.2 a) Bar coater applicator for fabricating coated steel samples. b) Set-up for corrosion tests in an aqueous solution of sodium chloride. c) Epoxy vinyl ester coated steel corrosion test sample after scribing and 120 h exposure to salt water.

4.3.2 Self-healing Coating with Doctor Blade Type Coater

In our previous section (4.3.1), it was shown that the variation in coating thickness associated with the bar coater application method strongly influenced the oxidation progression. Consequently, no consistent observations could be made from control tests performed on the samples coated on cold rolled steel sheets using the bar coater. Our coating deposition efforts were then directed to establish a more reliable and repeatable coating procedure. One promising coating tool is a doctor blade type coater which is more appropriate for thick coatings. The coating thickness can be controlled through a micrometer and the coating layer thickness could be varied from 25.4 to 12,700 μm. The applicability of the doctor blade type coater was investigated for the self-healing coating. To make samples for corrosion testing, the self-healing solution was coated on cold rolled steel sheets by a doctor blade type coater. The mixed self-healing coating solution was applied on metal substrates by a pipette and it was spread out by dragging the doctor blade type coater. The thickness of coated layer was controlled by dial adjusting of coater. In the experimental demo pictures (figure 4.3), it could be observed that the coating is relatively uniform.

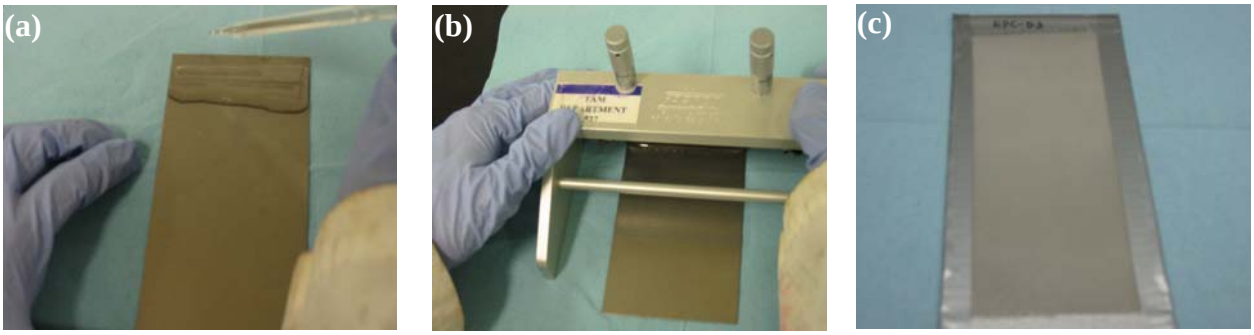

Figure 4.3 Procedure for surface coating fabrication with doctor blade coater. a) Application of coating solution by pipette. b) Coating thickness adjustment by threaded dials. C) Coated steel test sample.

4.4 Anti-corrosion Property of the Self-healing Coatings

The properties of self-healing coatings based on phase separated PDMS healing agents and microencapsulated catalyst were first evaluated through corrosion testing and compared to control samples missing at least one component required for self-healing to confirm the self-healing mechanism (figure 4.4). All samples contain adhesion promoter, without it, delamination of the coating occurred, invalidating the healing test. Damage was applied by scribing an X through the coating and into the substrate using a razor blade.

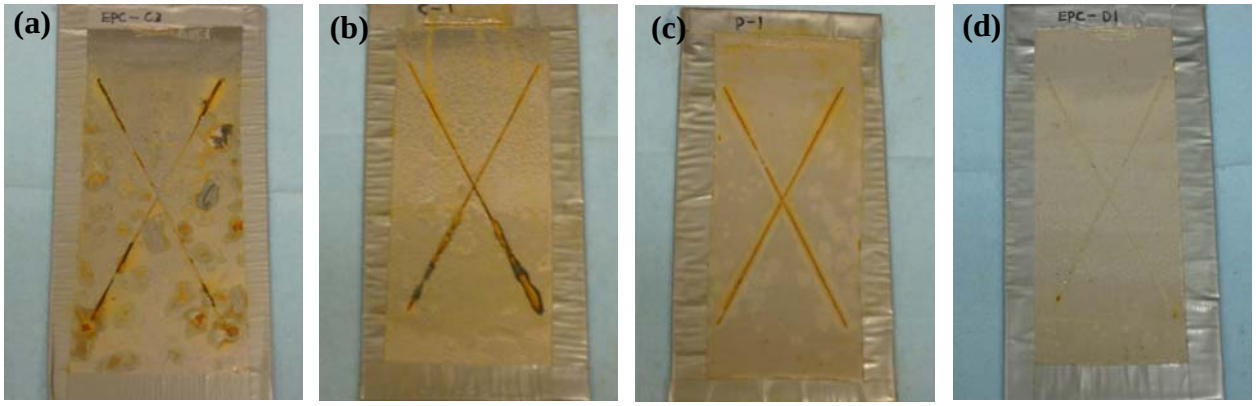

Figure 4.4 Corrosion test results for control and self-healing coatings. The polymers are composed of a, matrix (epoxy vinyl ester) and adhesion promoter (methylacryloxy propyl triethoxy silane, 3 wt%); b, matrix, adhesion promoter, and 3 wt% of tin catalyst (dimethyldineodecanoate tin containing microcapsules); c, matrix, adhesion promoter, and phase separated PDMS healing agent (12 wt% mixture of HOPDMS and PDES); d, the self-healing coating consisting of matrix, adhesion promoter, microencapsulated catalyst, and PDMS healing agent. The corrosion test samples are 75 x 150 mm^2 (width x length). Samples were healed at 50 °C. Images are taken after immersion in salt water for 120 hours.

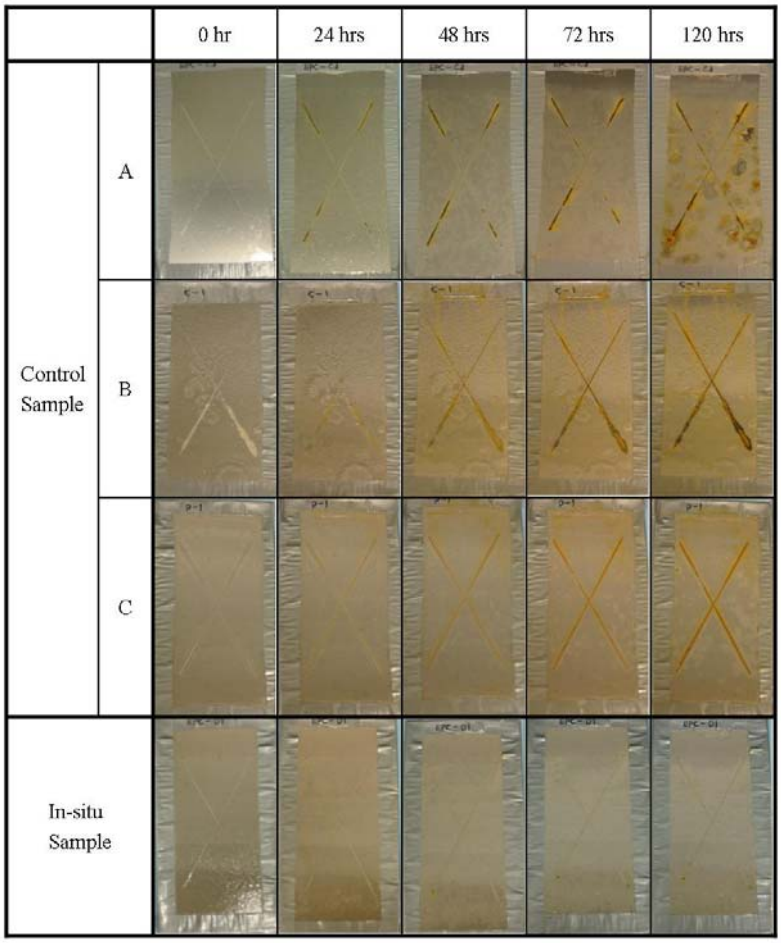

Figure 4.5 Corrosion test result of specimens of control and in situ samples according to dipping times in 5 wt% NaCl aqueous solution. Polymer coating solution is composed of control a, matrix (epoxy vinyl ester) and adhesion promoter (methylacryloxy propyl triethoxy silane, 3 wt%); control b, matrix, adhesion promoter, and microencapsulated tin catalyst (dimethyldineodecanoate tin, 3 wt% of total microcapsules); control c, matrix, adhesion promoter, and phase separated PDMS healing agent (12 wt%, mixture of HOPDMS and PDES); *In situ*, matrix, adhesion promoter, microencapsulate catalyst, and PDMS healing agent (self-healing). The size of corrosion test samples is 75×150 mm^2 (width ×length). Samples were healed at 50 °C.

Coatings were allowed to self-heal for 24 hours at room temperature (~20 °C), 30 °C, or 50 °C. The samples were subsequently immersed in a salt water solution. All control samples rapidly corroded within 24 hours, while the self-healing samples did not show any evidence of corrosion (red rust) even after 120 hours in salt water (figure 4.4 & 4.5). This experiment was highly repeatable, and the self-healing nature of the coating was not dependent on minor variations in composition or coating thickness. The self-healing coatings consistently protected the substrate from corrosion for 120 hours.

4.5 Electrochemical Test

Along with morphological and corrosion tests, a quantitative measure of the quality of a coating is an electrochemical test. Here we measure the steady-state conduction between the metal substrate and an overlying 1M NaCl electrolyte, at a constant potential of 3V.

4.5.1 Electrochemical Test Facility

As already described, the anti-corrosion properties of self-healing coated specimens was qualitatively confirmed by corrosion tests in salt water. In this section, a quantitative electrochemical test was applied to verify the anti-corrosion property of the self-healing coatings. An electro-chemical cell is made of 4 cm glass tube filled with 1 M NaCl in water (figure 4.6).

The cell is attached on the specimen with two part epoxy adhesive. The anode is connected to the platinum electrode and the cathode is connected to the sample. The current value of the samples is measured at a constant voltage through the cell using 236A Potentiostat/Galvanostat (PerkinElmer).

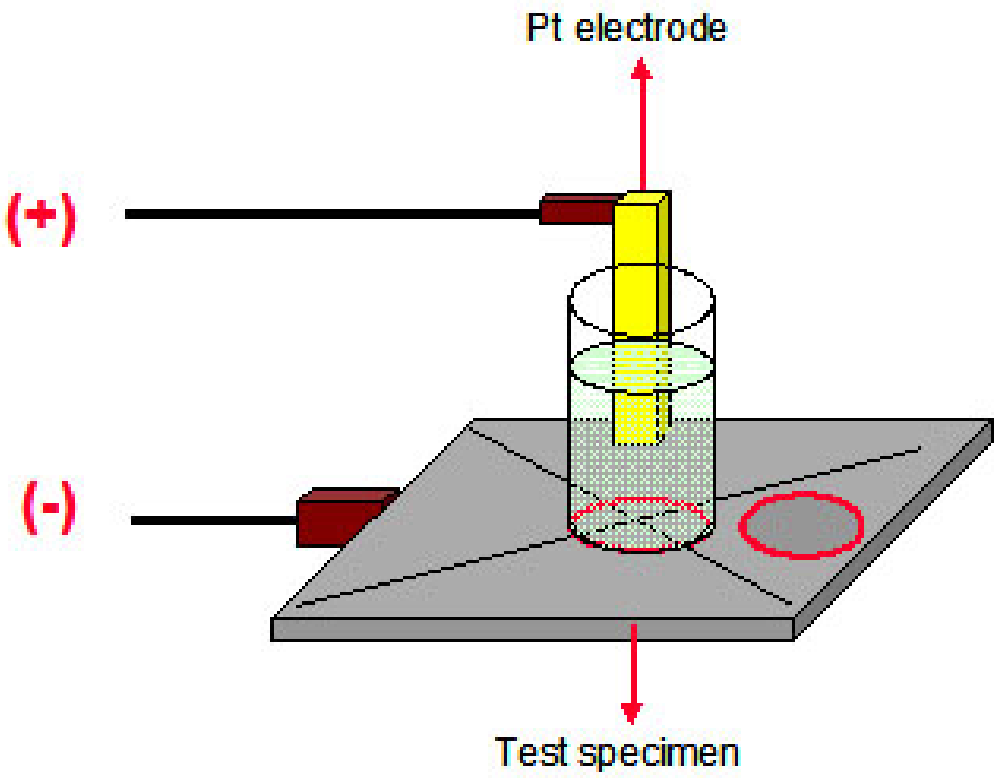

Figure 4.6 Electrochemical corrosion test set-up. The current is measured both over the scratched region and away from the scratch (red circle to right).

4.5.2 Electrochemical Current

To compare the electrochemical properties of both control samples and self-healing samples, the electrochemical current values was measured at a constant voltage. The test specimens were prepared by polymer coating on a metal substrate. Then they were scribed by a razor blade and followed by healing reaction at 50 °C for 24 hours. Figure 4.7 shows the electrochemical current of the test specimens at constant voltage (100 mV) in a cell containing pure water. The final current of control sample was 2.6 $\mu A/cm^2$ while the current was almost zero for *in situ* sample. The control sample also exhibited a slowly increasing current increasing up to

~100 seconds due to electrochemical etching of the damaged part of metal substrate, which probably increased the effective surface area.

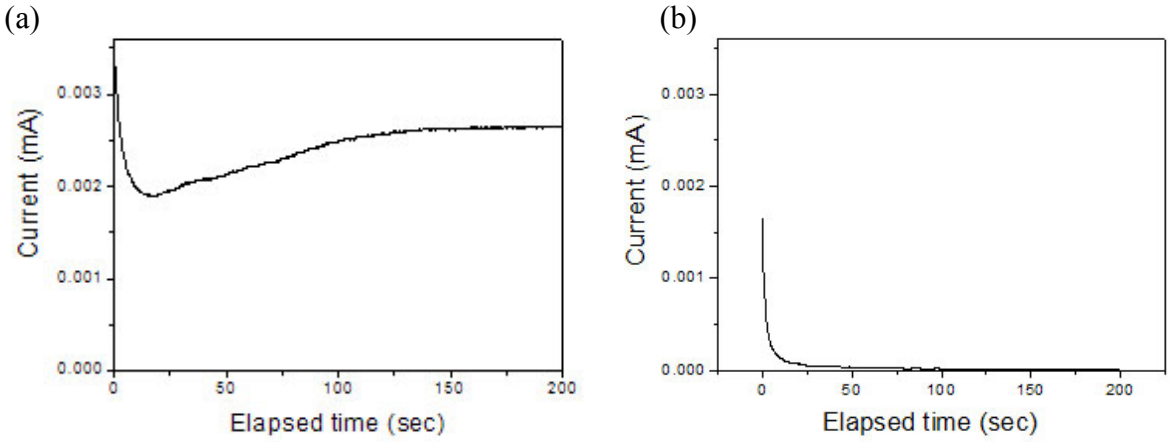

Figure 4.7 Electrochemical test result of polymer coated metal substrate in pure water. (a) Scratched part of control sample and (b) scratched part of self-healing sample.

The electrochemical current value of samples was also compared in a salt water containing cell. The current passing through the control and self-healing polymer coatings before scribing are almost identical, ~0.34 $\mu A/cm^2$ (figure 4.8a). After scratching, samples were allowed to heal and were tested in the electrochemical cell. The current passing through self-healing samples ranged from 12.9 $\mu A/cm^2$ - 1.4 mA/cm^2 (4 samples) while the current passing through the control sample was much larger, 26.6 - 58.6 mA/cm^2 (3 samples). Typical data is presented in figure 4.8b. The experimental data from the electrochemical tests is also summarized in table 4.1. It should be noted that the control sample was evolving gas during the experiment, so the current was probably kinetically limited. There was no gas evolution from the self-healing sample.

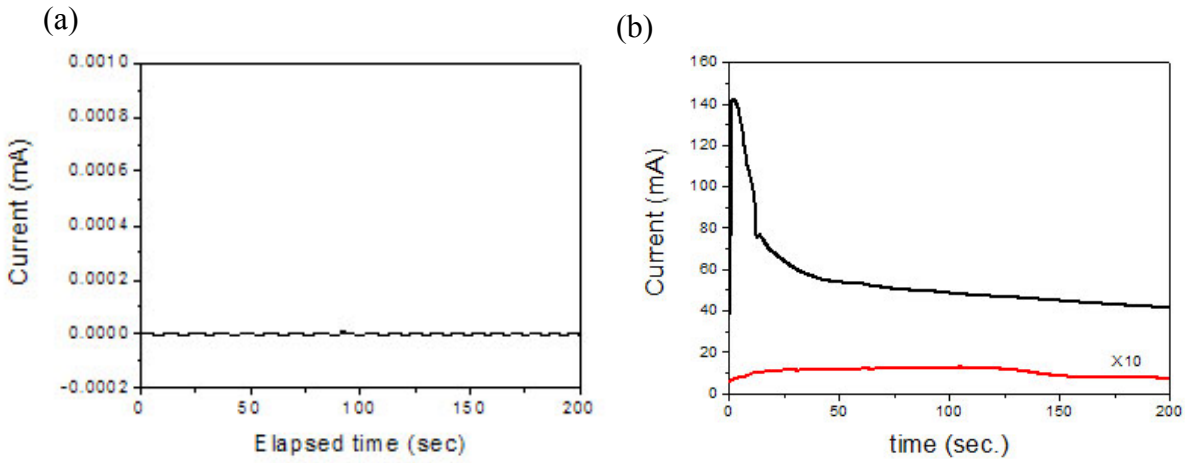

Figure 4.8 Electrochemical test result of polymer coated metal substrate in 1 M sodium chloride aqueous solution. (a) Unscratched part of specimens and (b) Scratched part of control (black) and self-healed sample (red).

Table 4.1. The electrochemical current values of the test specimens by electrochemical tests.

Damage	Current value	
	Control	Self-healing coating
Before scribing	0.34 μA/cm^2	0.32 μA/cm^2
After scribing	26.6 mA/cm^2	12.4 μA/cm^2
	41.3 mA/cm^2	0.59 mA/cm^2
	58.6 mA/cm^2	0.74 mA/cm^2
		1.4 mA/cm^2

4.6 Surface Morphology of the Self-healing Coatings

Corrosion prevention is only indirect evidence that the substrate has been passivated. To better evaluate morphology of the self-healing coating, scanning electron microscopy (SEM) were collected from self-healing and control samples (figure 4.9). It is very apparent that the

damage is significantly filled by cured PDMS in the self-healing coating, while the cut extends well into the metal substrate in the control sample (figure 4.9).

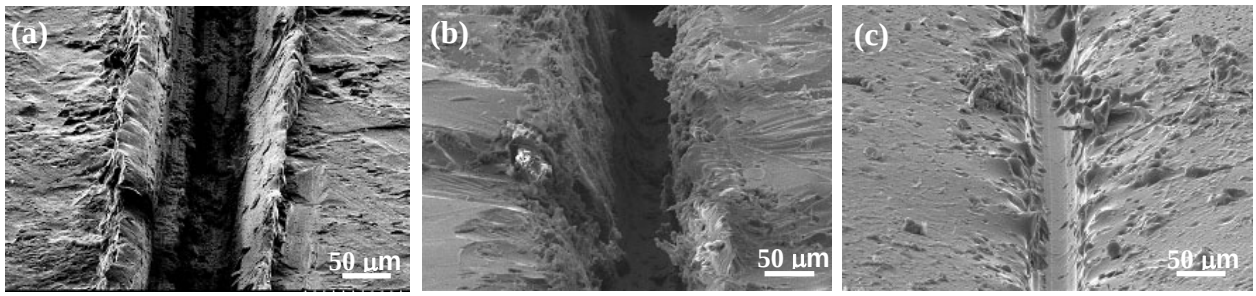

Figure 4.9 SEM acquired from metal substrate, control, and self-healing coatings. SEM of a scratch in (a) metal substrate, (b) control, and (c) self-healing coating after allowing for healing.

4.7 Cross Sectional Observation

The healed surface of the control and self-healing coated samples was investigated in the previous section (chapter 4.6). However, for more detailed observations, it was attempted to observe evidence of successful self-healing through cross sectional observations using optical microscopy and SEM.

4.7.1 Optical Microscopy

For the cross sectional observation, the specimens were cut by slow speed diamond saw, followed by mounting in epoxy resin and polishing with diamond paste (1 μm grid). The healing effect of self-healing polymer coating is first investigated by optical microscopy. In a cross sectional view of a self-healing polymer coating on a metal substrate, it can be observed by optical microscopy that the scratch damage on a metal substrate seems to be successfully covered by the healed self-healing coatings (figure 4.10).

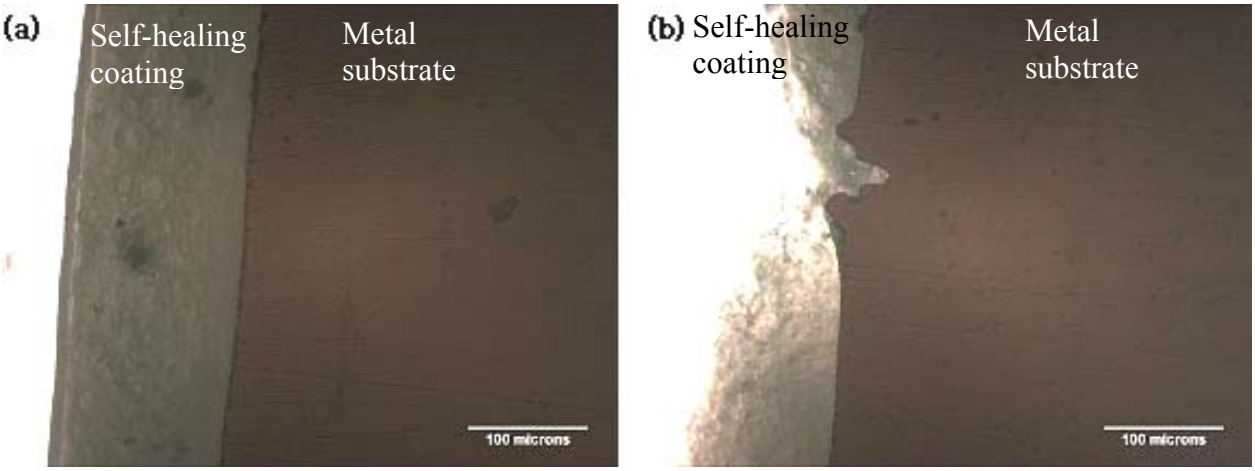

Figure 4.10 Cross sectional view of the self-healing coatings on a metal substrate by optical microscopy. (a) Undamaged part and (b) damaged part of the self-healing coated sample.

Next, it was investigated whether the damaged part of metal substrate is covered by healing agent or not. It could be observed that the scribed damage was penetrated into a certain depth of a metal substrate and covered by healing agent. If the damage was not covered by polymer layer, it would show serious corrosion in the salt water dipping. So, this can explain the excellent anti-corrosion property of self-healing samples during the corrosion test.

4.7.2 Scanning Electron Microscopy

The healing reaction of the self-healing polymer coatings is also investigated by SEM for higher magnification observation. The procedure for sample preparation was the same as the optical microscopic observation. The self-healing polymer coating layer and metal substrate could be observed by SEM. However, it was difficult to distinguish between epoxy molding compound and PDMS healing agent in the damaged part even by back scattered imaging (figure 4.11).

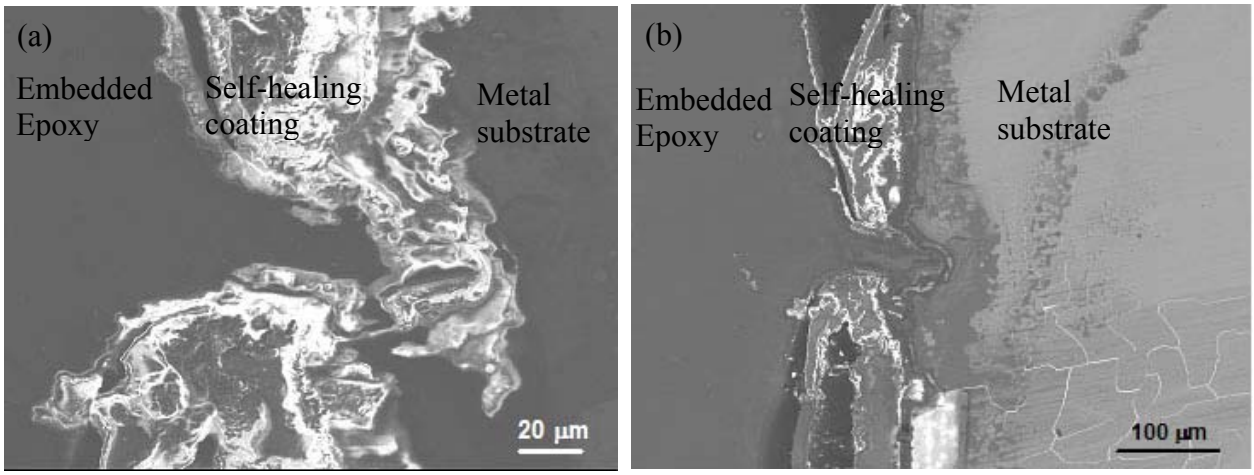

Figure 4.11 Cross sectional view of the self-healing coatings on a metal substrate by scanning electron microscopy. (a) Secondary electron image of sample 1 (image was taken from the scratched region) and (b) back scattered image of sample 2.

The same elements were basically observed in the damaged and undamaged parts of specimens (carbon, oxygen, silicone, and iron). The purpose of this elemental mapping was to observe different elemental distributions between epoxy and PDMS healing agent. However, the result revealed that the elemental distribution was not effective to observe the healed region (figure 4.12). It was suspected that the sample surface might be covered by healing agent due to the secondary healing reactions during the polishing process. For our next step, it was intended to use electroless nickel coating to obtain more obvious images to determine the details of the successful healing reactions. The electroless nickel should highlight the interface between epoxy and healing agent enabling direct SEM observation, even if secondary healing is taking place.

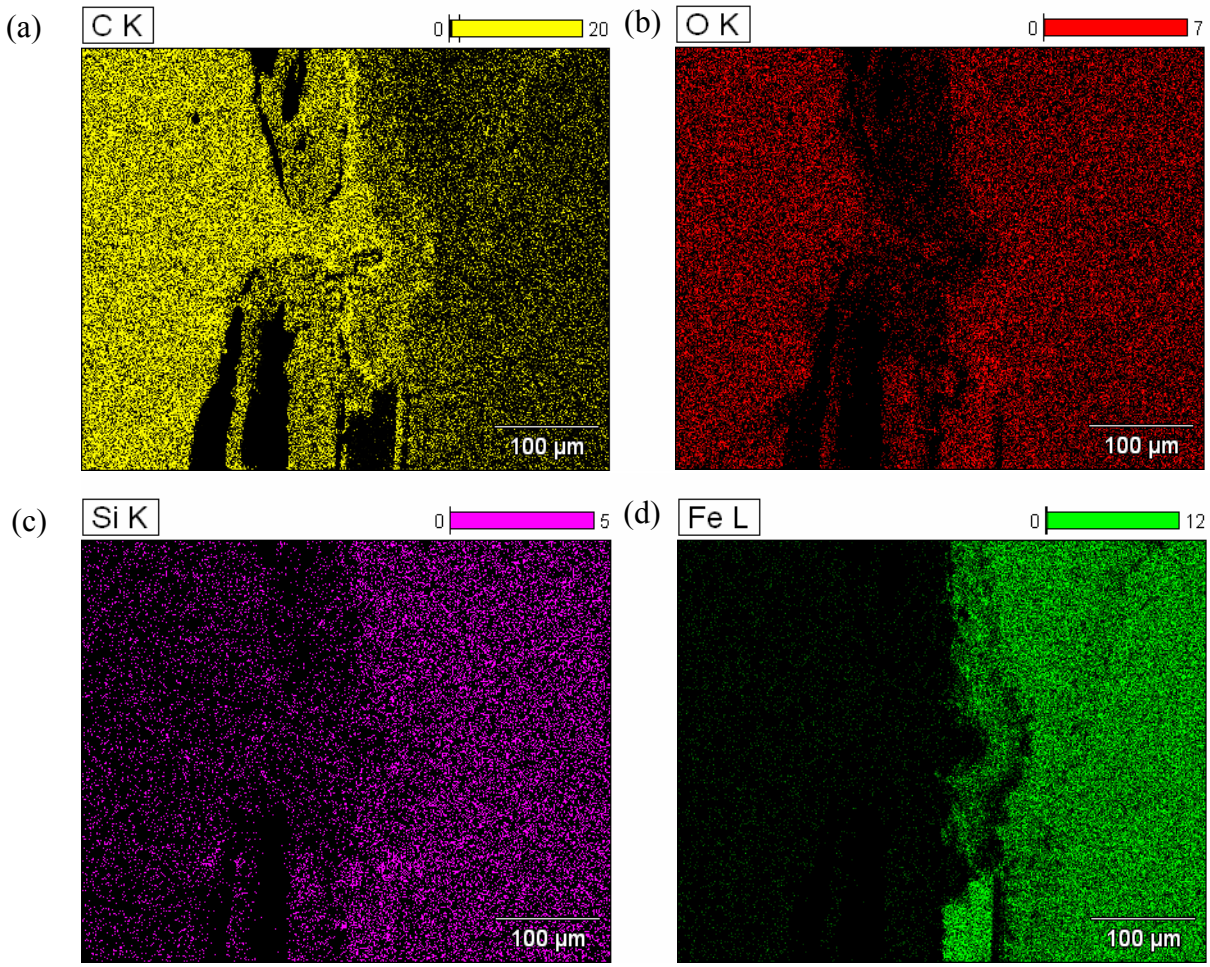

Figure 4.12 Cross sectional view of the self-healing coatings on a metal substrate (sample in figure 4.11b) by elemental mapping of scanning electron microscopy for (a) carbon, (b) oxygen, (c) silicone, and (d) iron.

4.7.3 Electroless Nickel Coating

Electroless nickel coating was induced to obtain a more definitive marker of the healed regions of the sample. The nickel layer is applied to the sample surface before the mounting process, highlighting the interface between the epoxy molding compound and healing agent (figure 4.13). The electroless nickel coating was performed using a commercially available

solution (20-8192 EDGEMET®KIT), was composed of pre-cleaning and main coating solution (solutions A&B). The sample treatment procedure is outlined in table 4.2. The thickness of the nickel layer is proportional to dipping time of the sample in the coating solution.

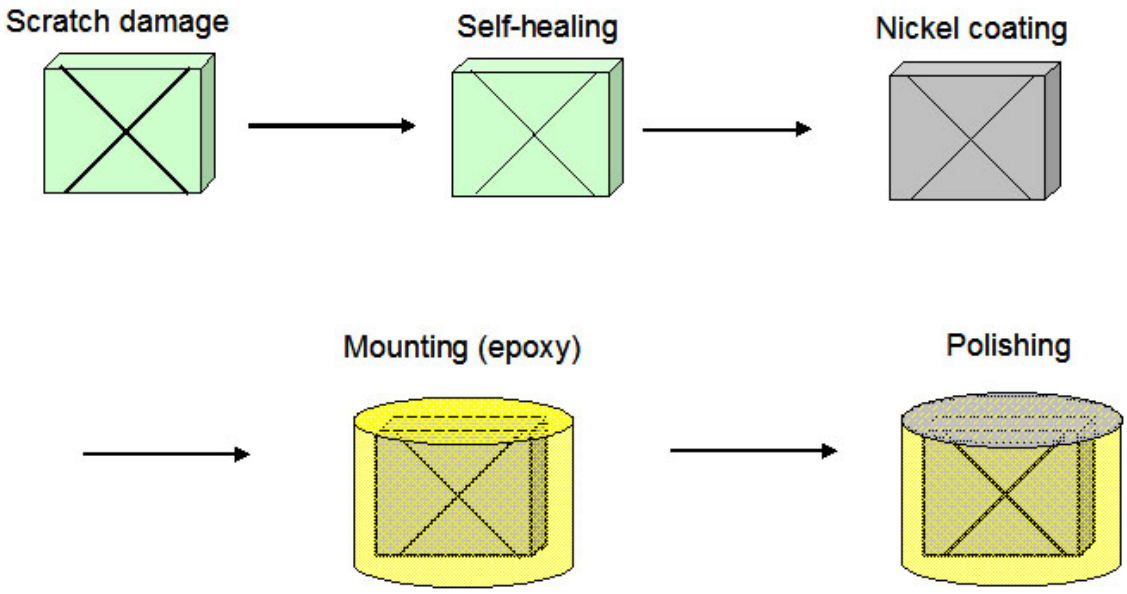

Figure 4.13 Procedures of sample preparation for cross sectional view of the self-healing coatings on a metal substrate by scanning electron microscopy with electroless nickel coating.

In a cross sectional view of self-healing coated sample, the highlighted interface could be observed by electroless nickel coating layer (figure 4.14), which distinguished the healing agent from epoxy molding compound. The nickel interface showed that the damaged part of metal substrate was not filled by epoxy molding compound. It could be also confirmed that the damaged part was covered by polymeric material, PDMS healing agent, by carbon mapping (figure 4.15). Thus, it was proved that scratch damage was healed by healing agent through self-healing reaction. In addition, nickel coating layer and metal substrate were pronounced by

elements mapping such as nickel and iron. This observation provides additional evidence of the successful healing reaction of self-healing coatings.

Table 4.2. Procedures of electroless nickel coating with 20-8192 EDGEMET®KIT.

Step	Purpose	Bath Composition	Comments	Time
1	Cleaning	Any available solvent-acetone, trichloroethane, MEK, etc.	Use gentle agitation	2 min
2	Cleaning	25-35 pellets of NaOH in one cup of distilled water	Save and re-use. Hold specimen with clamp	2 min
3	Cleaning	Pre-clean, full strength	Save and re-use	5-30 sec.
4	Application of EDGEMET®	Equal parts of solution A and B – minimum amount 75ml of each	Use at approx. 185 ºF Use only once	2 hours or longer

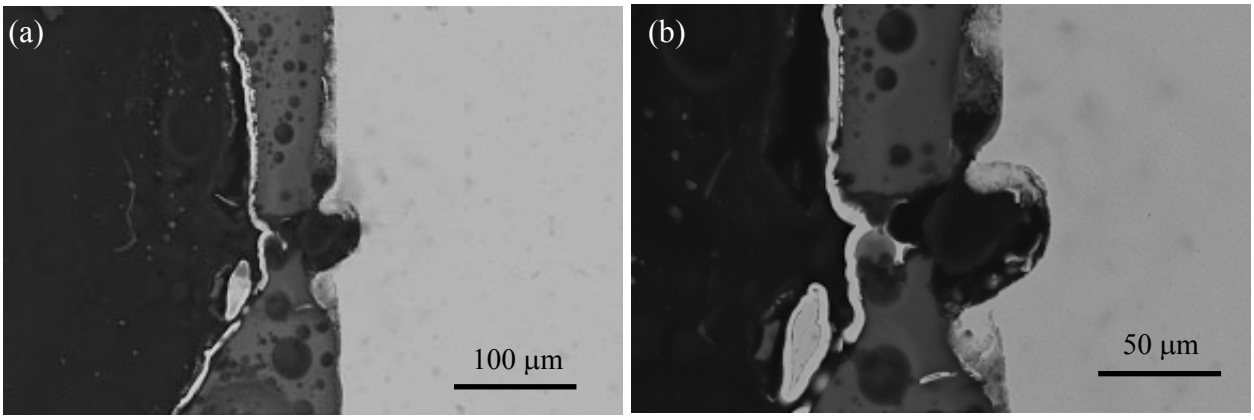

Figure 4.14 Cross sectional view of the self-healing coatings on a metal substrate by scanning electron microscopy with electroless nickel coating at the interface between epoxy molding and self-healing coated sample. (a) Lower magnification and (b) higher magnification.

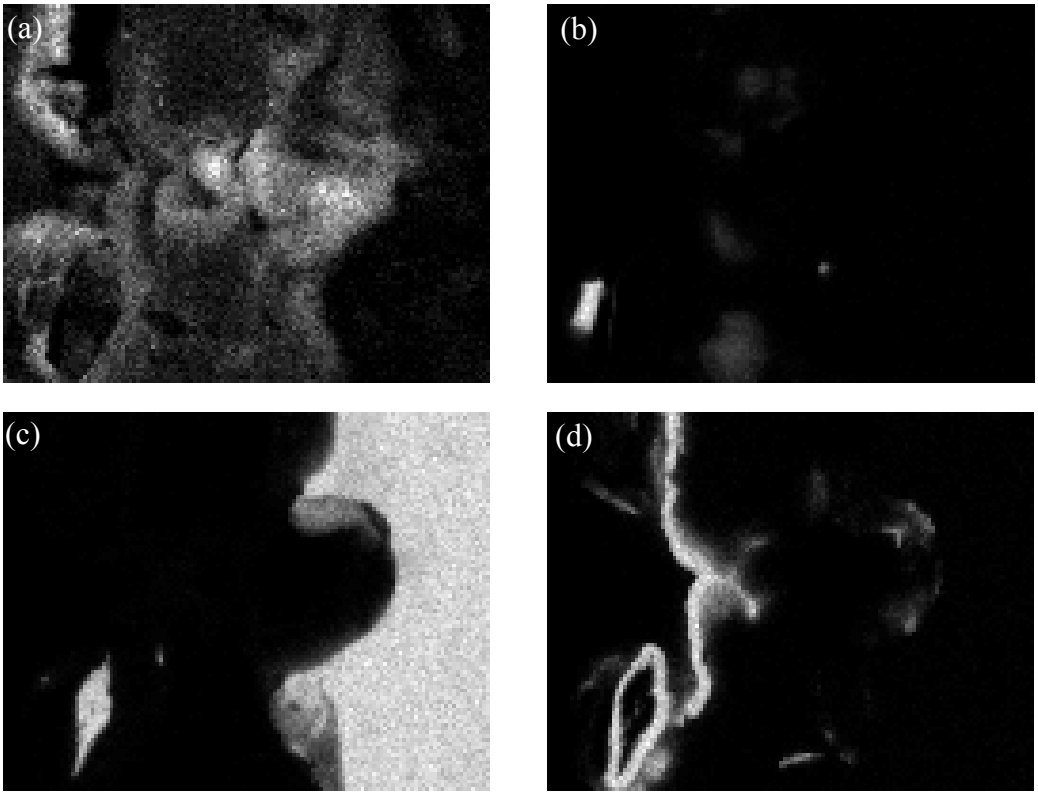

Figure 4.15 Cross sectional view of the self-healing coatings on a metal substrate with electroless nickel coating at the interface between epoxy molding and self-healing coated sample by elemental mapping of scanning electron microscopy for (a) carbon, (b) silicone, (c) iron, and (d) nickel.

4.7.4 Direct SEM Observation

In principle, it would be much better if we could obtain images of self-healing without mounting the samples in epoxy. The electroless nickel experiments do provide evidence of successful healing reactions. However, direct SEM observation would give clearer evidence. For direct polishing of samples without mounting, a special polishing tool was used to hold small metal samples (figure 4.16), preventing fluctuating of samples during polishing, providing an evenly polished surface.

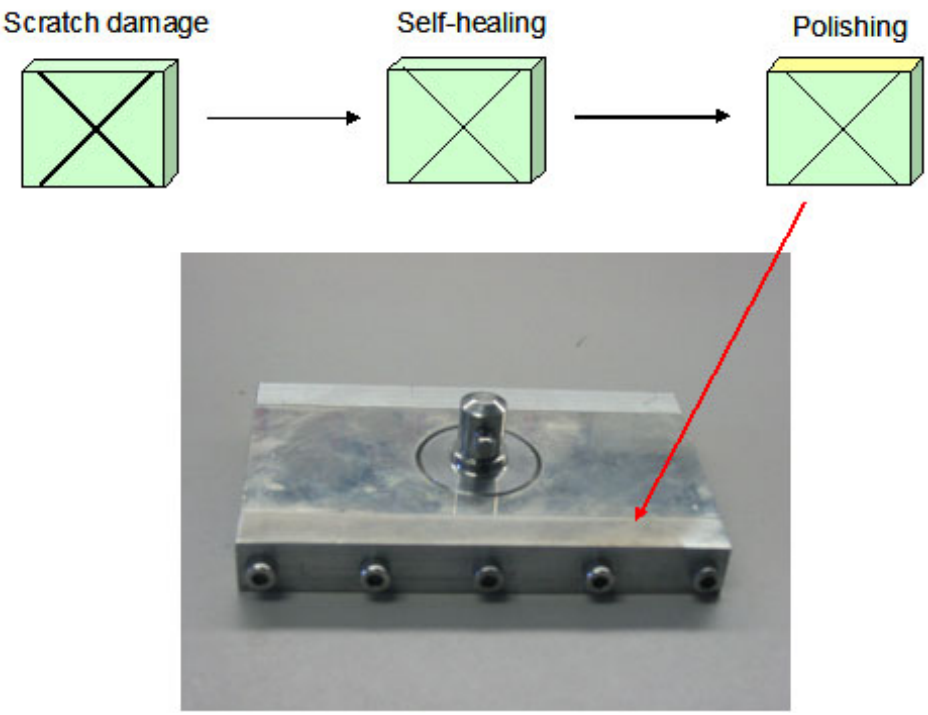

Figure 4.16 Procedures of sample preparation for cross sectional view of the self-healing coatings on a metal substrate by scanning electron microscopy without epoxy molding.

In this observation, SEM images show the cross sectional view of samples by direct SEM observation without epoxy molding (figure 4.17). However, the scratches were completely filled due to secondary self-healing from liquid PDMS released during the polishing process. As a result, the entire damaged part of polymer layer is filled with healing agent through secondary healing reactions, and it is difficult to determine the interface between secondary healing and the original self-healing reaction (figure 4.17). Basically, the self-healing is working very well. A number of attempts to circumvent this problem were tried including extraction of healing agent with hexane and ultrasound, and filling of the crack with wax prior to polishing, but both

approached did not work. In the next section a more, however still not completely successful approach, the procuring of the healing agent through a high temperature treatment is described.

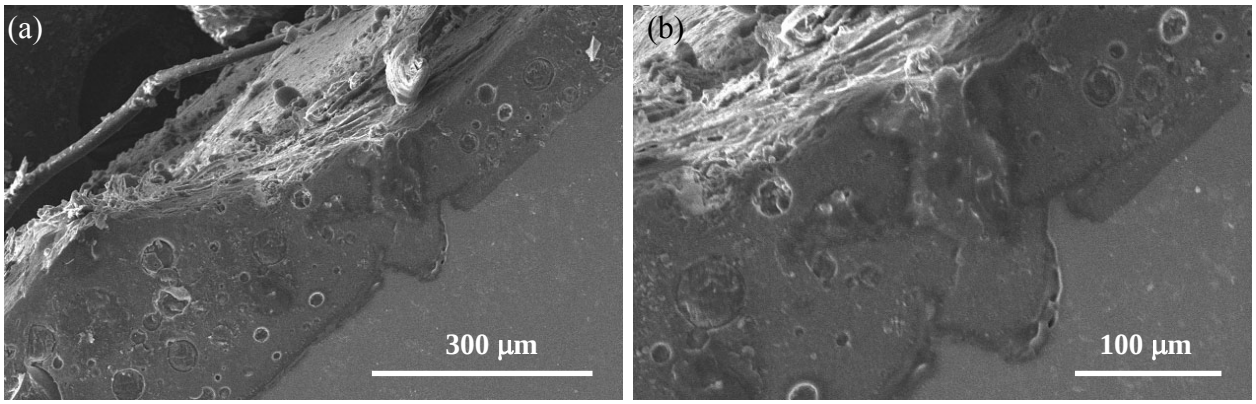

Figure 4.17 Cross sectional view of the self-healing coatings on a metal substrate by scanning electron microscopy without epoxy molding. (a) Lower magnification and (b) higher magnification.

4.7.5 Heat Treatment

To avoid secondary healing, self-healing coated samples were put into a convection oven at 170 °C for 24 hours after healing reaction, driving the thermal polycondensation reaction of the healing agent, hydroxyl end-functionalized PDMS (HOPDMS) and polydiethoxysiloxane (PDES). This reaction only takes place above 150 °C unless the catalyst is present (the case for self-healing). Now during polishing, no liquid PDMS is released, and SEM images of self-healed samples could be collected (figures 4.18).

The problem during the heat treatment was that the polymerized healing agent on the side edges of the damage groove appeared to delaminated from the matrix, so it could not provide the perfect image of the successful self-healing (figure 4.19). However, the presence of cured PDMS healing agent on the bottom of the damaged regions is clearly present. Thus, now have

clear SEM evidence that self-healing coatings can effectively cover scratch damage in metal substrates. Consequently, the images of the successful self-healing coatings which proved the protection of the damaged surface were achieved through the SEM observation in a surface and cross sectional observation.

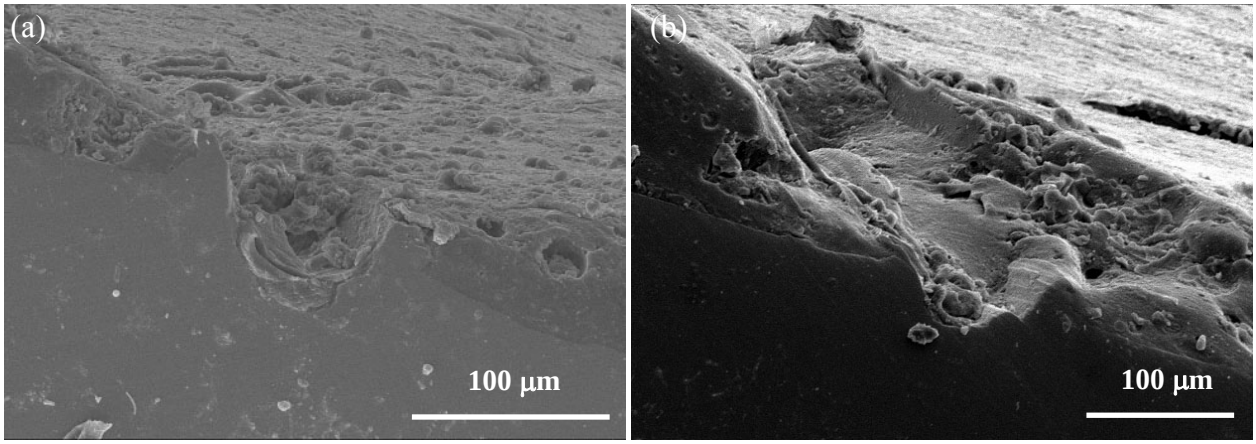

Figure 4.18 Cross sectional view of the self-healing coatings on a metal substrate treated at 170 °C for 24 hours by scanning electron microscopy. (a) Sample 1 and (b) sample 2.

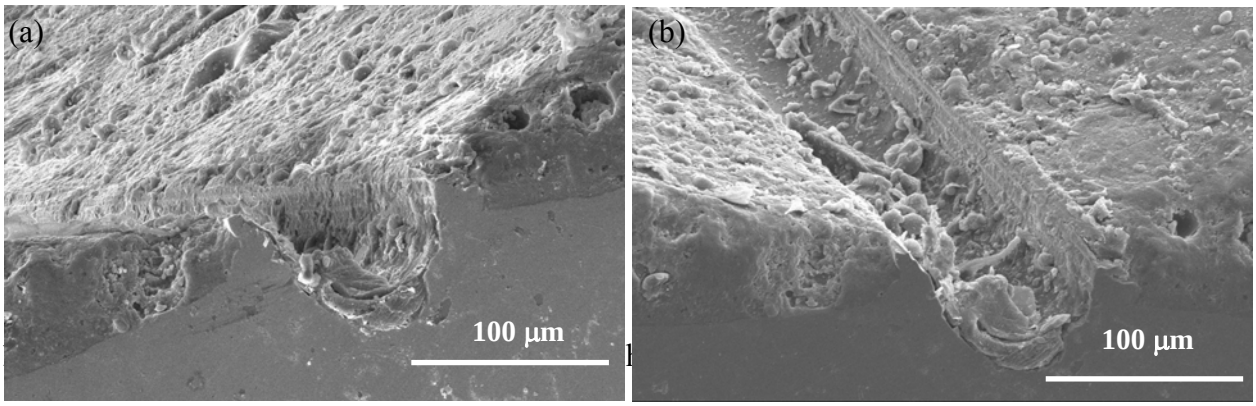

170 °C for 24 hours by scanning electron microscopy. Samples are tilted for observing the bottom surface of damages after healing reaction. Tilted images of sample 1 by (a) 30° and (b) 60°.

4.8 Surface Profile

Using profilometry, the surface morphology of damaged and subsequently healed test samples were compared to confirm the successful self-healing. The surface topography of polymer coated specimens was measured for both control samples and self-healing samples. Surface profilometry (Sloan Dektak^3 ST stylus surface profilometer) can measure minute physical surface profile down to a few nm as a function of position using a diamond stylus (tip diameter 2.5 μm), in contact with a sample. The surface profile of metal substrate and polymer coating layer was first investigated (figure 4.20). The metal substrate showed a surface roughness of 5 μm (figure 4.20a). The polymer coating layer had a much larger surface profile which ranged by 50 μm (figure 4.20b), most of this variation was caused by the large size of the microcapsules; smaller microcapsules will almost certainly result in smoother samples.

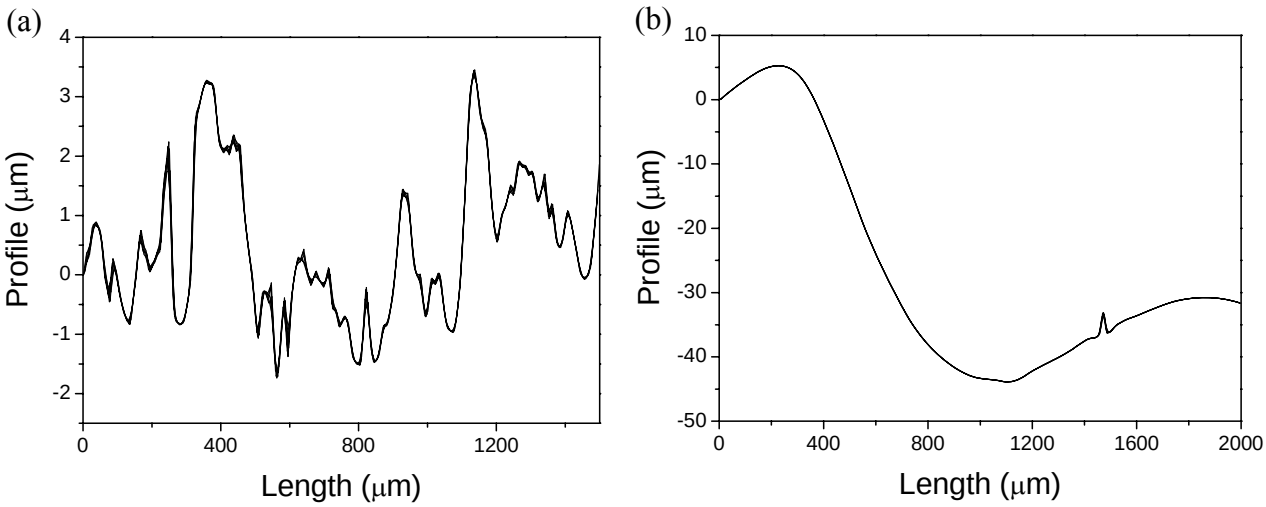

Figure 4.20 Surface profile of undamaged parts of test sample by surface profilometry. (a) metal substrate and (b) polymer coating layer.

Profilometry provides similar evidence for crack infilling as SEM observation (figure 4.21). The depth of cut in the control samples was ~120 μm, while the cut depth in the self-healing sample was considerably less, between 40 and 70 μm, depending on if the cut is

measured as starting from the initial top of the sample, or from the edge of the cut. The gradual slope of the surface of the coating away from the edge of the cut gives some insight into the mechanism for crack healing. The material that fills in the crack has to be provided from somewhere, the slumping on either side of the crack is strong evidence that PDMS healing agent has been released from either side of the cut, and has flowed into the cut. The smaller size of the microcapsules was used for the surface profilometry because of the thickness limitation (130 μm) of the profilometry instrument. The surface morphology above the thickness limitation was indicated by red line so that we could not observe the profile beyond the range (~130 μm).

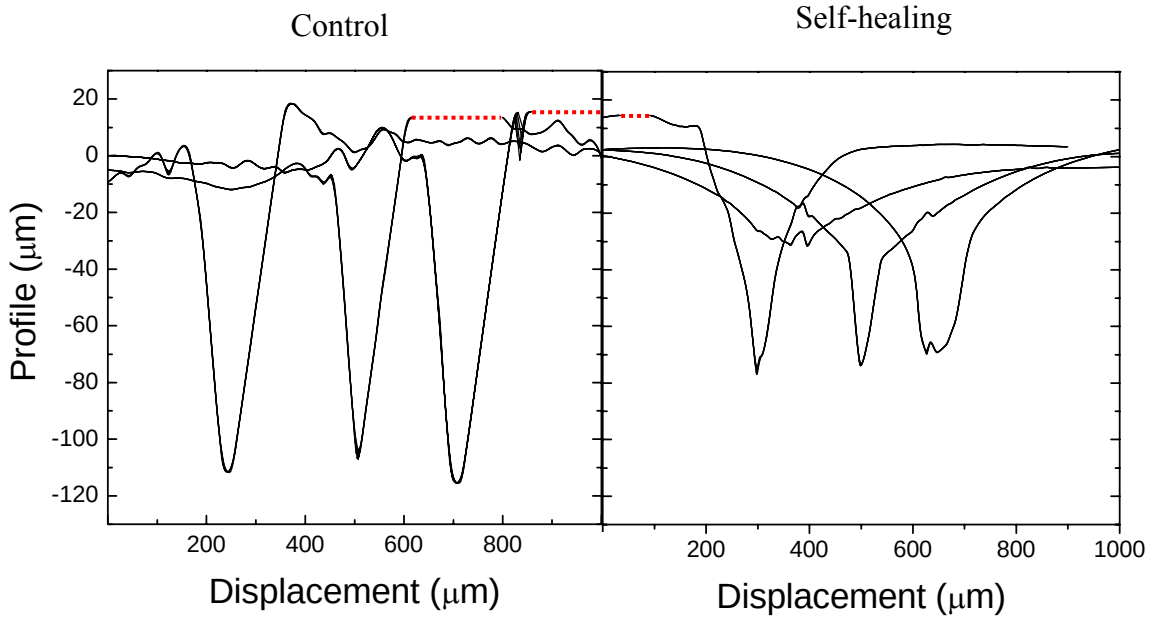

Figure 4.21 Surface profile of collected from control (no self-healing) and self-healing coatings after damage and sufficient time to allow healing reactions to take place. Red dots indicate the surface morphology beyond the thickness limitation by instrument.

4.9 Conclusions

The healing effect in damaged parts of the polymer composite was confirmed in the previous chapters when an internal crack was propagated into matrix material. In this chapter, the excellent anti-corrosion effect of the self-healing coatings was successfully demonstrated by a corrosion test, immersion of the scribed specimens after healing in salt water. For self-healing coatings, structural recovery is secondary to the ability to physically reseal surface damage. We were able to demonstrate a self-healing coating system based on phase separated healing agents and microencapsulated tin catalysts in a matrix for surface protection against corrosion. The electrochemical study provided a quantitative comparison of the self-healing coatings, which showed a lower electrochemical current value than the control sample. The morphology of the self-healed coatings was investigated by microscopic observation and surface profilometry. Consequently, it was proved that the self-healing coatings successfully protected the scratch damage, which resulted in corrosion prevention of the metal substrate in corrosive environments.

4.10 Experimental

The synthetic method for tin catalyst containing microcapsules by interfacial polymerization with polyurethane shell is described in chapter 2.

4.10.1 Coating Fabrication

The coating solution was cured using benzoylperoxide (BPO) and dimethylaniline (DMA) as the initiator and activator, respectively. 1 wt% BPO was dissolved in the prepolymer. After the BPO was completely dissolved, the mixture of HOPDMS and PDES was added into the prepolymer with mechanical stirring, followed by degassing under vacuum. The microcapsules containing tin catalyst were then mixed with the degassed solution and 0.1 wt% DMA, followed

by a final degassing. The doctor blade coater offers a robust coating thickness controlled by dial adjustments on the tool and also allows for thicker coatings. Coating layers of uniform thickness are obtained by depositing a self-healing solution with a pipette at one end of a cold rolled steel sheet (75×150 mm^2, width×length) and then dragging the blade coater along the length of the metal substrate to spread out the solution evenly. Self-healing samples with a coating of epoxy vinyl ester (ASHLAND, DERAKANE 510A-40), 3 wt% adhesion promoter (Gelest, methylacryloxy propyl triethoxy silane), 12 wt% PDMS healing agent (Gelest, mixture of HOPDMS (S27) and PDES) and 3 wt% of tin catalyst (Gelest, dimethyldineodecanoate tin) containing microcapsules were cured at room temperature for 24 hours, giving a coating thickness of approximately 100 μm.

4.10.2 Corrosion Test

A salt water set-up (NaCl in aqueous solution) was utilized for corrosion tests. To simulate surface damage, samples were scribed on the coated side from corner to corner in the shape of an "×" with a razor blade in the length of 10 cm each. The scratched samples were then healed at room temperature, 30°C, and 50 °C for 24 hours in a convection oven and then submersed in 5 wt% aqueous solution of sodium chloride. Before the specimen dipping, the cut edges of samples are shield by adhesive tape for preventing the corrosion from the exposed metal. The corrosion propagation of specimens was monitored and documented at 24 hours intervals.

4.10.3 Electro-chemical Test

An electro-chemical cell is made of 1.8×5 cm (diameter×length) glass tube filled with 1M concentration of sodium chloride aqueous solution. The cell is attached on the specimen with two part epoxy adhesive. The anode is connected to the platinum electrode and the cathode is connected to the sample. The current value of the samples is measured at a constant voltage (3 V) through the cell by using 236A Potentiostat/Galvanostat (PerkinElmer Instrument) equipment. The test specimens for scratching damage were × scribed with a razor blade and followed by healing at 50 °C for 24 hours.

4.10.4 SEM Sample Preparation for Cross-sectional Observation

The test samples were cut to approximately 1×1 cm^2 size by low speed diamond saw after healing reaction. Specimens were cleaned by deioinzed water and ethyl alcohol in ultrasonic bath. For direct polishing of samples without mounting, we used a special polishing tool to hold small metal samples, preventing fluctuating of samples during polishing, providing an evenly polished surface. To avoid secondary healing, we put self-healing coated samples into a convection oven at 170 °C for 24 hours after healing reaction, driving the thermal polycondensation reaction of the healing agent, HOPDMS and PDES. This reaction only takes place above 150 °C unless the catalyst is present (the case for self-healing).

4.10.5 Surface Profilometry

Polymer coated specimens after healing reaction were used for the measurement of surface topography prior to corrosion test. Surface profilometry (Sloan $Dektak^3$ ST stylus surface profilometer) can measure minute physical surface profile down to a few nm as a function of position with a diamond stylus (2.5 μm diameter), in contact with a sample.

4.11 References

1. S. H. Cho, H. M. Andersson, S. R. White, N. R. Sottos, P. V. Braun, *Adv. Mater.* **2006,** *18*, 997-1000.

2. S. R. White, N. R. Sottos, P. H. Geubelle, J. S. Moore, M. R. Kessler, S. R. Sriram, E. N. Brown, S. Viswanathan, *Nature* **2001** *409,* 794-797.

3. E. N. Brown, S. R. White, N. R. Sottos, *J. Mater. Sci.* **2004,** *39,* 1703-1710.K. Jud, H. H. Kausch, *Polymer Bulletin (Berlin, Germany)* **1979,** *1,* 697-707.

4. M. R. Kessler, S. R. White, *Journal of Polymer Science, Part A: Polymer Chemistry* **2002,** *40,* 2373-2383.

5. E. N. Brown, M. R. Kessler, N. R. Sottos, S. R. White, *Journal of Microencapsulation* 2003, **20**, 719-730.

6. J. D. Rule, E. N. Brown, N. R. Sottos, S. R. White, J. S. Moore, *Adv. Mater.* **2005,** *17,* 205-208.

7. X. Chen, M. A. Dam, K. Ono, A. Mal, H. Shen, S. R. Nut, K. Sheran, F. A Wudl, *Science* **2002,** *295,* 1698-1702.

8. C. S. Coughlin, A. A. Martinelli, R. F. Boswell, *PMSE Preprints,* **2004,** *91,* 472-473.

9. D. Therriault, S. R. White, J. A. Lewis, *Nature Materials*, **2003,** *2,* 265-271.

10. M. D. Gilbert, J. C. Hines, S. F. Cogan, *Proceedings from the American Society for Composites,* **2001,** Technical Conference16th, 26-32.

11. G. H. Koch, M. P. Brongers, N. G. Thompson, Y. P. Virmani, J. H. Payer, FHWA funds Cost of Corrosion Study. Report FHWA-RD-01-156, September 2001.

CHAPTER 5

TWO MICROCAPSULE SELF-HEALING SYSTEM

5.1 Investigation for Self-healing Coating Media

To develop the self-healing coating system, we investigated coating media for the self-healing coatings. First of all, epoxy resin was considered as a coating medium. Epoxy is a very widely used coating medium for industrial use because of its useful properties. However, it can not be directly used in PDMS self-healing system based on the phase separated healing agent in a matrix because amine curing agent may polymerize PDMS liquid droplets. Thus, another curing agent, melamine was investigated. The polymerization of both PDMS and epoxy was observed in the presence of melamine curing agent at various temperatures (table 5.1). In this test, it was intended to find the temperature where melamine just polymerizes epoxy but does not polymerize PDMS. However, melamine curing agent polymerized PDMS and epoxy together after a certain temperature (around 85 °C).

To solve the curing system restriction, other coating medium such as epoxy vinyl ester, acrylic resin, and polyurethane were considered. Among these, epoxy vinyl ester is used for one microcapsule self-healing coating system which utilizes phase separated PDMS liquid droplets as a healing agent and tin catalyst containing microcapsules. Previously, the excellent healing property of one microcapsule self-healing system with epoxy vinyl ester matrix was already confirmed, so that it should be applicable for the self-healing coatings. Another possible try would be two-microcapsule self-healing system which includes PDMS containing microcapsules as well as tin catalyst containing microcapsules. Thus, PDMS healing material can survive during the matrix polymerization with a curing agent but it could meet tin catalyst in the case of

microcapsule rupture. It is expected that the two-microcapsule self-healing system can also increase the system durability after long time aging and will be precisely described in chapter 5.

Table 5.1. Result of thermal curing reaction of melamine curing agent for epoxy and PDMS after 24 hours according to temperatures.

Temperature (˚C)	PDMS	Epoxy
Room temperature	Low viscous liquid	-
50	Low viscous liquid	-
75	Low viscous liquid	Transparent liquid
85	Slight viscous increase	Polymer (brown)
100	Viscosity increase (gel)	Polymer (brown)

5.2 Two Microcapsule Self-healing System for Epoxy Matrix

For the self-healing system previously described in this thesis, a one microcapsule self-healing system composed of phase-separated PDMS liquid droplets and catalyst containing microcapsules in an epoxy vinyl ester matrix was used. We already confirmed the healing property of the self-healing composite and the promising anti-corrosion property of self-healing coatings with this one microcapsule system. However, this one microcapsule self-healing system is not useful for other specific matrices such as epoxies formulated with amine based curing agents because the amine curing agent can also polymerize the PDMS based healing agent. So, a two-microcapsule self-healing system which is composed of PDMS containing microcapsules and catalyst containing microcapsules was developed. With this configuration, we can avoid system restriction and improve system durability after very long aging.

To compose the two microcapsule self-healing system, it was necessary to make PDMS containing microcapsules which protect the healing agent from the amine curing agent during epoxy matrix polymerization. PDMS containing microcapsules were successfully synthesized by urea-formaldehyde microencapsulation (figure 5.1) with modifications as noted in the experimental section. The urea-formaldehyde microencapsulation method was used for DCPD encapsulation in the previous methodology [1-3]. The size of PDMS containing microcapsules can be easily controlled according to the mechanical stirring speeds. The PDMS containing microcapsules can be embedded with tin catalyst containing microcapsules and an appropriate adhesion promoter in the matrix, which results in a two microcapsule self-healing system.

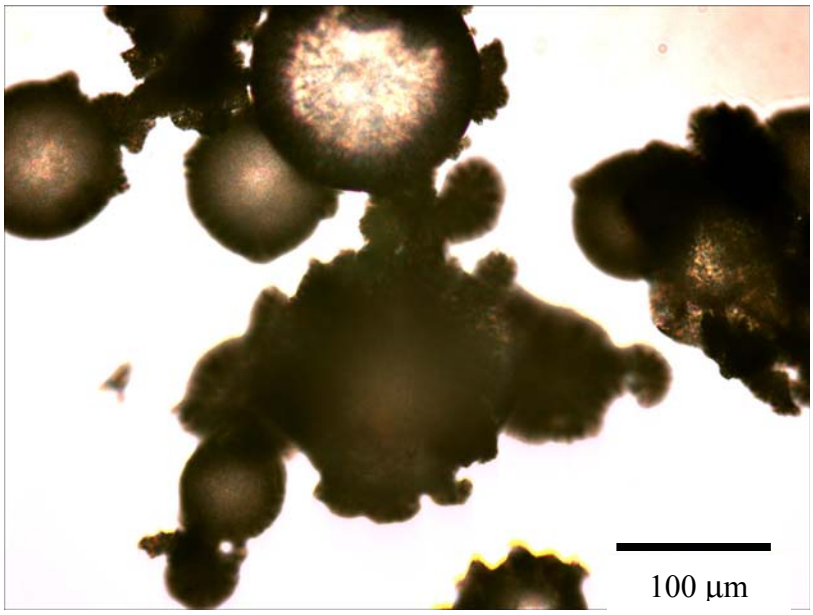

Figure 5.1 Optical microscopic images of PDMS containing microcapsules.

The healing property of the two microcapsule self-healing system was investigated using a fracture test with the TDCB sample geometry. First of all, the composition effect was investigated according to the amount of PDMS containing microcapsules and catalyst containing microcapsules. In the test result, the maximum load of healed samples increases as the amount

of healing agent increases (figure 5.2). The amount of catalyst containing microcapsules was proportional to the amount of the amount of the PDMS containing microcapsules. However, the slight amount change of catalyst containing microcapsules does not greatly change the healing property. The highest average maximum load of the sample healed at 50 °C was around 20 N, which is a 17 N lower value than observed in the one microcapsule self-healing system. The primary reason might for the lower strength was suspected that there was no adhesion promoter used in this two microcapsule system yet.

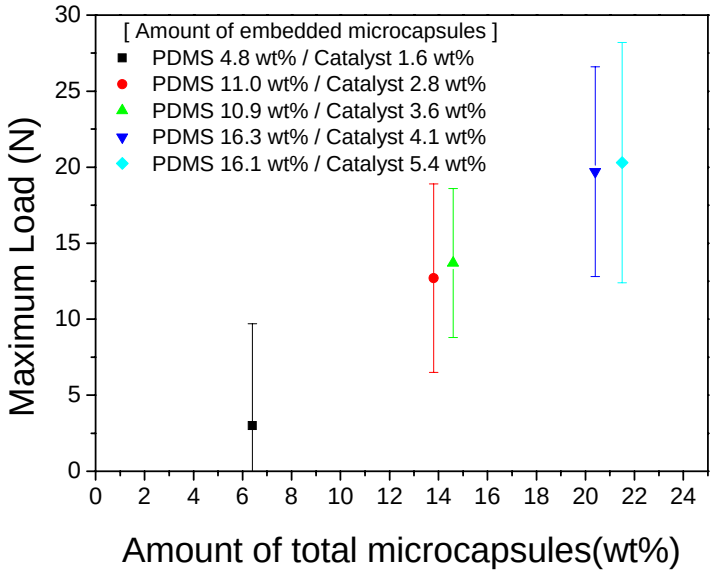

Figure 5.2 Maximum load changes of healed TDCB specimens according to the amount of PDMS and catalyst containing microcapsules. The samples were healed at 50 °C.

The purpose of the adhesion promoter is to improve adhesion strength between epoxy matrix and PDMS healing material. The chemical structure of the adhesion promoter for epoxy vinyl ester has carbon double bonds for reacting with vinyl ester matrix and ethoxy groups for hydroxyl groups of PDMS. This adhesion promoter will not be effective in an epoxy system because the double bonds will not react with the epoxy matrix. Thus, a new adhesion promoter,

(3-trimethoxysilylpropyl)dimethylene triamine ($C_{10}H_{27}N_3O_3Si$), which has amine groups to react with epoxy matrix and methoxy groups to react with hydroxyl groups of PDMS was investigated. The healing property of TDCB samples containing adhesion promoters was first confirmed by manually injecting a healing agent into the crack plane. The maximum load of samples without adhesion promoter was around 25 N. With the adhesion promoter used for epoxy vinyl ester matrix system, the maximum load was only slightly increased, as expected, but with the new adhesion promoter, the maximum load was 50 N (figure 5.3).

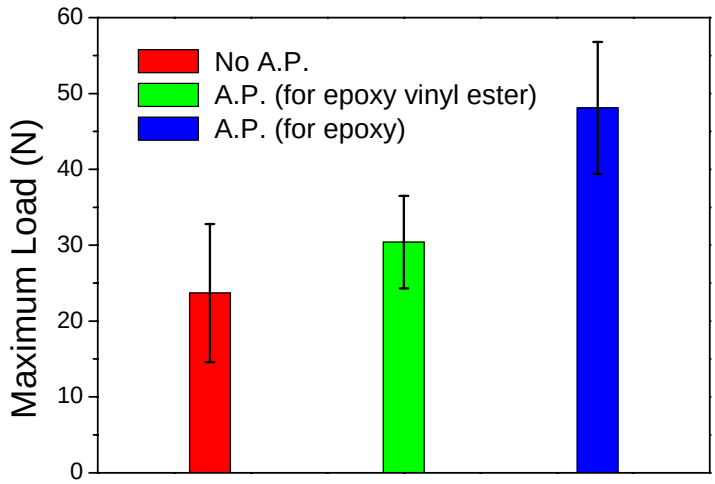

Figure 5.3 Maximum load values of manually healed TDCB specimens by injecting PDMS healing agent according to adhesion promoter change.

The new adhesion promoter was then investigated in the two microcapsule self-healing system with in situ samples. Although the new adhesion promoter for epoxy matrix shows the improvement of adhesion strength (figure 5.4), it is still necessary to find a more effective adhesion promoter, which at least in theory, will lead to further improvement of the healing properties of the two-microcapsule self-healing system.

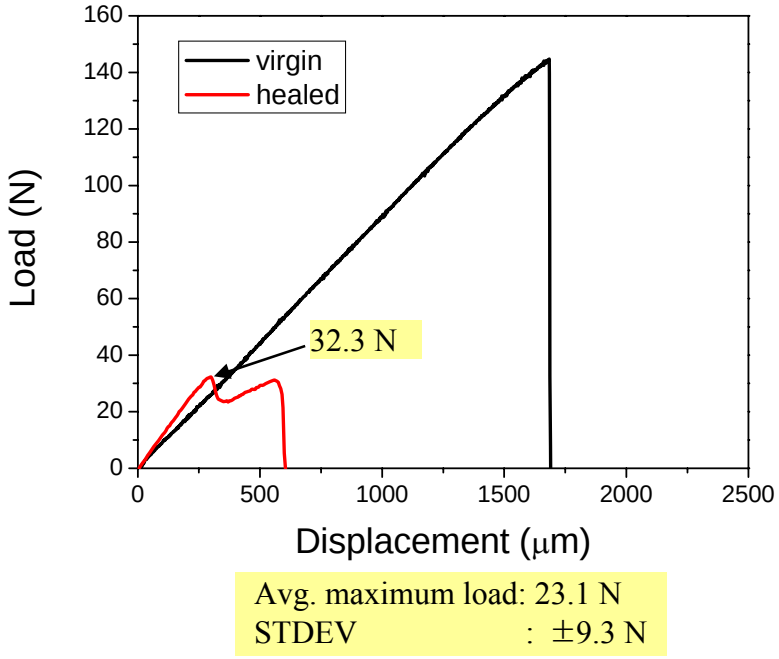

Figure 5.4 Monotonic fracture test results of two microcapsule self-healing polymer (TDCB geometry) for virgin and fractured samples healed at 50 °C. The self-healing composite is composed of epoxy with amine curing agent, 3 wt% of adhesion promoter ((3-trimethoxysilylpropyl)dimethylene triamine), 14 wt% of PDMS (S32, viscosity 1,600 cP) containing microcapsules, and 3 wt% of tin catalyst (dimethyldineodacanoate tin) containing microcapsules.

5.3 Temperature Dependence of the Healing Property

In the previous section (section 5.2), the healing properties of the two-microcapsule self-healing system as a function of composition ratio were investigated at 50 °C. The two-microcapsule self-healing system is designed for general matrix application with limited system restrictions. In two capsule systems, both healing agents are protected from the matrix, thus matrix-healing chemistry incompatibilities are greatly reduced. In this section, the healing property of the optimized (ratio of healing agent, catalyst, and adhesion promoter) two-

microcapsule self-healing system was investigated at different healing temperatures. Figure 5.5 is the monotonic test result of a two-microcapsule self-healing system composed of epoxy matrix, PDMS containing microcapsules, and tin catalyst containing microcapsules healed at 30 and 50 °C. 3wt% of the adhesion promoter was also mixed with the epoxy matrix prior to add other healing components. The average maximum load of the healed samples using the two microcapsule self-healing system was slightly lower than the one microcapsule self-healing system. It was also determined that the healing property at 30 °C was not as good as at 50 °C, which was the same trend observed the one microcapsule self-healing system.

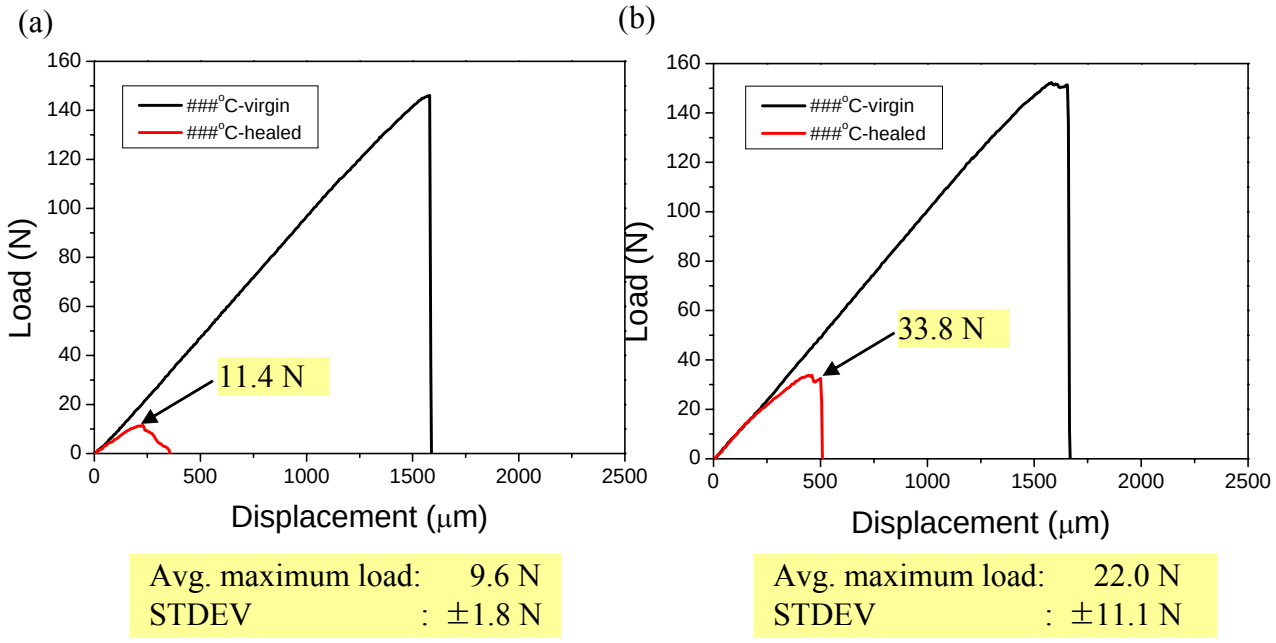

Figure 5.5 Monotonic fracture test results of two microcapsule self-healing polymer (TDCB geometry) for virgin and fractured samples healed at a) 30 °C and b) 50 °C. The self-healing composite is composed of epoxy with amine curing agent, 3 wt% of adhesion promoter [(3-trimethoxysilylpropyl)dimethylene triamine], 14 wt% of PDMS (S32, viscosity 1,600 cP) containing microcapsules, and 3 wt% of tin catalyst (dimethyldineodacanoate tin) containing microcapsules.

5.4 TKAS Catalyst synthesis

To improve the healing properties of PDMS self-healing systems at lower temperature, a number of commercially available organotin catalysts with greater catalytic activity than the original catalyst were previously investigated (chapter 3). That resulted in improved healing at near room temperature. Through a combination of a lower viscosity healing agent and a more effective catalyst some degree of healing was achieved at room temperature, however further improvements were still necessary. Thus, improved organotin catalysts were still investigated for further improvement of the healing property at lower temperature. Consequently, tetrakis(acetoxydibutyltinoxy)silane (TKAS, $Si[OSn(n\text{-}C_4H_9)_2OOCCH_3]_4$), a highly effective new organotin catalyst was synthesized and encapsulated for curing PDMS. This new catalyst does not require moisture for activation, potentially enabling self-healing coatings. Thus, this self-healing system can be applied in environments for applications ranging from aerospace to subsurface healing, where water may not be present. Figure 5.6 is a reaction scheme for polycondensation of PDMS with a tin catalyst [4]. If an alky ester tin catalyst is used, it needs contact with moisture for activation, where it is converted to an alkyl hydroxyl tin [4]. This intermediate compound reacts with alkyl alcoxy silane and forms a tin compound containing a Sn-O-Si linkage [4]. This organotin compound reacts with hydroxyl-terminated PDMS and forms highly polymerized PDMS [4]. This scheme led us to synthesize a new catalyst which contains a Sn-O-Si linkage. The final chemical structure of this new catalyst is $Si[OSn(n\text{-}C_4H_9)_2OOCCH_3]_4$.

The TKAS catalyst was synthesized based on US patent 4,137,249 [5]. The experimental set-up for the TKAS synthesis is shown in figure 5.7. The final product of this procedure is organotin silicone compound containing a Sn-O-Si linkage, and the by-product is

ethyl acetate. Much improved catalytic activity is also expected because this catalyst can directly drive the polycondensation reaction.

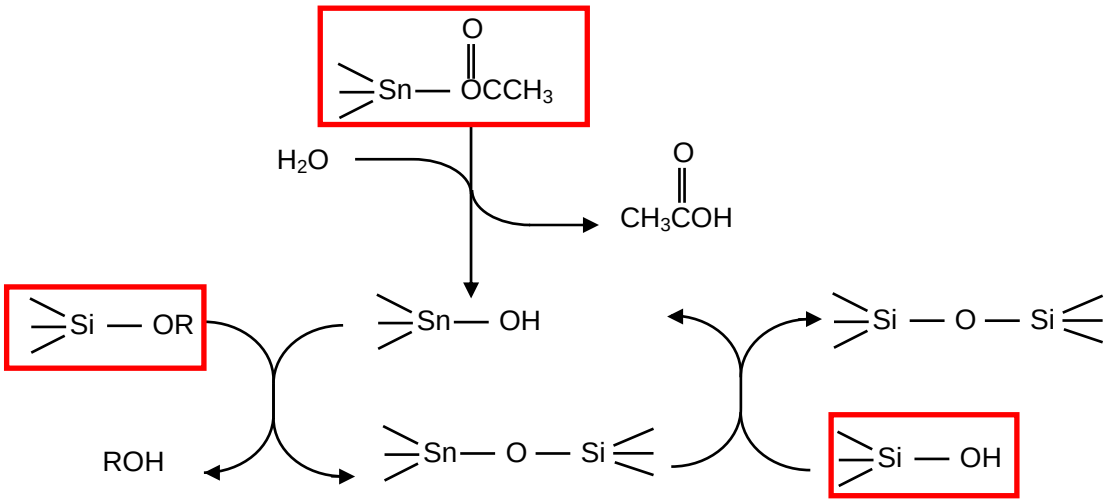

Figure 5.6 Reaction scheme for the polycondensation of hydroxyl end functionalized PDMS with an alkyl ester tin catalyst in the presence of moisture (adapted from [4]).

Figure 5.7 Experimental set-up for synthesis of the TKAS catalyst.

5.5 Microencapsulation of the TKAS Catalyst

Self-healing requires the microencapsulation of the TKAS catalyst. The catalyst is dissolved in chlorobenzene, filtered it through a glass micro-fiber and created microcapsules by interfacial polymerization (polyurethane shell). This microencapsulation method is similar to the original tin catalyst encapsulation. The urea-formaldehyde microencapsulation was also tried, but that did not yield high quality capsules even at low catalyst concentrations. Figure 5.8 is an optical microscopic image of the new catalyst containing polyurethane microcapsules. To confirm the healing property, small scale tests were first performed with the bullet shaped samples. The samples were composed of epoxy vinyl ester, adhesion promoter, 12 wt% of phase separated PDMS, and 4wt% of catalyst containing microcapsules. In these tests, very promising results were observed at lower temperature. Thus, we moved to TDCB sample tests using these new catalyst containing microcapsules and the other required components.

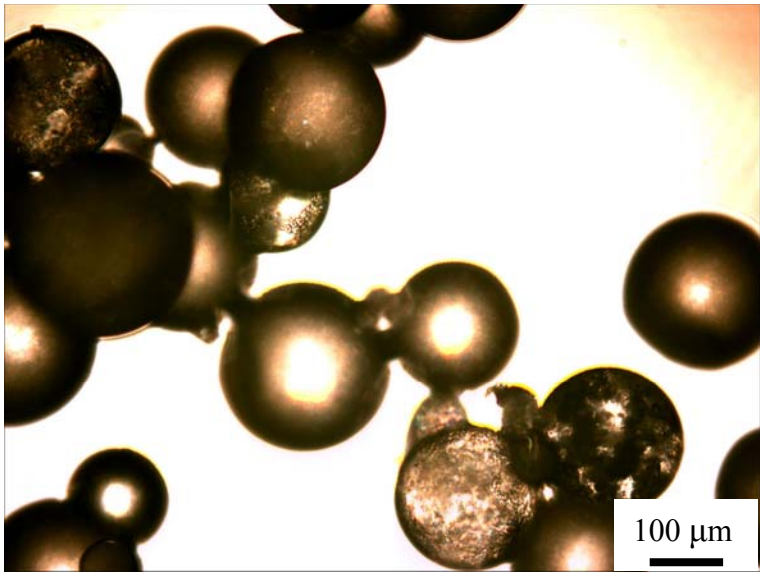

Figure 5.8 Optical microscopic image of newly synthesized catalyst containing microcapsules.

5.6 Healing Property with the TKAS Catalyst

The healing performance of the self-healing polymer composite containing the TKAS catalyst containing microcapsules, the synthesis and properties of which is previously described, was investigated. The TKAS catalyst was dissolved in chlorobenzene by 2 wt%, which is then encapsulated by the urethane microencapsulation method. As described in the previous section, the improved healing property was expected, especially at lower temperatures, due to the higher catalytic activity of the TKAS catalyst. Figure 5.9 is the monotonic test result of the two-microcapsule self-healing polymer with the TKAS catalyst containing microcapsules healed at room temperature and 30 °C.

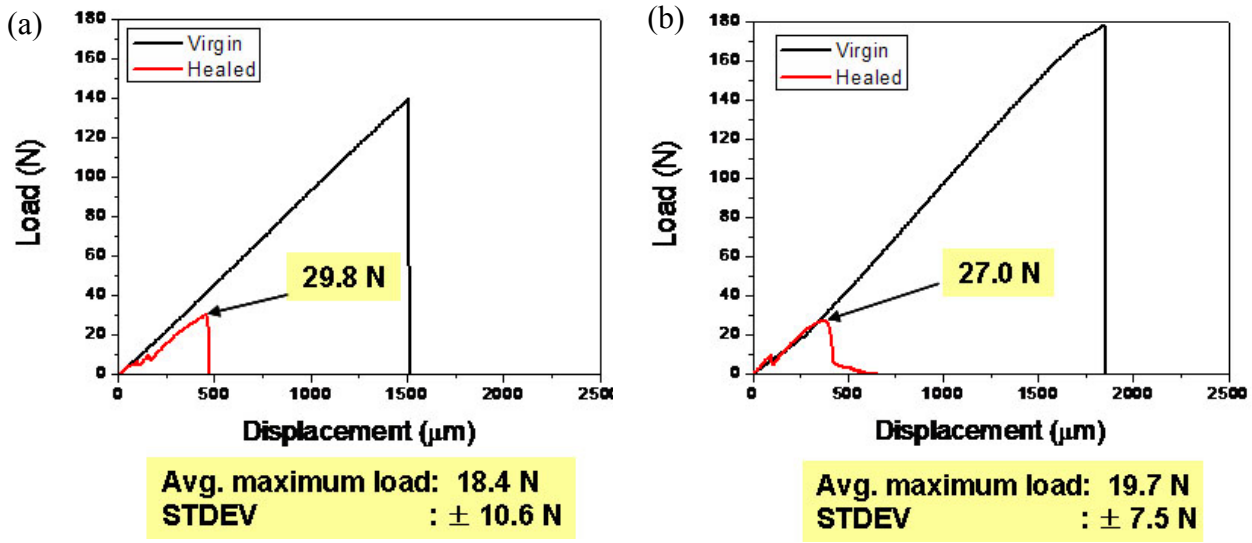

Figure 5.9 Results from monotonic fracture tests with TDCB geometry for virgin samples and fractured samples healed at a) room temperature and b) 30 °C using the TKAS catalyst. The self-healing composite is composed of epoxy with amine curing agent, 3 wt% of adhesion promoter ((3-trimethoxysilylpropyl)dimethylene triamine), 14 wt% of PDMS (S32, viscosity 1,600 cP) containing microcapsules, and 3 wt% of TKAS catalyst containing microcapsules.

The average maximum load of the healed samples were greatly improved by adding the TKAS catalyst containing microcapsules, and almost the same healing property was achieved at room temperature as when healed at 30 °C.

The healing property was also compared with the samples healed at 50 °C for the one microcapsule system and the two-microcapsule system by monotonic fracture test. The healing property of the one microcapsule system had a slightly higher maximum load than the two-capsule system (figure 5.10). However, the two-microcapsule self-healing polymer also showed good healing performance with the new catalyst containing microcapsules. Better healing occurs at 50 °C (figure 5.10a) compared to lower temperatures (figure 5.10a-b), but the lower temperature healing should still be within acceptable range for many applications such as coatings.

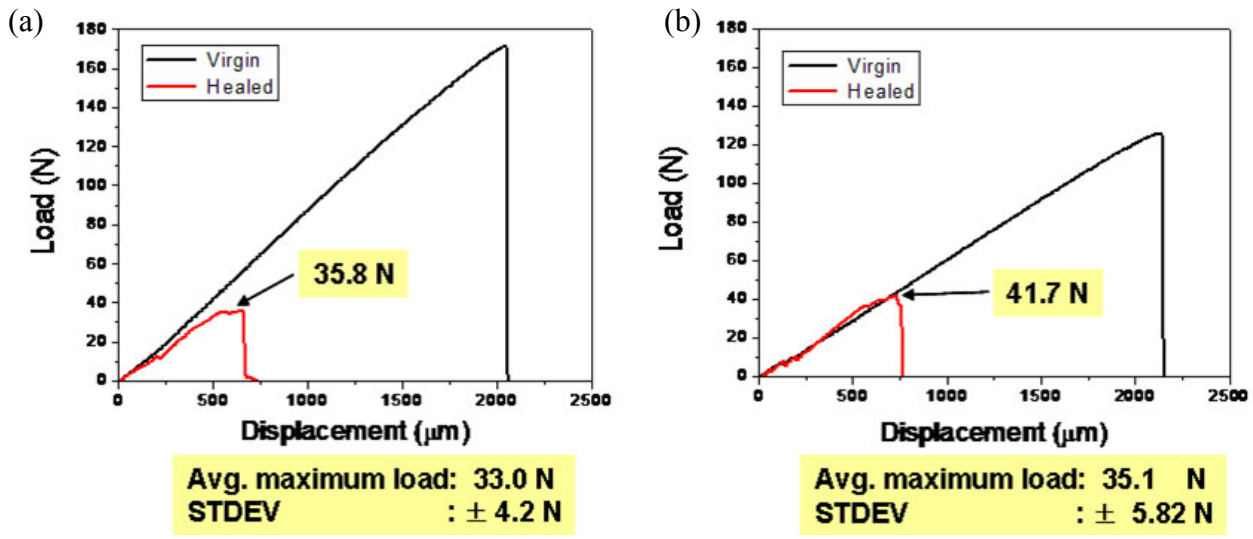

Figure 5.10 Results from monotonic fracture tests (TDCB geometry) for virgin samples and fractured samples healed at 50 °C for (a) two microcapsule containing system and (b) one microcapsule containing system. The amount of TKAS catalyst containing microcapsules added in the sample was 3 wt%.

The most important advantage of the two-capsule system is that it can be used in almost any polymer matrix, while the one capsule system has matrix limitations. Given the motivation to explore the use of this system for coatings applications, the anti-corrosion property of coatings containing the two-microcapsule self-healing system was investigated for our next step.

5.7 Self-healing Coatings with Two Microcapsule System

The anti-corrosion property of two microcapsule containing self-healing coatings was investigated in this section by the scribed specimen immersion in salt water. The anti-corrosion property between control samples and an in situ sample was also compared the same as the previous one microcapsule system (figure 5.11).

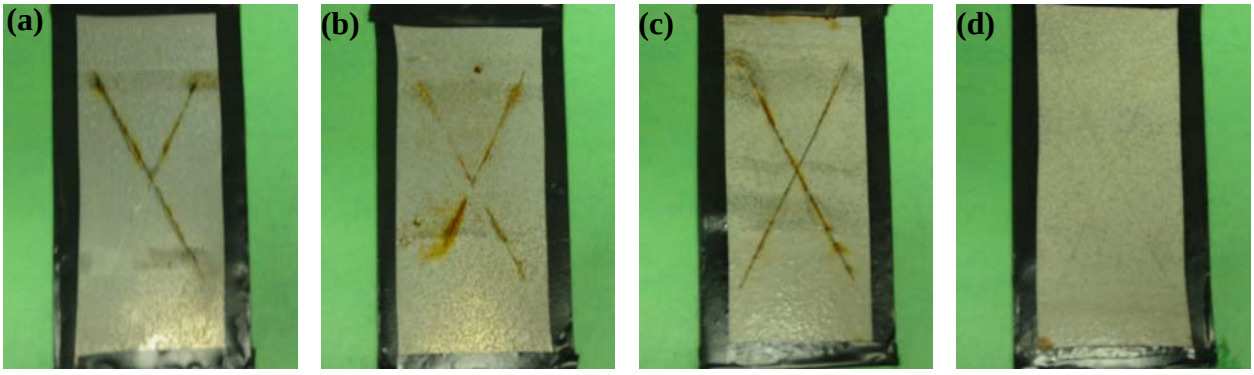

Figure 5.11 Corrosion test result of specimens of control and in situ samples healed at 50 °C after 120 hours in 5 wt% NaCl aqueous solution. Coating solution is composed of (a) matrix with 3 wt% of adhesion promoter; (b) matrix, 3 wt% of adhesion promoter, and 3 wt% of catalyst containing microcapsules; (C) matrix, 3 wt% of adhesion promoter, and 14 wt% of PDMS containing microcapsules; (d) matrix, 3 wt% of adhesion promoter, 3 wt% of catalyst containing microcapsules, and 14 wt% of PDMS containing microcapsules (*in situ* sample).

The self-healing coating solution was composed of epoxy matrix with amine curing agent, 3 wt% of adhesion promoter, 14 wt% of PDMS containing microcapsules, and 3 wt% of catalyst containing microcapsules. The curing condition was at room temperature for 24 hours and post cure at 30 °C for another 24 hours. Samples were healed at 50 °C for 24 hours after scribing with a razor blade. The corrosion test result after 120 hours revealed that all the control samples showed red rust on the scribed parts while the in situ sample did not show red rust (figure 5.11).

5.8 Healing in water environments

The anti-corrosion property of self-healing coatings healed in water environments was investigated in this section. Previously, the self-healing coatings healed in air were already confirmed as very successful. Thus, our next step was to investigate whether the self-healing coatings also efficiently operate under water environments. As a more aggressive test, the anti-corrosion property of the self-healing coatings healed under salt water and acidic or basic water was also investigated.

5.8.1 Healing in Pure and Salt Water Environment

First of all, the anti-corrosion property of the self-healing coatings healed in pure and salt water was investigated. The self-healing coating solution composed of the same components and composition as the samples healed in air (figure 5.11) was used in these experiments. Figure 5.11 shows the corrosion test result of the samples healed in water and salt water environments. The anti-corrosion property between control samples and *in situ* samples was compared the same as the previous experiments. Control samples are epoxy matrix with adhesion promoter and in situ samples are coated with the two-microcapsule containing self-healing coating solution.

In the result with the samples healed in pure water (figure 5.12a-b), *in situ* samples showed slightly better anti-corrosion property than control samples but the healing was not as effective as for samples healed in an air environment. It is suspected that the tin catalyst, and possibly the PDMS healing agent, may be washed out by water before polymerization initiates.

In the case of healing in salt water (figure 5.12c-d), the self-healing sample did not show any better anti-corrosion property than the control samples. The tin catalyst is likely very rapidly removed in salt water due to ion exchange reactions. The PDMS healing agent may also be washed out by the salt water.

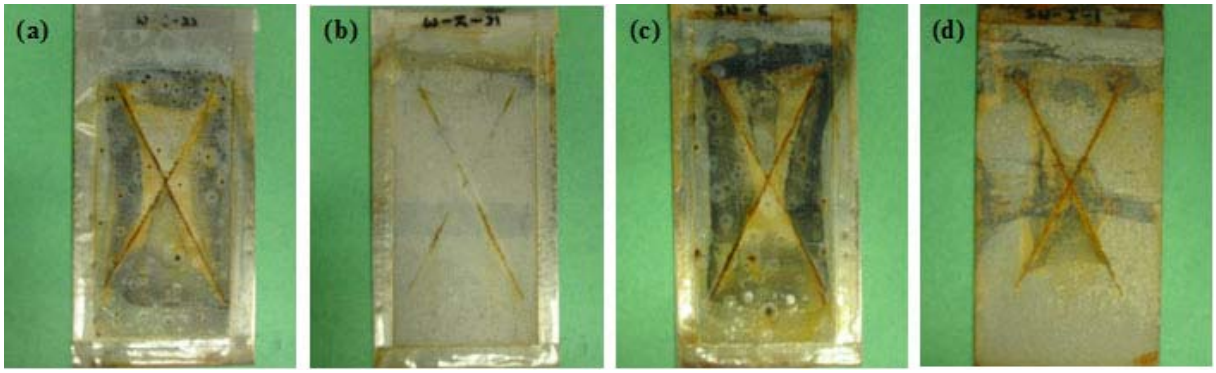

Figure 5.12 Corrosion test result of specimens healed at 50 °C after 120 hours in 5 wt% NaCl aqueous solution. The first set of (a) control and (b) *in situ* samples was healed in pure water, and the second set of (c) control and (d) *in situ* samples was healed in salt water (5 wt% NaCl aqueous solution).

5.8.2 Healing in water in different pH conditions

The anti-corrosion property of self-healing coatings healed in water with different pH conditions was also tested. The pH of the water bath was varied between 2 to 12 using the same sample preparation and corrosion test conditions. The corrosion test result of the samples healed in a water bath having pH 2, pH 4, pH 10, and pH 12 is shown in figure 5.13.

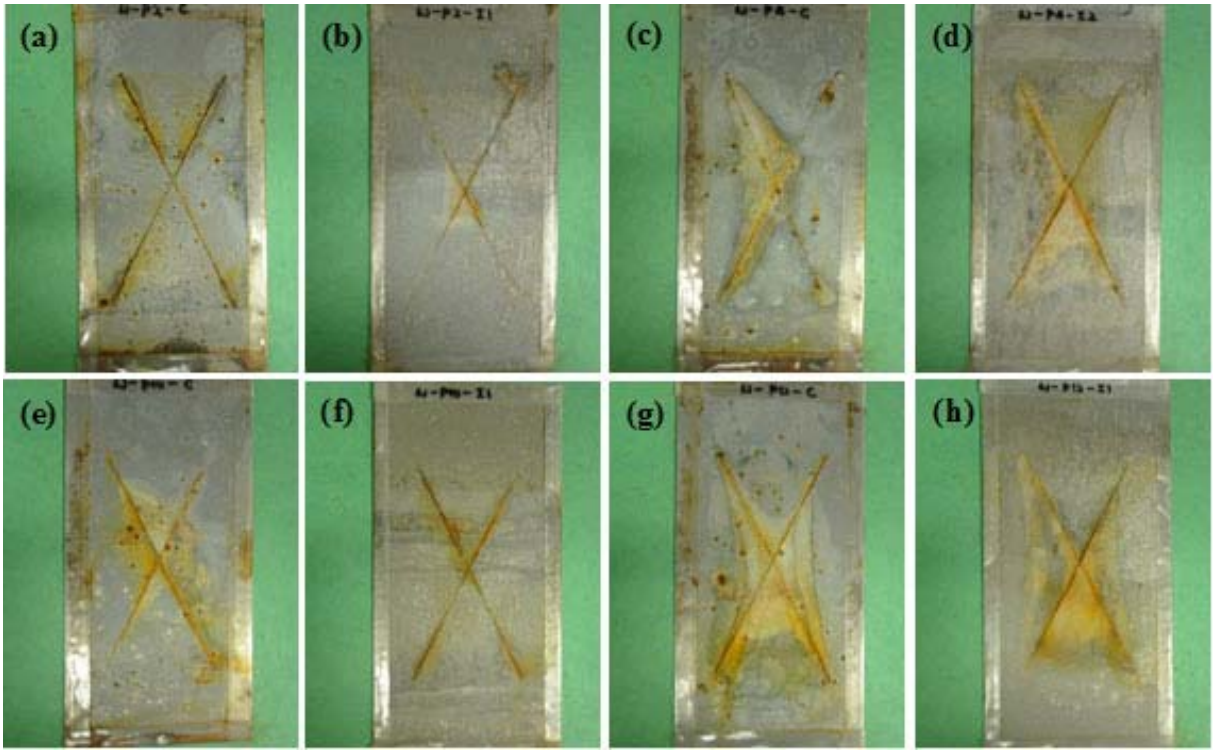

Figure 5.13 Corrosion test result of specimens healed at 50 °C after 72 hours in 5 wt% NaCl aqueous solution. (a) Control and (b) *in situ* sample healed in water bath having pH 2; (c) Control and (d) in situ sample healed in water bath having pH 4; (e) Control and (f) in situ sample healed in water bath having pH 10; (g) Control and (h) in situ sample healed in water bath having pH 12.

In these results, in-situ samples healed in water with pH 2 showed a better healing property, especially within a short time range of the corrosion test, than other samples. This may be because PDMS poly-condensation can be catalyzed by the presence of an acid. So, even if the tin catalyst is being removed by the water, the acidic water may provide the necessary catalytic properties to heal the polymer. The metal substrate is generally very corrosive in acid environments. If the scribed area is not protected by a polymer layer, it would have serious red

rust on the damaged part as shown in the control samples. However, the in situ samples show some anti-corrosion property in the acidic condition indicating self-healing is taking place. However, the self-healed samples do not show good anti-corrosion properties under other pH conditions, similar to the lack of healing observed under pure and salt water environments.

To get good healing property in water environments, PDMS and catalyst loss problems before polymerization need to be solved. A better catalyst would be helpful for the PDMS and catalyst loss problems of self-healing coatings in the case of healing in water environments because rapid reaction could prevent the loss of components.

5.9 Adhesion Strength of Self-healing Coatings

To get a better healing property, we first need to solve the delamination problem of the coating layer because some test samples showed delamination during the corrosion test. Even if the self-healing sample has a good healing property, it would be useless in the case of de-lamination problem. The delamination problem also hindered an accurate evaluation of the anti-corrosion property of the test specimens.

5.9.1 Chemical Treatment with Silane Coupling Agent

Initially, the anti-corrosion properties of two microcapsule containing self-healing coatings healed at low temperature was investigated. The anti-corrosion property of control samples and an in situ sample were compared using the same procedure as for the previous one microcapsule containing self-healing system. However, the serious adhesion problems in the two microcapsule system were encountered, which caused delamination from the metal substrate during corrosion tests (figure 5.14).

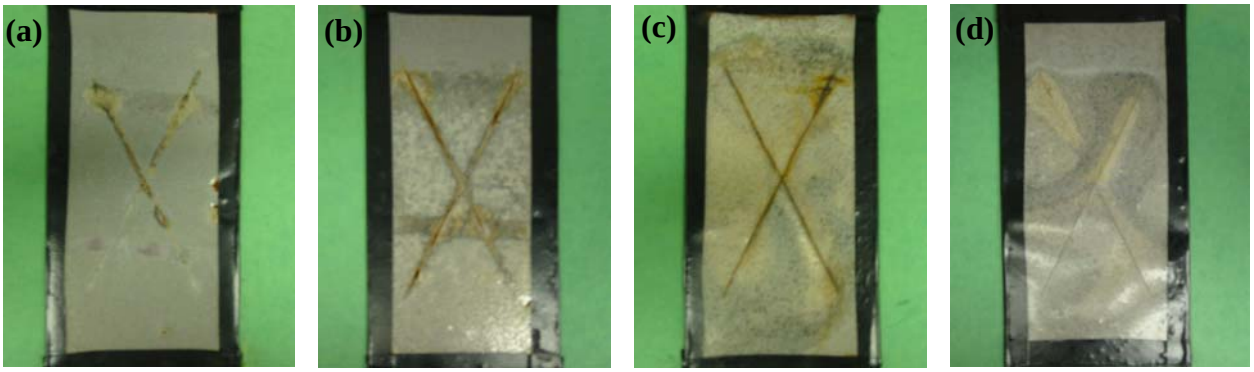

Figure 5.14 Corrosion test result of specimens of control and in situ samples healed at 30 ℃ after 120 hours in 5 wt% NaCl aqueous solution. Coating solution is composed of (a) matrix with 3 wt% of adhesion promoter; (b) matrix, 3 wt% of adhesion promoter, and 3 wt% of catalyst containing microcapsules; (C) matrix, 3 wt% of adhesion promoter, and 14 wt% of PDMS containing microcapsules; (d) matrix, 3 wt% of adhesion promoter, 3 wt% of catalyst containing microcapsules, and 14 wt% of PDMS containing microcapsules (*in situ* sample).

For our first attempt, it was expected that the delamination problem would be solved through treatment of the substrate with the silane coupling agent (γ-glycidoxy propyl trimethoxysilane) which should induce chemical bonding between the polymer coating layer and metal substrate. Basically, the silane coupling agent has functional groups which can connect to hydroxyl groups on the metal substrate and the epoxy matrix (figure 5.15). For the silane treatment, 1 wt% aqueous solution of silane coupling agent was sprayed on a metal substrate and dried it at room temperature. However, it did not significantly improve the adhesion problem. Another attempt for the silane treatment was to mix 3 wt% of silane coupling agent with the self-healing coating solution but this was also not very effective.

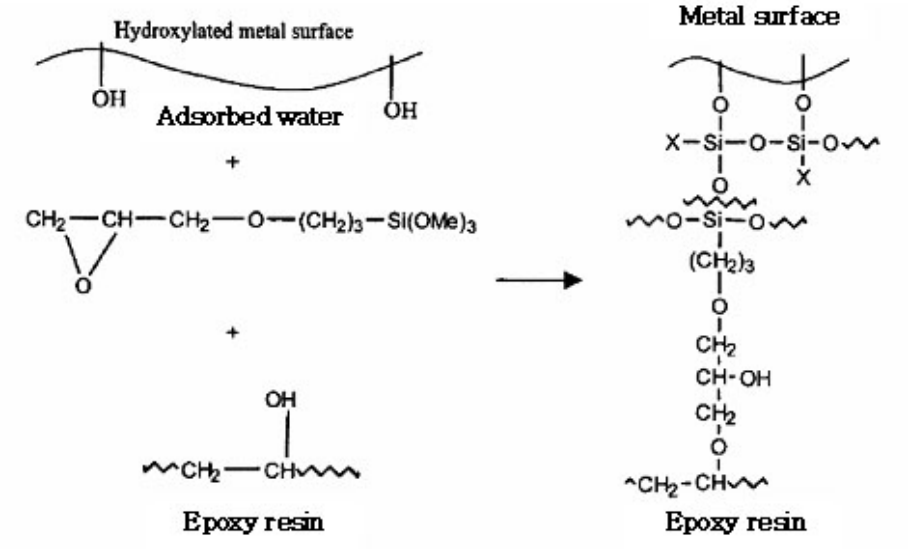

Figure 5.15 Reaction scheme for forming adhesion bonds by reaction of γ-glycidoxy propyl trimethoxysilane with epoxy on a metal surface [adapted from reference 4].

5.9.2 Mechanical Treatment with Sand Blasting

In another attempt to increase the adhesion strength between the self-healing coating and the metal substrate, the substrate was mechanically abraded by sand blasting. This increases the surface roughness of the substrate, which should improve the adhesion strength. To confirm the effect of mechanical treatment, self-healing coatings were applied to the mechanically treated metal substrate, followed by scratch damage, healing reaction, and corrosion test in salt water. However, the corrosion test result (figure 5.16) was not very promising. The test samples did not show good adhesion, especially specimens healed at low temperature. Furthermore, the anti-corrosion property of the self-healed sample could not be evaluated due to delamination during the corrosion test.

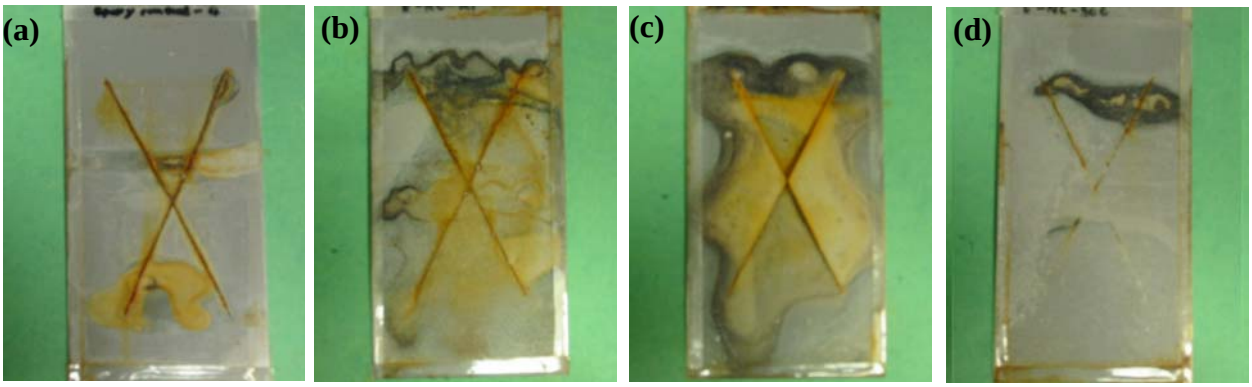

Figure 5.16 Corrosion test result of specimens of control and *in situ* samples healed at 30 °C after 120 hours in 5 wt% NaCl aqueous solution. Coating solution is composed of (a) matrix with 3 wt% of adhesion promoter; (b) matrix, 3 wt% of adhesion promoter, and 3 wt% of catalyst containing microcapsules; (C) matrix, 3 wt% of adhesion promoter, and 14 wt% of PDMS containing microcapsules; (d) matrix, 3 wt% of adhesion promoter, 3 wt% of catalyst containing microcapsules, and 14 wt% of PDMS containing microcapsules (*in situ* sample). Metal substrates were treated by sand blasting to induce mechanical adhesion.

5.9.3 Primer Coating

In the previous work, it was evident that the chemical treatment with silane coupling agent and the mechanical treatment by sand blasting did not improve the adhesion strength of the self-healing polymer coating layer. Thus, it was necessary to induce another coating layer at the interface between the self-healing polymer and metal substrate.

A primer bottom coating was applied on a metal substrate prior to the self-healing coating to increase the adhesion strength between the self-healing coating and metal substrate. Commercially available epoxy based primer (KUKDO Chemical, KU-420K40) was coated by doctor blade type coater (50 μm thick). After complete curing of the primer layer, a self-healing

coating was applied on the top layer, followed by scratch damage, healing reaction, and corrosion test. To compare the anti-corrosion property of specimens according to healing temperatures, control and self-healing samples were healed at room temperature, 30 °C, and 50 °C. The new organotin catalyst, which showed the best healing property in the previous experiments, was used for the self-healing sample to obtain good healing property at low temperature. After 120 hours of corrosion test in 5 wt% salt water, the control sample showed very serious red rust on the scratched part while the self-healing sample showed an excellent anti-corrosion property even at room temperature (figure 5.17). Furthermore, the previous adhesion problem was solved by this primer treatment.

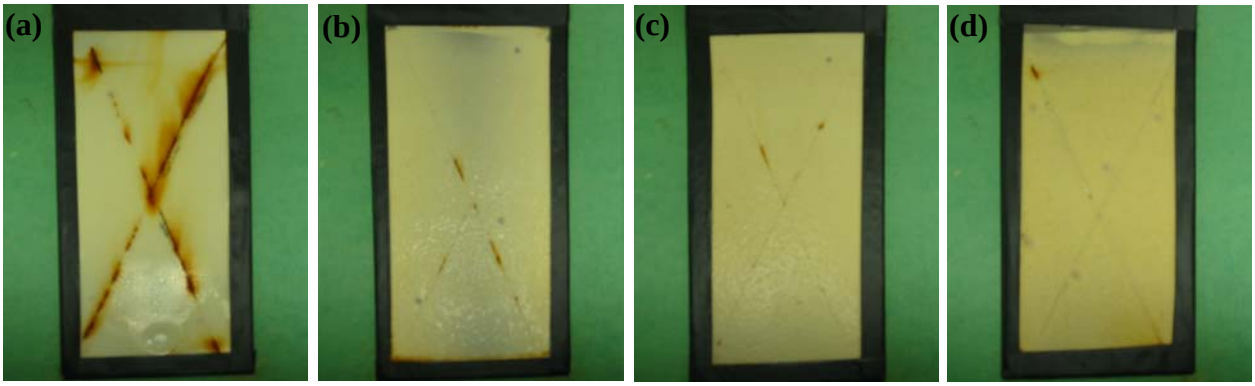

Figure 5.17 Corrosion test result of specimens of (a) control and *in situ* samples healed at (b) room temperature, (c) 30 °C, and (d) 50 °C after 120 hours in 5 wt% NaCl aqueous solution. The self-healing coating solution is composed of epoxy with diethylenetriamine (DETA), 3 wt% of adhesion promoter, 14 wt% of PDMS containing microcapsules, and 3 wt% of tin catalyst (synthesized, $Si[OSn(n\text{-}C_4H_9)_2OOCCH_3]_4$) containing microcapsules. Metal substrates were coated by primer bottom layer to induce adhesion strength prior to the self-healing coating.

5.10 Dual Layered Self-healing Coatings

In order to develop a commercially optimized self-healing coating system, it is necessary to investigate the general compatibility of self-healing coatings with commercialized paints and to confirm its good anti-corrosion effect. Furthermore, we need to investigate dual layer self-healing coatings, which are composed of the actual self-healing coating in a bottom layer. A conventional coating layer can be applied over the self-healing layer for protection and to improve the appearance (the self-healing coating can be rough due to the incorporated microcapsules). The commercialized epoxy based coating solution (International Marine Coatings, Intergard 264) was used for the matrix solution. The components for two microcapsule self-healing coating system were applied for the self-healing coatings (figure 5.18).

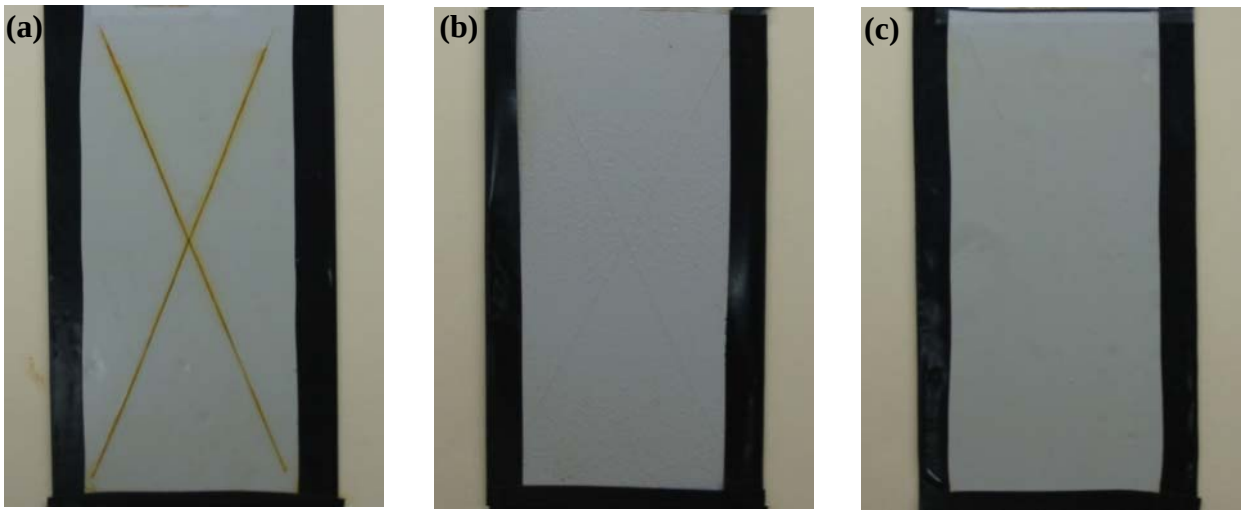

Figure 5.18 Corrosion test result of specimens of (a) control and *in situ* samples with (b) one layered self-healing coating and (c) dual layered self-healing coating healed at 50 °C after 120 hours in 5 wt% NaCl aqueous solution. The control sample is coated by Intergard 264. The self-healing coating solution is composed of Intergard 264, 3 wt% of adhesion promoter, 14 wt% of PDMS containing microcapsules, and 3 wt% of tin catalyst (DMDN-Sn) containing microcapsules.

In corrosion test the result (figure 5.18), the dual layered self-healing coatings showed improved surface appearance as well as promising anti-corrosion property the same as the one layered self-healing coatings, while the control sample showed serious corrosion propagation on the scribed part.

5.11 Conclusions and Outlook

In this chapter, a two microcapsule self-healing system composed of matrix with an adhesion promoter, healing agent containing microcapsules, and catalyst containing microcapsules was created. PDMS containing microcapsules were synthesized by a urea-formaldehyde microencapsulation method according to the previous methodology [3] with some modification. Although the healing property of the two microcapsule self-healing system was slightly lower than the one microcapsule self-healing system, it could have significant merits for general matrix application with minimal system restrictions. To solve the poor adhesion strength between the polymer coating and metal substrate, a primer bottom coating prior to the self-healing coatings was applied. The two microcapsule self-healing system with the new organotin catalyst was very effective at low temperature, so that the good healing property at room temperature was achieved both in the composite and coatings. It was expected that the self-healing coatings can greatly extend the lifetime of polymer coatings on substrate materials. One microcapsule or dual microcapsule self-healing systems can be applied according to the matrix system. For confirming general compatibility, it was investigated the anti-corrosion property of commercialized coating solutions with the PDMS based self-healing components. Furthermore, the dual layer self-healing coating was developed for more advanced application, which is

composed of the actual self-healing coating in a bottom layer and the blank polymer layer for protection and outer appearance.

5.12 Experimental

Experimental details for the synthesis of tin catalyst containing microcapsules and TDCB sample tests were covered in Chapter 2, and those for coating sample fabrication and corrosion tests were covered in Chapter 4.

5.12.1 Microcapsule Synthesis

Tin catalyst containing microcapsule is modified using a DMDN-Sn catalyst (Gelest, Dimethydineodecanoate tin) for better catalytic activity due to the shorter organic chain. Preparation of PDMS containing microcapsules is performed by *in situ* polymerization with urea-formaldehyde shell. The method for urea-formaldehyde microencapsulation is described by White et al. in Nature [1]. Basically, PDMS healing agent with lower molecular weight can be directly encapsulated by urea-formaldehyde microencapsulation, but the high molecular one needs to be diluted with a solvent such as n-Heptane. Urea (5.0 g) followed by resorcinol (0.5 g) and ammonium chloride (0.5 g) were dissolved in water (200 ml) in a 600 ml beaker. A 2.5 wt% solution of ethylene maleic anhydride copolymer (50 ml) was added to the reaction mixture and the pH of the reaction mixture was adjusted to 3.5. The reaction mixture was agitated at 700 r.p.m. and to the stirred solution 60 ml of mixture of HOPDMS (58 ml) and PDES (2 ml) was added to achieve an average droplet size of 120 μm. 37% formaldehyde (12.667 g) solution was added to the agitated emulsion and then the temperature was raised to 55 °C and maintained for 4 hours. After 4 hours, the reaction mixture was cooled to room temperature and the microcapsules were separated.

5.12.2 Sample Preparation for Fracture Test with TDCB Geometry

The test samples were cured at room temperature for 24 hours and then post cured at 30 °C for another 24 hours. The specimens were tested until breaking, followed by healing at 50 °C for 24 hours. For the test of temperature dependence, the test specimens were healed at room temperature, 30 °C and 50 °C.

5.12.3 Synthesis of TKAS Catalyst

0.1 mol of di-n-butyltin diacetate and 0.025 mol of tetraethylsilicate were first mixed in a round flask. The mixed solution was heated to 150 °C while stirring under anhydrous conditions. The reaction by-product, ethyl acetate, was distilled off at atmospheric pressure. The ethyl acetate started to condense at 130 °C, and was considerably distilled off after 15 minutes at 150 °C. The solution was cooled with an ice bath, and the purified TKAS was harvested by filtration. The TKAS final product had the form of wax-like spherulites, which dissolved in an organic solvent such as petroleum ether, cyclohexane, ethyl acetate, dichloroethane, carbon tetrachloride, acetone, and chlorobenzene. 1 g of the TKAS activator was dissolved in 10 milliliters of chlorobenzene under stirring at 80 °C. The solution was filtered through a sintered-glass filter and cooled by means of ice bath.

5.12.4 Microencapsulation of the TKAS Catalyst

The microencapsulation method for the TKAS catalyst by urethane microencapsulation is almost similar to the previous to other organotin catalyst encapsulation with some modification of tin catalyst concentration (2 wt%) in chlorobenzene.

5.12.5 Corrosion Test of the Samples Healed in Water Environments

For the corrosion tests, samples were coated with the dual microcapsule self-healing system which is composed of epoxy matrix, 3 wt% of adhesion promoter ((3-trimethoxysilylpropyl) dimethylene triamine), 14 wt% of PDMS containing microcapsules, and 3 wt% of catalyst (dimethyldineodecanoate tin) containing microcapsules. The substrates were coated with this self-healing system, cured at room temperature for 24 hours and at 30 °C for another 24 hours. These samples were × scribed with a razor blade and followed by healing in a water bath at 50 °C for 24 hours. Each water bath contained pure water, salt water (5 wt% sodium chloride aqueous solution), and water with different pH conditions (pH 2, pH 4, pH 10, and pH 12). The corrosion test was performed by immersing the specimens in 5 wt% sodium chloride aqueous solution at room temperature.

5.13 References

1. S. R. White, N. R. Sottos, P. H. Geubelle, J. S. Moore, M. R. Kessler, S. R. Sriram, E. N. Brown, S. Viswanathan, *Nature* **2001**, *409*, 794-797.
2. E. N. Brown, *Fracture and Fatigue of a Self-healing Polymer Composite Material*, University of Illinois at Urban-Champaign, 2003.
3. E. N. Brown, M. R. Kessler, N. R. Sottos, S. R. White, *Journal of Microencapsulation* **2003**, *20*, 719-730.
4. E. P. Plueddemann, *Silane Coupling Agents;* Plenum press, New York, NY, 1991.
5. F. W. Van der Weij, *Macromol. Chem.* **1980**, *181*, 2541-2548.
6. E. Wohlfarth, W. Hechtl, P. Hittmair, Burghausen, Germany, US Patent, 1976.

CHAPTER 6

CONCLUSIONS

My research aimed to develop a new self-healing system by introducing environmentally stable healing chemistry and demonstrating the concept of phase separated healing agents in polymer matrices. Phase separation of the healing agent is an approach that may be applicable to a broad class of new healing chemistries for structural polymers. Using the environmentally stable self-healing system, we studied the self-healing effects of polymer composites for structural materials and polymer coatings with anti-corrosion functionality by re-sealing surface cracks during weathering and mechanical damage of the coating layer.

To develop the self-healing system, we studied the chemistries for matrix polymerization, the room temperature healing reaction of polydimethylsiloxane (PDMS) healing agent, and the microencapsulation of catalyst materials through interfacial polymerization. The self-healing properties of the developed system were investigated by fracture testing composites or corrosion testing coated specimens. We also established a scientific basis for the self-healing system we developed that used the polycondensation of phase separated droplets of PDMS driven by the breaking open of microencapsulated catalysts to drive healing.

Importantly, the polycondensation reaction of PDMS is accomplished at room temperature using a catalyst which is highly stable against water and oxygen. The microcapsules of the organotin catalyst consist of a polyurethane shell material formed through the interfacial polymerization of urethane with a chain extender in organic solvent. The self-healing efficiency of the polymer composite is evaluated by comparing the fracture toughness of virgin and self-healed samples. The addition of acryl ethoxy silane to the matrix as an adhesion promoter

significantly improved the healing efficiency of the polymer composite. The self-healing system was optimized to apply to low temperature healing by changing the viscosity of the healing agent and inducing the catalyst with higher catalytic activity. Thus, the excellent self-healing properties of a chemically stable polymer composite were demonstrated, even under water environments.

Nevertheless, we think an even more important application of this self-healing system is for coatings. In our study, a new paradigm for self-healing polymer coatings which provides very good corrosion resistance to metal substrates was demonstrated, even after deep scratch damage. Polymer coatings are commonly applied to metal substrates to prevent corrosion in environments such as high humidity and salt water. If the polymer coating has been breached, for example by cracking or scratches, it loses its effectiveness, and corrosion can rapidly propagate across the substrate.

In this thesis, we demonstrated the effectiveness of self-healing polymer coatings based on the dispersion of PDMS healing agents in those coatings. The anti-corrosion properties of the self-healing polymer on metal substrates were investigated by a corrosion test; i.e., salt water dipping. Remarkably, the self-healing coatings showed excellent anti-corrosion effect on the scratched parts, while control samples that did not include all the necessary healing components revealed corrosion propagation on the damaged parts. Scanning electron microscopy (SEM) revealed that the damage in the self-healing system was effectively covered by the polymerized healing agent. The depth difference of damaged parts between the control and the self-healed samples provided other evidence of a successful healing reaction, which coincided with the SEM observation. The quantitative comparison of the anti-corrosion property by electro-chemical tests proved that the self-healing coatings had an excellent anti-corrosion property. The poor

adhesion strength between the polymer coating and metal substrate could be overcome by applying a primer layer at the interface. Eventually, we obtained an excellent anti-corrosion effect with self-healing coatings in the case of scratch damage at room temperature.

In order to develop a commercially optimized self-healing coating system, we investigated the general compatibility of self-healing coatings with a commercialized epoxy based coating solution (International Marine Coatings, Intergard 264) and confirmed its good anti-corrosion effect. For more advanced self-healing coatings, we will investigate the dual layer self-healing coating, which is composed of the actual self-healing coating in a bottom layer and the blank polymer layer for protection and outer appearance.

We can apply a one microcapsule system for easy manufacturing or a dual microcapsule system for general matrix and curing agent application without system restriction in both the composite and coatings. In particular, due to the environmental stability of PDMS poly-condensation, the self-healing coating may be used in severe environments such as high humidity, marine, and aerospace applications. Furthermore, the self-healing coatings are highly effective for forming an anti-corrosion barrier. So, the self-healing coatings can extend the lifetime of the coated layer on the substrate materials and can reduce the frequency of repair for anti-corrosion coatings.

AUTHOR'S BIOGRAPHY

Soo Hyoun Cho was born on August 24, 1970 in Jin-hae, Republic of Korea. He graduated from Pohang University of Science and Technology (Republic of Korea) with a B.S. in Chemical Engineering in February of 1993. He received his M.S. degree in February of 1995 at Pohang University of Science and Technology where he worked under the supervision of professor Chan-Eon Park. During his M.S. degree period, he studied the phase separation behavior of thermoplastic in thermoset matrices. From the spring of 1995 until the fall of 2002, he worked in the technical research laboratory in POSCO (Republic of Korea). As a research engineer, he developed various polymer coating solutions for many fields of industrial application, such as automobile and electric home appliances. In the fall of 2002, he began his Ph.D. work with Professor Paul V. Braun in Materials Science and Engineering at the University of Illinois at Urbana-Champaign. During his Ph.D. period, he also joined the Autonomic Materials System Group to perform interdisciplinary research. After completing his Ph.D., Soo Hyoun will join a company research center as a senior researcher, where he will develop advanced polymeric materials.